New in vitro model of traumatic brain injury to assess biomaterial based regenerative strategies

Raja Haseeb Basit

A thesis submitted for the degree:
Master of Philosophy in
Neuroscience

Neural Tissue Engineering Keele

October 2020

Keele University

Abstract

Penetrating traumatic brain injury (pTBI) causes significant neural damage and debilitation. The management of pTBI is largely supportive currently, with no clinically established regenerative therapies. Researchers have previously evaluated the regenerative potential of biomaterial constructs called hydrogels in pTBI. To screen biomaterials for regenerative application, clinically predictive models of pTBI are required. However, there is a lack of facile, high throughput, pathomimetic in vitro pTBI models capable of evaluating biomaterial implantation.

This thesis aimed to develop methods to i) establish a high throughput and facile culture system containing the major glial cell types, which play an important role in biomaterial handling in the central nervous system ii) introduce reliable and characterizable penetrating lesions into the cultures iii) implant DuraGen Plus™ – an Food and Drug Administration (FDA) approved neurosurgical grade biomaterial into the lesion iv) visualize cell-biomaterial interactions using simple light microscopy v) refine the model to establish a high throughput neuronal model containing all of the neural cell types.

The findings of this study show that the key pathological features of injury seen in pTBI can be reliably replicated, in this novel, facile, high throughput, multi-glial model. Specifically, peri-lesional astrocytes have markedly different responses to injury versus distal astrocytes showing hypertrophic palisading astrocytes and glial fibrillary acidic protein (GFAP) upregulation analogous to reactive astrogliosis in vivo. In addition, microglia and oligodendrocyte precursor cells (OPCs) were observed to infiltrate the lesion core similar to processes seen in pTBI models in vivo. Furthermore, DuraGen Plus™ could be implanted into the lesions to visualize cell-biomaterial interactions. Finally, early pilot data shows that use of an alternative chemical medium can further support the growth of neurons, resulting in a model containing all neural cell types in a technically simple and high throughput experimental system.

Contents page

List of tables and figures

Chapter 1: General introduction

Tables

Figures

Chapter 2: Materials and Methods

Tables

Figures

Chapter 3: Establishing a technical method to develop an in vitro multi-glial TBI model to evaluate cellular responses to biomaterial implantation

Figures

Chapter 4: Characterizing the micro-mixed glial injury model

Figures

Acknowledgements

First and foremost, I would like to thank my supervisor Professor Divya Chari. Without her unwavering support, I would not have been able to produce this thesis. I am particularly thankful for her clear direction, encouragement and guidance throughout the year, enabling me to persevere with my project. On a personal note, I would also like to thank you for your excellent supervision, in the face of an unexpected, global pandemic. These novel circumstances must have been challenging not only for the students, but also yourself, so thank you.

I would also like to thank Dr Stuart Jenkins, without whom I would not have been able to get involved in such a project. I really appreciate your support, advice and direction and I am in a debt of gratitude to you, so thank you.

A special thanks to **all** of the Neural Tissue Engineering Keele group members, whom have helped me along the way and contributed towards my development as a scientist. Farhana Chowdhury and Jessica Wiseman, I appreciate your time and effort, teaching me laboratory skills required to complete this thesis.

Finally, I would like to take this opportunity to thank my family whom have given their unwavering support throughout the year.

Abbreviations

2D	Two-dimensional
3D	Three-dimensional
ATLS	Advanced Trauma Life Support
BBB	Blood brain barrier
CNS	Central nervous system
CSF	Cerebrospinal fluid
CT	Computerized Tomography
Cy3	Cyanine 3
DAB	3,3'-diaminobenzidine
DAMPS	Damage-associated molecular patterns
DAPI	4′,6-diamidino-2-phenylindole
ECM	Extracellular matrix
FITC	Fluorescein isothiocyanate
FDA	Food and Drug Administration
GCS	Glasgow Coma Scale
GFAP	Glial fibrillary acidic protein
Iba1	Ionized calcium-binding adapter
ICC	Immunocytochemistry
ICP	Intracranial pressure
IED	Improvised explosive device
IL	Interleukin
FBS	Foetal bovine serum
MAI	Myelin-associated inhibitors
MAG	Myelin-associated glycoprotein
NDS	Normal donkey serum
NG2	Neural glial antigen
NOGO	Neurite outgrowth inhibitors
OMGP	Oligodendrocyte myelin glycoprotein
OPC	Oligodendrocyte precursor cell
PAMPS	Pathogen-associated molecular patterns
PBS	Phosphate buffered saline
PEG	Polyethylene glycol
PFA	Paraformaldehyde

PS Picrosirius

PMN Polymorphonuclear

PNS Peripheral nervous system

pTBI Penetrating Traumatic brain injury

SCI Spinal cord injury

TBI Traumatic brain injury

TNF Tumor necrosis factor

Tuj1 Purified anti-neuron-specific class III beta-tubulin

US United States

USA United States of America

Chapter 1

General introduction

1.1.1 Epidemiology of traumatic brain injury

Globally, traumatic brain injury (TBI), affects around 10 million people annually, with around 1.7 million cases of TBI occurring within the United States (US) (1,2). The mortality rate for TBI is 30 per 100,000 or an estimated 50,000 deaths in the US. Within the US, TBI is the leading cause of death in individuals under 44 (3). In 2014, 56,800 people died from TBI-related deaths; 2,529 deaths were among children. In the US, the total annual direct cost of TBI management is estimated at $48 billion dollars, whilst the indirect costs such as productivity losses is estimated at $56 billion US dollars (2).

1.1.2 The classification of TBI

TBI can broadly be classified by two distinct aetiologies; closed TBI or penetrating TBI (pTBI) (4). Closed TBI results from an injury to the head without dural breach, often by a blunt object. pTBI results from an object possessing enough energy to pierce the skin, skull, dura and enter the brain (5). TBI aetiology is multifactorial, however falls and being struck with or against an object represents most cases ***(figure 1***).

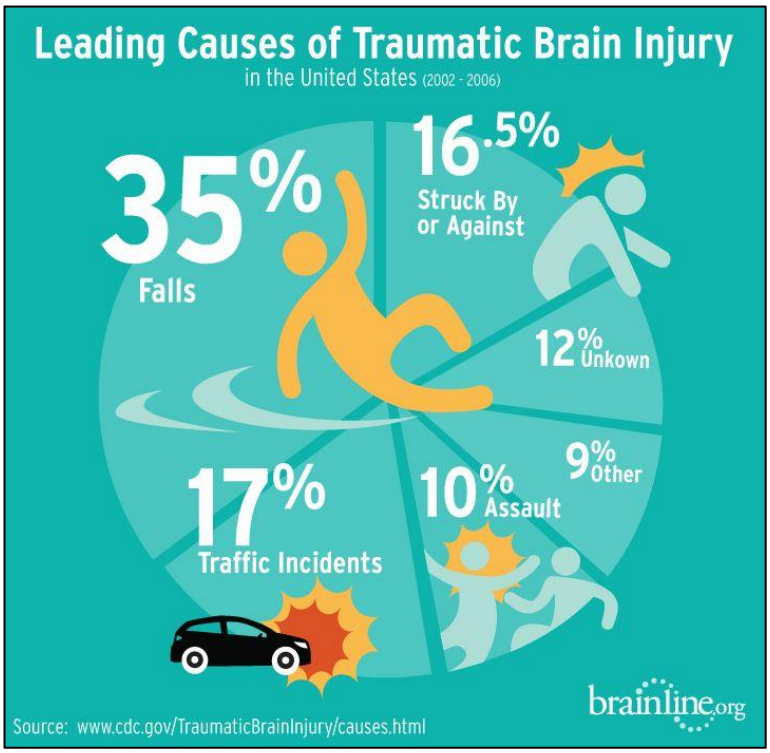

Figure 1: Infographic representing the causes of TBI (6)

pTBI is the most lethal form of TBI, with approximately 70-90% of patients dying prior to hospital admission and 50% of those whom reach the hospital die during resuscitation in the emergency department (7). pTBI survivors are a minority and given that these patients often have to live with severe debilitation, this review will focus on pTBI including the aetiology, pathophysiology and management of this pathology (8). pTBI is prevalent in many different populations, particularly civilians living in areas with a high incidence of violence, and military personnel (8). Of the 333,169 US military TBI deaths recorded between 2000 -2015, 4,904 were classified as pTBI (7). Furthermore, 32,000 -35,000 civilian deaths in the US are as a result of pTBI (7). pTBI can result from any object which breaches the dura and enters the brain. Unsurprisingly, gunshots are the most common cause of pTBI (9). However, wounds induced from knives, nails, screwdrivers and ballpoint pens have also been described (10). In addition, within military populations shrapnel from improvised explosive devices also cause pTBI (11).

1.1.3 pTBI causes severe tissue damage

The clinical quantification of the severity of TBI is often carried out using scales such as the Glasgow Coma Scale (GCS) seen in ***table 1*** (12).

ADULT		INFANT
Eye opening	**E**	**Eye opening**
Spontaneous	4	Spontaneous
To speech	3	To speech
To pain	2	To pain
No response	1	No response
Best motor response	**M**	**Best motor response**
Obeys verbal command	6	Normal movements
Localizes pain	5	Localizes pain
Flexion - withdraws from pain	4	Withdraws from pain
Flexion - abnormal	3	Flexion - abnormal
Extension	2	Extension
No response	1	No response
Best verbal response	**V**	**Best verbal response**
Oriented and converses	5	Coos, babbles
Disoriented and converses	4	Cries but consolable
Inappropriate words	3	Persistently irritable
Incomprehensible sounds	2	Grunts to pain/restless
No response	1	No response

Table 1: Different components assessed in the Glasgow coma scale (13)

The GCS categorizes TBI in three distinct categories; mild, moderate and severe (14). Mild TBI represents 75-85% of all TBI and is most often seen in the context of closed TBI. In addition, mild TBI is the most common TBI affecting military personnel, and has been reported to affect around 15.2% to 22.8% of returning service members (12). Branded as the "silent epidemic" mild TBI is characterized with a GCS of 13-15 and presents typically with subtle concussive symptoms, including memory and cognitive impairments (15). Although patients with mild TBI make a complete neurological recovery, up to 30% suffer with prolonged behavioural changes. Patients with moderate TBI have a GCS of 9-13. Indeed, pTBI almost always presents as severe TBI. Here, patients have a GCS of 3-8 and it is often characterized by a prolonged loss of consciousness, inability to speak and open the eyes and unresponsiveness to commands (16). Lower GCS scores typically correlate with a poor prognosis (17).

1.1.4 pTBI management is supportive and lacks regenerative treatments

pTBI is a neurosurgical emergency until proven otherwise (18). The management can be described in two distinct phases; acute stage management and secondary rehabilitative management. Patients should initially be assessed according to current Advanced Trauma Life Support (ATLS) guidelines and be subjected to a full A-E (airway, breathing, circulation, disability, exposure) approach and undergo primary resuscitation (19). Post-resuscitative GCS scores should also be obtained, and if a score less than 8 is achieved the patient must be intubated (20).

Computerized Tomography (CT) scans are the neuroimaging gold standard, providing key information which guides subsequent management (21). Current acute management strategies are largely supportive and involve intracranial pressure (ICP) monitoring and aggressive early surgical wound debridement with or without decompressive craniotomy/craniectomy and closure of the dura to form a watertight seal (22). Together, these measures have shown to improve prognosis as they limit cerebral oedema and post-trauma infection (11). Specifically, the bacterium *Staphylococcus aureus* is the most common

cause of infection (23). The increased risk of infection can be attributed to a variety of factors; firstly, penetration of the brain including the skin, skull and meninges breaches the normal “brain sterility” and exposes the brain to external pathogens. Secondly, the penetrating foreign objects are unsterile and thus carry an intrinsic risk of infection. Thirdly, hair, bone fragments and cerebrospinal fluid (CSF) leaks within the brain pose a potential risk of infection (3). Thus, early broad-spectrum prophylactic antibiotics are often administered in addition to surgical wound debridement. In addition to infection, the presence of necrotic brain tissue and foreign bodies are sometimes associated with post-traumatic epileptic seizures, thus anti-seizure drugs also form a part of the management (24). To promote long term recovery, patients are also managed from a biopsychosocial approach and patient rehabilitation involves many members of the multidisciplinary team; neurosurgeons, neurologists, nurses, physiotherapists, psychiatrists, speech and occupational therapists (25).

Currently, as discussed above, pTBI management is largely supportive, with no clinically established regenerative therapies. Thus, the development of such regenerative therapies is of paramount importance. However, to understand how regenerative therapies could potentially help pTBI patients one must first have an awareness of why regeneration is limited within the CNS.

1.2.1 The central nervous system has a limited capacity for repair

The central nervous system (CNS) is unique among physiological tissues in that it has an intrinsically low regenerative capacity (26). Limited CNS regeneration is multifactorial including; limited regenerative capacity of adult neurons, scarring, inflammation and inhibitory chondroitin sulphate proteoglycans (CPSGs) (27).

1.2.2 Myelin-associated inhibitors are a barrier to repair

One theory as to why the CNS environment is inhibitory is due to the presence of myelin-associated inhibitors (MAIs).

Firstly, injury in the CNS and axonal damage increases the presence of the myelin breakdown products, which are in themselves inhibitory. Three main inhibitors within myelin have been identified; neurite outgrowth inhibitors (NOGO), myelin-associated glycoprotein (MAG) and oligodendrocyte myelin glycoprotein (OMGP) (27). These molecules have been shown to be the main inhibitors to regeneration early in injury, prior to the maturation of the glial scar.

NOGO-A is the most common isoform of NOGO, a transmembrane protein expressed by oligodendrocytes (28). Studies have demonstrated the inhibitory actions of NOGO, by studying NOGO-A knockout mice. Interestingly, NOGO knockout mice have reduced inhibitory effects on neurite outgrowth in vitro (27).

MAG is a transmembrane glycoprotein produced by oligodendrocytes, although MAG is also found in the peripheral nervous system (PNS). Normally MAG plays a key role in neuronal development by promoting axon growth in young neurons, whilst inhibiting axonal growth in mature neurons (26). Furthermore, research has shown a role for maintaining axonal integrity in disease states. However, MAG has been shown to limit neurite outgrowth in vitro by interacting with the neuronal receptors, nogo66 receptor-1, nogo66 receptor -2, paired immunoglobulin-like receptor b and gangliosides (29). Thus, MAG is often considered as both a growth promoting and growth inhibitory agent.

OMGP is a glycosylphosphatidylinositol (GPI) linked protein produced both by oligodendrocytes and neurons. Like MAG, OMGP is also found in the PNS. In vivo studies have demonstrated that OMGP has inhibited axonal sprouting post CNS injury (30).

All three MAIs have been shown to inhibit neurite outgrowth in vitro and are postulated to inhibit growth in vivo (27). One well understood mechanism which is common to the MAIs, is their interaction with glycosylphosphatidylinositol linked NOGO receptor (NGR). Upon MAI interaction with the receptor, NGR activates p75NTR which in turn activates Rho – the main mediator of inhibition (29).

Of relevance to pTBI, the glial scar has been shown to be inhibitory to regeneration in several ways. The dense network of hypertrophied reactive astrocytic processes and surrounding extracellular matrix (ECM) form a barrier to axonal growth and regeneration (31). Huang et al demonstrated that regenerated axons were “pinched” by the glial scar, indicating that regeneration must be targeted prior to maturation of the glial scar (32). When regenerating axons are unable to complete regeneration, they form dystrophic end bulbs – a morphological fate which characterizes regeneration failure.

Furthermore, astrocytic production of CSPGs has shown to inhibit regeneration both in vitro and in vivo (32–34). CSPGs are a family of ECM proteins and consist of a protein core to which chondroitin sulphate chains are covalently attached. The chondroitin sulphate chains are major inhibitory molecules. Increased production of CSPGs has been demonstrated within the glial scar by reactive astrocytes (32). CSPGs are membrane bound yet astrocytes can also secrete them into the extracellular space (33). Adult sensory neurons have been shown to undergo axonal regeneration when transplanted into the corpus callosum provided they are transplanted with minimal trauma to the surrounding tissue (35). Interestingly, when there is increased trauma, or indeed a lesion site, regeneration stops as the axons approach the lesion as there is a high concentration of CSPGs (34).

Different theories, as to why CSPGs are inhibitory have been proposed, including CSPGs acting as a negatively charged boundary which actively inhibits the growth of regenerating

axons (36). Furthermore, there is additional evidence that CSPGs inhibit a variety of growth promoting molecules such as fibronectin and L1 (33). Interestingly, like myelin inhibitors CSPGs also mediate inhibition through NOGO receptors (32). In addition, receptor tyrosine phosphatase is able to bind CSPGs yet also has a role in axonal growth inhibition (37). Specifically, two members of the leukocyte common antigen related subfamily of receptor tyrosine phosphatases, protein tyrosine phosphatases$^{1}/_{4}$ and leukocyte common antigen related bind CSPGs with high affinity and mediate suppression of axon elongation by CSPGs.

As discussed above, the CNS has an intrinsically limited regenerative capacity. It is important to understand however, the key pathophysiological responses to pTBI as it is these responses which partially contribute to the hostile and inflammatory environment which can be inhibitory to repair.

1.3.1 pTBI results in neuroinflammation and glial scarring - both inhibitory to repair

Previous literature has classified both microglia and astrocytes as the two principal immunocompetent cell types within the central nervous system (CNS) (38). These cells mediate neuroinflammation and the glial scar, two features seen in pTBI (39). Understanding these processes requires an understanding of the roles of microglia and astrocytes.

1.3.2 Microglia are the major immune cell type of the CNS

Microglia are resident tissue macrophages of the CNS and represent ca 20% of all glia (40). Generally, microglia drive and resolve inflammation within the CNS. Microglial role and function is largely dependent on the activation state (40,41).

M0 represents the unactivated microglial activation state, seen under normal physiological conditions, typically ramified (***figure 2***). M1 represents pro-inflammatory microglia typically seen in response to CNS insults including tissue damage (42,43). M1 microglia are typically described as amoeboid (42,43).

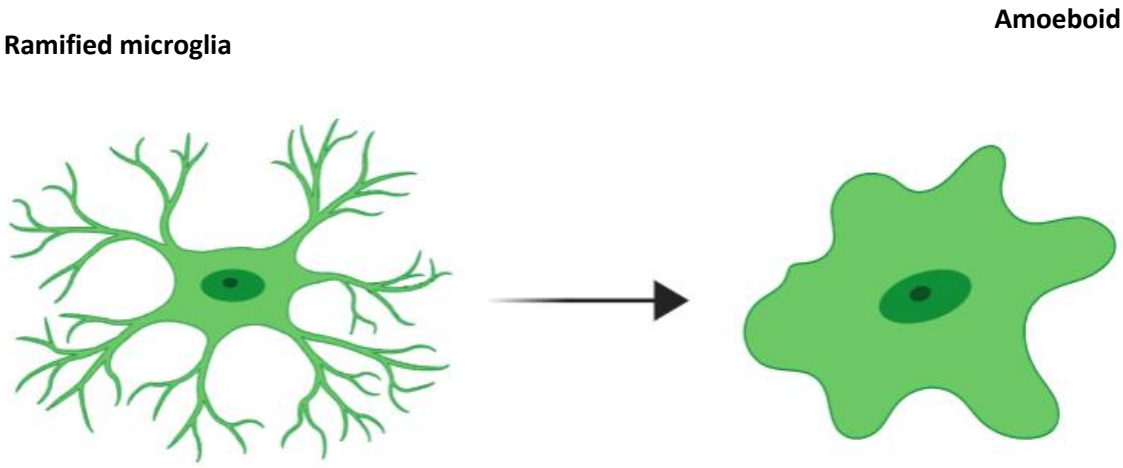

Figure 2: A schematic demonstrating the morphological changes ramified microglia undergo in response to CNS trauma

Note how amoeboid microglia are rounded as ramified microglia have undergone process retraction.

1.3.3 M0 microglia monitor tissue for damage and infection

Ramified microglia represent ca 20% of all glial cells within the adult brain parenchyma. With regards to their morphology ramified microglia have a high membrane branches **:** cytoplasm ratio (40) (***figure 3***).

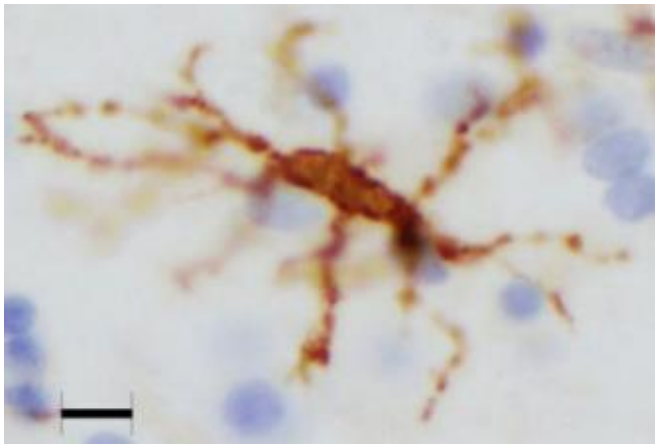

Figure 3: Immunohistochemistry micrograph of a ramified microglial cell which is highly processed and displaying classical resting morphology. Scale bar: 10 µm (44).

In healthy tissue, ‘resting’ (M0) microglia are constantly surveying tissue for damage associated molecular patterns/ pathogen associated molecular patterns (DAMPS)/(PAMPS) (45). Although previously it was considered that resting microglia were inactive, recent literature suggests that ramified microglia undertake a variety of functions under resting physiological conditions; scanning the surrounding microenvironment for possible insults. Zanier et al (2015) suggests that microglia are “never resting” and that ramified microglia have a crucial role in not only metabolite removal but also clearing debris and toxic factors released as a by-product of neuronal injury (46). In addition, further roles include: to optimize neural circuits and maintain neuronal activity through synaptic pruning whilst also optimizing conduction through synapses by maintaining neurotransmitter signalling (47).

1.3.4 M1 inflammatory microglial responses combat infection and clear cellular debris

Pro-inflammatory responses to trauma/infection results in loss of ramified microglial processes and the presence of amoeboid microglia (48). Amoeboid microglia are a highly motile, phagocytic cell and thus are morphologically similar to monocytes and macrophages (***figure 4***).

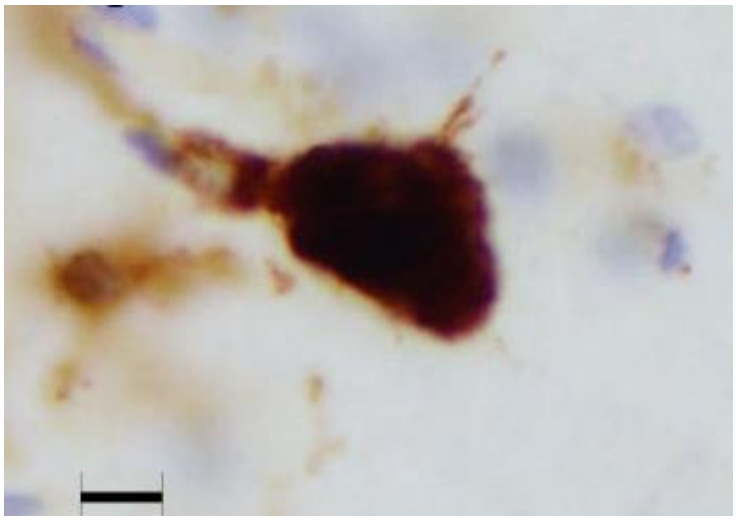

Figure 4: Immunohistochemistry micrograph of a microglial cell showing classical signs of M1 activation

Note the lack of processes and rounded morphology. Scale bar: 10 µm (44)*.*

Exposure to pro-inflammatory stimuli induces reactive microglia to release pro-inflammatory cytokines such as tumour necrosis factor (TNF) alpha, interleukin (IL) 1 beta , and also protease enzymes and reactive oxygen species (ROS) (28,45,49–52). Reactive microglia primarily phagocytose damaged/apoptotic cells and cellular debris. Although the presence of M1 microglia is often seen as a sign of neuroinflammation, the process of M1 microglia phagocytosing cellular debris has shown promise in promoting regeneration. This is because cellular debris can be toxic and inhibitory to axonal regeneration, thus active phagocytosis and subsequent removal of this debris prevents debris mediated inhibition (53).

1.3.5 Is there a role for 'M2' microglia in CNS regeneration?

There is active debate with regards to the presence of M2 microglia, as currently there is evidence both for and against the existence of M2 microglia (52). Generally, researchers in favour of the M2 classification characterize these microglia as anti-inflammatory. For instance, Lively and Schlichter et al (2013), demonstrated that M2 microglia, upregulate MRC1(54). MRC1 is a transmembrane pattern recognition receptor which binds carbohydrates and is involved in pinocytosis and phagocytosis of immune cells. Specifically, microglial MRC1 upregulation has been associated with a neuroprotective microglial phenotype (52). M2 microglia are considered to exert an anti-inflammatory effect and be conducive to pro-repair as they release type 2 cytokines (transforming growth factor beta and IL-10), whilst also inhibiting pro-inflammatory cytokines. Furthermore, specifically IL-4 alternatively activated M2 microglia are neuroprotective and conducive to regeneration within the CNS as they promote both neurogenesis and oligodendrogenesis (55). Miron et al (2013) demonstrated that M1 microglia "switch" to M2 microglia during remyelination, oligodendrogenesis, which resulted in increased oligodendrocyte differentiation, thus providing evidence that M2 microglia may also have a pro-neuroregenerative role (56)(57).

Although there is evidence both for and against the M1/M2 microglial classification as presented above, more recently researchers have been in favour of a multidimensional

concept of microglial/macrophage ontogeny, activation and function (58). Researchers have studied the microglial phenotypes in relation to neurodevelopment, homeostasis, ageing, neurodegeneration and in vitro conditions through transcriptome studies (58–60). Overlaying disease specific microglial signatures has led to the identification of genes which are commonly expressed (although in different proportions) across all conditions/environments (58–60). These microglial genes have been referred as the microglial core gene signature and thus provides strong evidence in favour of microglia as a multidimensional cell type versus strict M1 versus M2 classification applying to each condition(58–60).

1.3.6 Astrocytes are the main homeostatic cells of the CNS

Astrocytes represent a major glial cell type representing 20%-40% of all glia (61). Astrocytes have a key role in the development of the CNS and formation of synapses, as they secrete a variety of growth inducing/inhibitory molecules responsible for axon guidance during development such as glutamate, adenosine triphosphate, cytokines and other signalling molecules such as adenosine and lactate (61). Astrocytes are also involved in neurotransmitter metabolism and regulate extracellular pH and potassium (38). Also, astrocytes maintain the integrity of the blood-brain barrier (BBB) and blood flow (62). Furthermore, during CNS development, astrocytes interact with other glial cell types including the microglia. Specifically, neonatal astrocytes cause neurons to upregulate the complement protein c1q which is localized selectively to immature synapses, thus phagocytic cells such as the microglia can recognize complement proteins and can remove these complement tagged cells, thereby clearing unwanted axons and synapses (61).

1.3.7 Astrocytes are key mediators in neuroinflammation

Astrocytes have been described as “active players” in neuroinflammation (63). In response to the specific inflamed milieu, astrocytes can secrete a variety of cytokines and chemokines, whilst also having a role in immune cell activation and migration (41).

Much like the M1/M2 microglia classification discussed above; a classification scheme applies to astrocytes. Both A1 and A2 reactive astrocytes been described (64). A1 astrocytes

are inhibitory to repair (64). A2 astrocytes on the other hand are considered to be “pro-repair”. Unlike microglial activation states, astrocytes are accurately classified according to the genes they upregulate. A1 astrocytes upregulate classical complement cascade genes whilst A2 astrocytes upregulate neuroprotective genes (61) (64).

The glial scar is characterized by reactive gliosis (section 1.3.8) and is often seen in response to CNS injury and evolves with time (31). Within hours after axonal injury, cellular debris such as myelin causes activation and proliferation of microglial cells which subsequently migrate into sites of injury (***figure 5***).

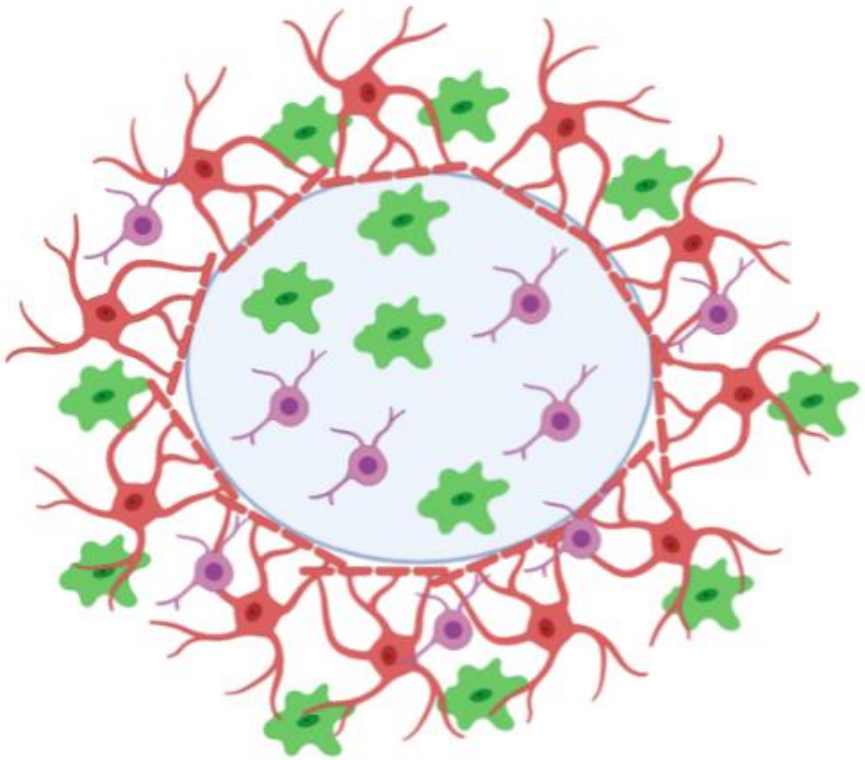

Astrocytes**- red cells** Microglia- **green cells** OPC**- purple cells.**

Lesion core**- light blue circle in the middle**

Figure 5: A schematic showing the hallmarks of the glial scar

Astrocytes are hypertrophic with process polarization towards the lesion core. Astrocytes have surrounded the lesion core. Microglia and OPCs infiltrate the lesion core prior to astrocytic responses.

Oligodendrocyte precursor cells (OPCs) are seen 3-5 days post-injury with or without meningeal cells and fibroblasts depending on meningeal damage. Astrocytes can become activated as early as 1 day post-lesion and hypertrophy and migrate towards the lesion. Astrogliosis is characterized by the presence of reactive astrocytes – hypertrophied astrocytes which upregulate a variety of genes and molecules including GFAP, and form a glial scar post-acute CNS insult (61). GFAP is a cytoskeletal protein and is used to identify astrocytes both in vitro and in vivo (31,37). Specifically, upregulation of GFAP signifies CNS injury and trauma (32).

Anatomically, the glial scar can be divided into two distinct zones. Firstly, the lesion core predominately contains NG2 positive glia, fibroblasts/pericytes (perivascular cells that wrap around capillaries) and macrophages. The outer layer surrounding the lesion core consists of reactive hypertrophic astrocytes with elongated, overlapping processes polarizing towards the lesion. The outer layer also consists of increased numbers of activated microglia which surround the lesion core (65).

1.3.8 pTBI results in astrogliosis and microgliosis

In pTBI, damaged cells release damaged-associated molecular patterns (DAMPS) which interact with microglial toll like receptors and subsequently activate them (66). Upon activation, microglia enter the lesion site following chemotactic signals, and phagocytose cellular debris (42). Furthermore, microglial responses to pTBI can be described in the following ways : increased staining intensity of microglial marker Iba1 (45,47,60), increased microglial numbers around and inside the lesion due to both microglial proliferation and migration at these sites and finally distinct morphological changes from normal resting microglia with a ramified morphology to activated and rounded microglia with a more amoeboid morphology (39,42,67,68). Also, microglia release inflammatory cytokines and chemokines which recruit further microglia and astrocytes (64,69). Specifically, microglial release of IL-1 alpha, TNF alpha and complement 1q has shown to activate A1 astrocytes which become activated from their resting state (64). Upon injury, resting and processed

astrocytes become reactive and hypertrophic. Reactive hypertrophic astrocytes form a barrier between damaged and healthy tissue known as the glial scar (62). To effectively form the glial scar around the injury track, the astrocytes must “accumulate” around the lesion (70). Astrocytic accumulation and recruitment in vivo has been characterized by forming elongated processes and polarizing towards the lesion and has been described as palisading astrocytes (70,71).

1.3.9 Neuronal response to pTBI

Neurons are electrically active cells responsible for the conduction of action potentials within the nervous system (72). Neurons have four main distinct regions: cell body, dendrites, axon and axon terminals (***figure 6***).

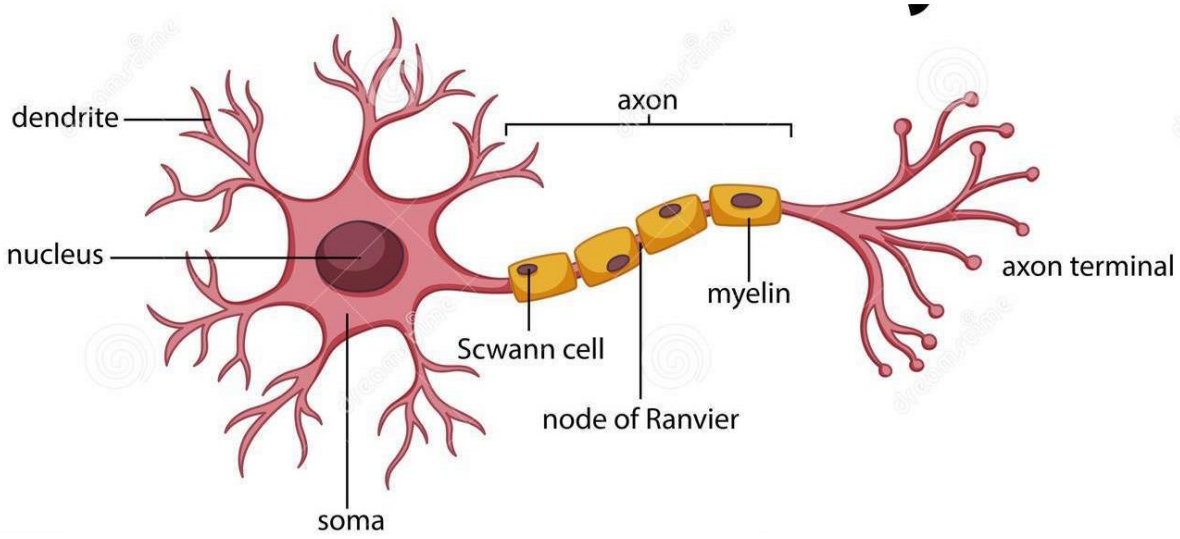

Figure 6: A schematic showing the anatomy of a neuron (73)

The cell body houses the nucleus and is the site of most of the neuronal protein synthesis. Likewise, the presence of lysosomes also makes the cell body the site of neuronal protein degradation (74). Axons are responsible for the conduction of action potentials away from the cell body. The dendrites allow interneuronal communication as dendrites receive chemical signals from axon termini of other neurons (75).

Generally, post-injury, most axons within the adult CNS are unable to spontaneously regenerate like they do in the peripheral nervous system (PNS), leading to significant functional impairment. Interestingly, Aguyao et al demonstrated that CNS axons can regenerate within a PNS environment, thus indicating that the PNS environment favours repair and that the CNS environment may be inhibitory to repair (76).

The neuropathological consequences of pTBI are often related to the impact velocity of the projectile (77). Low velocity projectiles such as shrapnel, or bullets discharged from a firearm with a low muzzle velocity enter the cranium and create a missile track leading to a laceration, shearing and compression of the brain along the track (10,77). High velocity projectiles include most bullets, where in addition to the missile track, upon impact high pressure shock waves transmit through the brain and create an additional temporary cavitation effect. The temporary cavity collapses and expands in a wave like pattern, compressing the brain against the skull. Each cycle of collapse and expansion is responsible for significant tissue damage and has been shown to cause neuronal shear injuries, epi/subdural hematomas and parenchymal contusions. Microscopically, widespread axonal injury and haemorrhage has been reported to be distributed throughout the cerebral hemispheres. Oehmichen et al found that away from the missile track, neurons are arranged in a wave like pattern suggesting axonal damage secondary to the temporary cavitation effect (11) (78). They microscopically characterized the cell destruction resulting from the missile track and found significant shearing of blood vessels, subsequently leading to haemorrhagic extravasation adjacent to the track (78) (***figure* 7**).

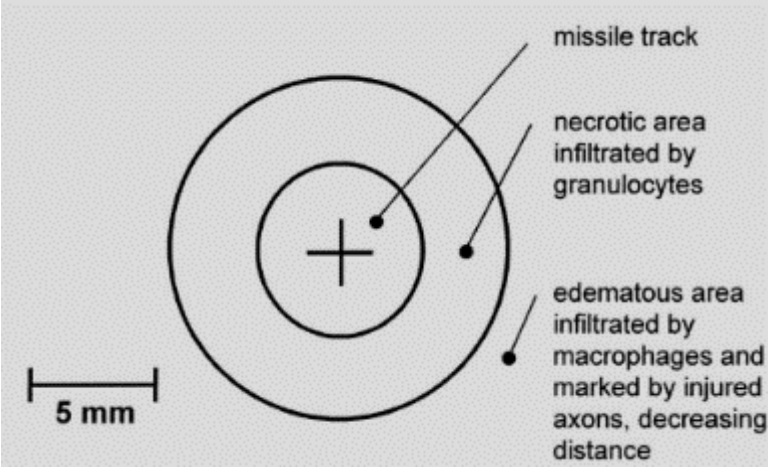

Figure 7: *A* schematic demonstrating the different zones surrounding the missile track

Here, immediately surrounding the missile track is the necrotic zone, whilst the edematous area surrounds the necrotic area where extensive neural damage is still seen (11).

Within the haemorrhage, there were distinct necrotic zones of astrocytic and neuronal destruction. Furthermore, within the necrotic zones, polymorphonuclear (PMN) leukocytes acts as scavengers and appear within 1 day post-injury. Immediately surrounding the necrotic zone, is an edematous area with substantial numbers of macrophages. Loss of large amounts of brain tissue has been shown to cause edema formation which correlates with higher mortality, possibly because edema leads to secondary complications such as intracranial hypertension. Furthermore, within the oedematous zone, axonal fragmentation, clumping and varicose changes are seen. The degree of axonal damage correlates inversely with distance away from the track.

1.3.10 OPC response to pTBI

Oligodendrocytes are a glial cell type responsible for axonal myelination within the CNS, with one oligodendrocyte capable of myelinating around 40-50 axons (41). Myelination allows saltatory conduction throughout the CNS. In addition to myelination, oligodendrocytes provide trophic support to neuronal cells through lactate release.

OPC responses to traumatic injury within the CNS has been studied extensively. There is a consensus amongst researchers that neural glial antigen positive $(NG2)^+$ cells proliferate and accumulate around and in the injury site (79). Previous studies employing stab wounds to the brain and contusion injuries to the spinal cord have led to a local increase in the number of $NG2^+$ glia. Rabchevsky et al found an increased number and density of OPCs in the ventral-lateral funiculus of rats 2 days after contusion injury (80). McTigue et al reported a 3-5-fold OPC infiltration increase within lesioned tissue (81). Hampton et al found that in response to a cortical stab wound, OPCs infiltrate into the peri-lesional area from as little as 2 days post-lesion (82). In addition, it was noted that the OPCs appeared hypertrophic with many processes and increased NG2 immunoreactivity within 1.5mm of the lesion. Interestingly, in response to injury OPCs have also been reported to increase NG2 expression, withdraw finely branched processes and increase cell body size. The reaction of OPCs to cortical stab wounds has also been studied extensively. Buffo et al (2005) found a 3-fold increase in the density of OPCs surrounding a cortical stab at 7 day post-lesion, whereas Tatsumi et al (2008) reported 5-6-fold increase (83). As mentioned previously, the glial scar has 2 anatomical zones; the lesion core and the astrocytic zone surrounding the lesion core. In response to spinal cord injury, $NG2^+$ cells have been known to populate lesion cavities, 2 days after injury (79). Furthermore, Hughes et al (2013) found in response to a laser lesion of the cortex, OPCs proliferate and migrate into the vacated space (84).

Studies have shown that in response to generalised traumatic injury OPCs, which are normally in a quiescent state become activated (85). Post-brain injury mature oligodendrocytes are unable to produce new myelin sheaths and are often killed in the acute phase following injury (86). Renewal is thus dependent on the process of oligodendrogenesis. During injury, quiescent OPCs become activated and proliferate, and migrate towards the lesion and differentiate into mature oligodendrocytes (85). Oligodendrocytes are postmitotic cells, thus loss of these cells through injury is associated with a subsequent loss of myelination, which has been shown to contribute to cognitive

decline and can trigger depressive-like behaviour. Thus, formation of new oligodendrocytes post-injury is dependent on oligodendrocyte precursor cell (OPC) differentiation into oligodendrocytes.

1.3.11 Regenerative therapies are needed for pTBI management

The complex cellular responses to pTBI enables researchers to understand the pathophysiology and extent of pTBI injuries on a microscopic level, however these microscopic cellular responses translate clinically as significant cognitive and function impairment and debilitation, with severe cases resulting in death. Examples of current therapies being trialled include the potential of neural stem cell (NSC) transplantation into lesioned brain to facilitate functional recovery (87). However, although such therapies show promise, low cell viability post-transplantation means such therapies cannot maximise regeneration within the CNS. One potential solution to this is to transplant neural cell types in biomimetic biomaterials such as hydrogels into lesion sites to promote regeneration and reduce inflammatory processes (88–96).

1.4.1 Biomaterials such as hydrogels have been considered as a "pro-repair" strategy

As discussed above, the CNS has an intrinsically lower regenerative capacity versus other tissues and thus researchers have been focusing on developing biomaterials which are "pro-repair". One such class of biomaterials which is widely tested within the CNS includes **hydrogels**. Hydrogels are a three-dimensional network of hydrophilic polymers comprised of up to 90% water and can be synthesized from natural or synthetic polymers (92). The tissue-like, high-water content favours transplantation into soft tissues such as the CNS (97). Hydrogels can provide structural support to surrounding tissue and also serve as a trophic microenvironment via biomolecule and cell delivery. Specifically, tuneable hydrogel properties such as biomaterial stiffness (87,91,98,99) and thixotropic properties (90,99–105) makes hydrogels highly attractive biomaterials in regenerative research and clinical medicine (88–92,106). These specific properties are explored in turn in the following discussion.

1.4.2 Gel stiffness can be controlled, and influences biological responses

One major advantage hydrogels offer is the tuneable mechanical properties such as stiffness. Thus, for specific purposes one can tailor hydrogel stiffness to meet that need. For example, NSCs differentiate into three major cell types- neurons, astrocytes and oligodendrocytes. In general, NSCs and their subsequent differentiation is favoured in soft biomaterials with a relative stiffness of around 0.1-1 kPa (94,102,107,108). Extremes of stiffness including very soft biomaterials (<0.1 kPa) and very hard biomaterials (>100 kPa) have shown to be inhibitory to NSC viability, whilst glial differentiation is optimal in biomaterials with a stiffness of around 7-10 kPa. When cultured on hydrogel substrates, NSC preferentially differentiate into astrocytes on hard surfaces where as soft-intermediate stiffness (around 500 Pa) promotes NSC differentiation into neurons (94). Banjeree et al found a 17-fold increase in NSC number after 7 days in culture in alginate hydrogels of low stiffness, versus a 2-fold increase in the stiffest variant of their alginate hydrogel (94). Furthermore, at day 7, the highest levels of beta tubulin III (neuronal differentiation marker)

was observed in alginate hydrogels of low stiffness (183 Pa), and interestingly the modulus of brain tissues is also around 180 Pa. Thus, neural regeneration, proliferation and differentiation, can be induced by hydrogel scaffolds, depending upon their specific mechanical properties (109).

1.4.3 Thixotropic and bio adhesive properties can be altered to facilitate minimally invasive applications

The current trend in developing hydrogels for transplantation for regenerative therapies now emphasize “injectability” (90,100,103). Previously, hydrogels were implanted directly into the CNS/injury site, through a surgical procedure. Although effective, this process is not without limitations. Firstly, a surgical procedure is lengthier than an injection-based delivery system and will require multiple healthcare professionals to deliver this service. Secondly, surgery is invasive, which could be detrimental when considering hydrogels will usually be implanted into sites of injury and pathology. In addition, surgery also increases the risk of infection. Thus, injectable hydrogels provide a minimally invasive alternative to conventional surgery. In particular, this offers an attractive approach to fill cavities in pTBI. However, hydrogels are a jelly like, fibrous-cross linked polymer, composed of either natural substances- mimicking CNS extracellular matrix (ECM), or synthetic formulations (109,110). Thus understandably, to inject a hydrogel successfully, a hydrogel must possess thixotropic properties- the ability to withstand shear-thinning forces that hydrogels are subjected to as they the transit through a needle, and then subsequently gelate and “self-heal” at the target site without further intervention (100). Thus shear-thinning and thixotropic properties enable a pre-set 3D hydrogel construct tuned for a specific function ex-vivo, to then be delivered in vivo (99–101). Furthermore, injecting a pre-set shear-thinning hydrogel has inherent advantages over purely liquid hydrogel solutions which subsequently gelate; the host environment may affect the hydrogel during crosslinking in non, pre-set hydrogels (99). Hydrogels with shear-thinning properties gelate much more rapidly at their target site (101). Finally, pure liquid uncrosslinked hydrogels may leak into surrounding tissue or perhaps dilute with local fluid

changing the physicochemical properties and concentrations of substances within the hydrogels (92).

Furthermore, once a hydrogel is injected it is vital that the hydrogel remains in-situ at the target site and does not drift away. This is of importance when considering the role of hydrogels in forming “structural bridges” in pTBI management, thereby bridging the lesion made from the missile track and promoting regeneration. Thus, hydrogels for such purposes must intrinsically possess or can be engineered to have bio adhesive properties. For a hydrogel to be bio adhesive it must not drift away from the implanted site whilst also being cell adhesive. Oliviera et al reports that when injecting NSCs into the spinal cord intrathecally, the majority of cells sediment inferior to the cauda equina, and thus injecting NSCs within a bio adhesive biomaterial scaffold has been reported as novel solution (98, 106). Strategies to improve bio adhesion include modifying the surface of the biomaterials with ECM proteins such as laminin, fibronectin and collagen (87,103,106,112,113). Such strategies have shown to improve tissue integration, viability of transplanted cells and axonal regeneration. For example, increased neurite outgrowth was seen in a poly(ethylene glycol) (PEG) hydrogel coated with fibronectin versus hydrogel without coating (87,103,106,112,113).

1.4.4 Hydrogels offer pro-regenerative properties

Hydrogels are biomaterial scaffolds and act as a protective three-dimensional (3D) matrix which also supports cellular growth (87,92,105,110,112,114). For example, dopaminergic neurons only have a 1-5% post transplantation cellular viability. Interestingly, $1x10^{13}$ dopaminergic neurons need to be transplanted to yield a 1% post-transplantation survival (91,115). Adil et al (2017) transplanted neurons encapsulated in a hyaluronan-heparin matrix into rat striatum and demonstrated a 3.5-fold increased cell viability versus unencapsulated cells, and a 5.4 fold increase in TH^+ neuronal survival versus injection of traditional unencapsulated cells (91). Furthermore, it was noted that there was 2-fold increase in neurite outgrowth within the hydrogel. Hydrogels are porous structures and thus allow bilateral cellular movement. Furthermore, hydrogels can recruit host cells to promote differentiation

and proliferation at the lesion site and thus can act as a transitory neuromimetic milieu (104). This is of paramount importance when considering the neuropathological consequence of pTBI.

In addition, acellular biomaterial matrices have also been shown to possess regenerative properties. Hou et al found in a pTBI model that hyaluronic acid hydrogels modified with laminin disrupt glial scarring responses and promotes regeneration (116). Here, the hydrogel was implanted into a cavity for 6-12 weeks within the cortices of 8-week old Sprague-Dawley rat brains. The results showed that there was evidence of neurite regrowth, as myelinated axons could be seen infiltrating some of the implanted biomaterial, interestingly previous studies have also demonstrated that certain biomimetic biomaterials have promoted neurite outgrowth and angiogenesis into the implants (117,118). Furthermore, immunocytochemistry revealed that in control injured only cortices, an intense band of $GFAP^+$ astrocytes along the length of the lesion could be observed whilst in hydrogel implanted cortices, there was little GFAP immunostaining along the perimeter of the implant (116).

Furthermore, high magnification scanning electron microscopy revealed that blood vessels had grown into the 3D, porous hydrogel. Transmission electron microscopy (TEM) showed that there was evidence of cell migration into the implanted area; which was predominately glial cells, specifically morphologies consistent with astrocytes, microglia and macrophages could be identified (116). Here, astrocytes sent “pseudopod” like processes from the lesion margin into the implant, thus forming a structural bridge between lesion and implant (***figure 8a***) (116).

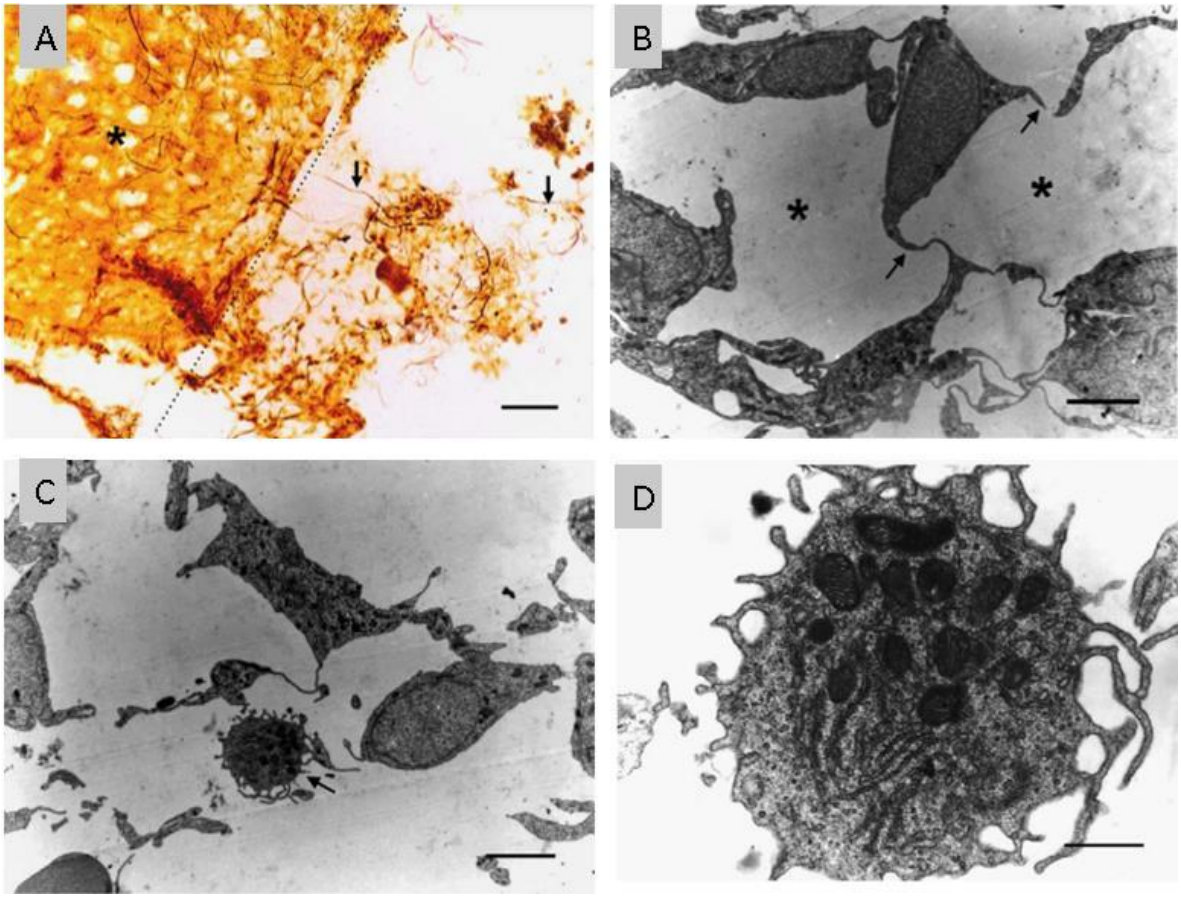

Figure 8: Micrographs demonstrating glial cell infiltration into an implanted biomaterial (hyaluronic acid-laminin hydrogel) (116)

Hyaluronic acid-laminin hydrogel implanted into the cortex of a lesion. ***A:*** *Silver staining on a coronal section 6 weeks post implantation. The implantation region is on the right of dotted line, and normal tissues (asterisks) on the left. Numerous argyrophilic processes (arrows) are revealed within the biomaterial.* ***B:*** *The implantation region 12 weeks under TEM. Cells that migrated into the implanted area are mainly glial cells. Gels have already degraded and left much empty space (asterisks) between cells. An astrocyte sends pseudopod-like extensions (arrows) and contacts with others, forming cell bridges between the spaces.* ***C:*** *Macrophages (arrow) presented in the implanted area 12 weeks post-implantation could be discerned easily under TEM because they had ample short extension on their surface and plentiful vesicles in the cytoplasm.* ***D:*** *High power of a macrophage with vesicles due to endocytosis****.*** *Scale bars A: 20 µm. B-C: 3 µm. D: 20 µm.*

High magnification TEM revealed that amoeboid microglia could be seen within the implant with numerous vesicles within the cytoplasm often containing degraded hydrogel (***figure 8d***). Thus, glial cell responses are critical to evaluate when studying the regenerative properties, a biomaterial possesses. Astrocytes are involved in biomaterial remodelling; specifically, astrocytic process extension and biomaterial infiltration bridges the lesion and provides structural support in turn allowing neurite outgrowth and angiogenesis within the implant. Secondly, microglia digest the biomaterial and influence the biodegradability profile. Currently, little is known about microglial dependent biomaterial degradation. Perhaps one could argue that highly immunogenic biomaterials lead to increased microglial infiltration and thus increased biodegradability rates which would thus limit the regenerative processes such as neurite outgrowth, astrocytic infiltration and angiogenesis into the implant.

However, in vivo models including Hou et al have a major disadvantage when studying glial cell-biomaterial interactions. Hou et al found on post-mortem analysis of the tissue sections that after 12 weeks in vivo the hydrogel had “wholly degraded” and left an empty space in the reparative tissue. Thus, definitive cell-biomaterial responses cannot be determined at later time points. A solution to this is to study glial cell-biomaterial interactions through live imaging. Live in vivo imaging is extremely challenging and thus in vitro models are needed where live imaging can easily be employed. Current in vitro biomaterial testing predominately involves culturing neural cells in 3D matrices and comparing their response to two dimensional (2D) controls. For example, primary rat cortical astrocytes cultured in 3D collagen type 1 hydrogels, were deemed less reactive than those cultured on 2D surfaces. Specifically, astrocytes cultured within the hydrogel displayed decreased GFAP and CSPG immunofluorescence in addition to a significant reduction in GFAP mRNA and neurocan (119). However, such models do not simulate an injury environment and therefore cannot be considered pathomimetic to traumatic injury and thus there is no guarantee that neural cells will have similar biomaterial induced responses in the context of an injury. Currently, there are very few, if any, high throughput, in vitro multi-glial, pathomimetic, pTBI models capable of supporting biomaterial implantation. Furthermore, one can see from ***figure 8a*** that at 6

weeks in vivo, the biomaterial cannot be clearly identified, resulting in the researchers guessing the biomaterial's location and determining cellular responses in the "implantation region". In addition to live imaging techniques**,** researchers could counterstain or counter immunolabel the hydrogel, however currently there are very few, if any studies which have utilized such an approach.

One key aspect which can limit CNS regeneration is immune and inflammatory responses to injury (15,18,24,68). This key response is also widely described in pTBI. Thus, it is vital for hydrogels to be biocompatible (95,97,103). Biocompatibility can be assessed by several key parameters. Firstly, post-transplantation hydrogels should be minimally immunogenic and thus should not induce an adaptive nor innate immune response (40,103). Secondly, hydrogels should not be cytotoxic (97). Thirdly, hydrogels are manufactured to be biodegradable, whether this is a controlled degradation rate for "smart release" of its contents or time dependent inevitable hydrogel degradation (104). Thus, subsequent hydrogel degradation products should not be immunogenic/cytotoxic; whether this is due to exposing cryptic immunoreactive sites or degradation into to novel products with immunoreactive profiles (95,103,107,113,120–122).

Thus, to improve hydrogel biocompatibility, two schools of thought typically exist with regards to hydrogel manufacturing. One classification includes synthetic hydrogels which are composed of specific chemical formulations with the intended purpose of being inert, minimally immunogenic and even anti-inflammatory/pro-repair (96,114). The second main classification includes "natural" hydrogels, which are created using the same components found within the host CNS ECM, thereby reducing the chance of rejection and recognition as a foreign object which could elicit an immune response (33,109,110).

Collagen, a key component of the host CNS ECM has been widely used to manufacture hydrogels (92,107,123–125). Firstly, collagen is relatively cheap and widely available. Secondly, collagen hydrogels have shown to possess significant regenerative capability, potentiating cellular growth, differentiation as well as providing structural support. Furthermore, studies have demonstrated acellular collagen matrices promote both

angiogenesis and neurogenesis post-surgical brain injury (126). Furthermore, Chen et al (2019), demonstrated that a collagen-glycosaminoglycan matrix hydrogel implanted into surgical brain injury rat models was neuroprotective and anti-inflammatory (124). Specifically, implantation of the biomaterial significantly reduced the density of activated microglia as well as a significant decrease in the tissue concentration of the pro-inflammatory cytokines IL-6, TNF alpha. Interestingly, there was a significant increase in the anti-inflammatory cytokine IL-10.

1.4.5 Limitations in relation to hydrogel testing

A major limitation of the Chen et al (2019) study and indeed most studies investigating hydrogel efficacy is that laboratory grade biomaterials are used, which are unapproved for human testing. Clinical grade biomaterials undergo an extensive and lengthy safety profiling process (up to seven years) by clinical safety governing bodies such as the food and drug administration (FDA), before approval for human use. Thus, even if research suggests hydrogel efficacy, there is no guarantee that such biomaterials will be suitable for clinical translation. Thus, increased testing with clinically approved neurosurgical grade biomaterials needs to be undertaken. One such biomaterial is DuraGen Plus™, an ultrapure medically approved, type 1 bovine collagen-based hydrogel widely used in duraplasty. DuraGen Plus™ use in duraplasty allows fibroblast infiltration to allow for dural repair. Furthermore, bovine collagen use to fill the cavity in pTBI has also been described (127). Before exploring the potential of DuraGen Plus™ further, it is worth noting that bovine collagens in this case or indeed any animal derived biomaterials pose significant ethical and religious concerns. Specific religious groups and animal activists may object to the use of xeno-products and thus synthetic biomaterials can provide an ethically viable alternative. DuraGen Plus™ is reported to be minimally immunogenic, whilst also being compatible and mouldable for neurosurgical application. Early scientific studies indicate DuraGen Plus™'s role as a neuroprotective and neuroregenerative matrix. Finch et al demonstrated DuraGen Plus™ use as a protective matrix for neural cell types as NSCs directly seeded onto the biomaterial had a cell viability over 94% (128). Finch et al also demonstrated that DuraGen Plus™ matrix

supports stem cells engineered with magnetofection technology and minicircle DNA vectors- a novel approach to cell engineering (129).

Thus, DuraGen Plus™ matrices show promise for neural regeneration and its regenerative capabilities should be assessed in pTBI. Shin et al (2015) demonstrated that implantation of DuraGen Plus™ into an in vivo rat contusion TBI injury model significantly improved cognition, reduction in lesion volume and reduced neuronal loss within the hippocampus versus sham injury rats (130). Although this study shows promise for TBI, currently there are no studies which investigate DuraGen Plus™'s efficacy in pTBI; the cellular responses of neural cells to this material have also not been documented in detail. To facilitate the development of such therapies, clinically predictive models of pTBI are required, within which potential therapies can be screened.

1.5.1 An overview of in vivo pTBI models

A variety of in vivo TBI models exist. These include the fluid-percussion model (115,125), the weight drop model (132), and the shock tube generated blast induced neurotrauma model (133). However currently, there are a limited number of in vivo pTBI models. Although not previously labelled as such in the literature, here the term large animal models will be used to describe those animals larger than rodents whilst small-animal models describe models of rodent size and smaller. Previously researchers focused on developing pTBI models in large animal models. Large animal pTBI models have introduced a ballistic injury in cats (134), dogs (135), monkeys (136) and sheeps (137). As discussed previously, pTBI results from any external insult which pierces the skull and enters the brain. Gunshot wounds and stab wounds to the brain represent common modes of trauma in both civilian and military populations. Thus, in vivo animal models have tried to replicate such trauma, through a variety of methodologies.

1.5.2 An overview of in vivo pTBI models in large animals

In the following discussion all animals used in the models were anesthetized. Zhou et al (1998) utilised the standard “Swedish missile trauma model” wherein 60 mongrel dogs were placed on a wounding frame and shot in the masseter muscle with a model 53 smooth bore rifle at a distance of 6 meters (135). The projectile was a 1.03-gram steel sphere shaped bullet. The aim of the study was to investigate cerebral injury associated with a maxillo-facial wound. The results showed cerebral hyperaemia, contusion, haemorrhage and haematoma. Microscopically, intracerebral micro-haematomas and necrosis of nervous cells was noted. Carey et al (1995), developed a pTBI model in mongrel cats where, the animals were placed on a stereotaxic frame. Researchers then removed the outer wall of the right frontal sinus allowing a missile to penetrate the intact posterior sinus wall (134). The bullet was a 2mm 31-mg steel sphere and when fired penetrated the right frontal bone into the right cerebral hemisphere. This model showed vasogenic oedema around the missile track, raised intracranial pressure, raised blood glucose, and respiratory arrest. Finnie et al (1993)

developed a pTBI model which involved physically restraining a sheep and firing a bullet from a 0.22 calibre rifle at a distance of 3 meters in the temporal region of the sheep's head (137). This resulted in tissue laceration, and stretch injuries to neurons, nerve fibres and blood vessels, as well as brain distortion. Thus, we can see that the glial responses to pTBI, have not been investigated in detail, rather macroscopic/clinically predictive features have been evaluated.

Evaluation of large animal pTBI models

Large animal pTBI models have inherent advantages over small animal models. Firstly, a larger brain to work with means introducing non-fatal injuries into brains is more facile. Secondly, due the larger brain size, these models provide closer mimicry to the human brain size. This also allows a similar injury which is encountered by a human for instance a bullet to be accurately replicated, since most bullets are larger than rodent brains thus the specific injury would not be accurately simulated in rodent brains.

The main disadvantage of such large animal models is that they are inherently low throughput and obtaining the resources to house and maintain these animals is expensive. Secondly, there are major ethical implication associated with large animal models over small animal models, as some would argue that larger animals are more sentient animals than rodents. In addition to this, these models are highly invasive/traumatic and raise major ethical concerns. Thirdly, the majority of these models focus on macroscopic pathological and physiological consequences of pTBI and not the cell-specific responses such as the glial response- which have key roles in pTBI.

1.5.3 An overview of in vivo rodent pTBI models

As discussed above large animal pTBI models have several limitations. Thus, researchers have focussed on more accessible and facile small animal in vivo models to facilitate research into pTBI pathophysiology.

Cernak et al (2014) developed an non-fatal in-vivo mouse pTBI model whereby a modified air rifle delivers a pellet which subsequently hits a small probe; the small probe then enters the brain (***figure 9***) (39).

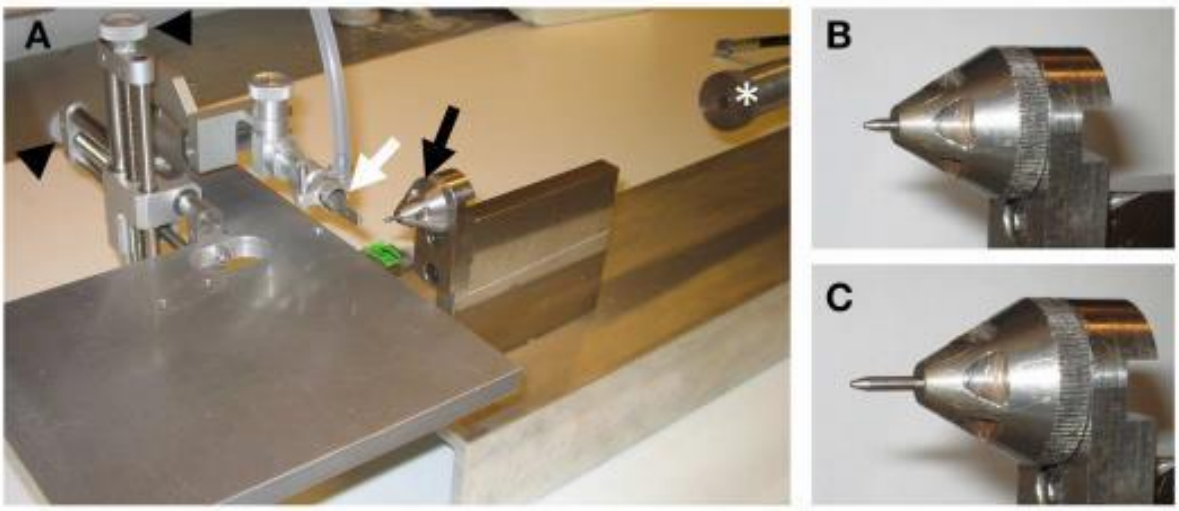

Figure 9: Overview of a penetrating device setup

A: *Overview of a penetrating device setup. White arrow- penetration rig mouthpiece, Black arrowhead – stereotactic manipulators. Black arrow – Probe holder, white asterisk- air-rifle barrel.* ***B/C:*** *Images of the probe holder before (B) and after (C) impact of pellet.*

The same model by Cernak and colleagues has previously been used in rats (67). Cernak et al found increased tissue destruction and neuronal degeneration in lesioned brains. Furthermore, reactive gliosis was also noted and was quantified by measuring staining intensity of GFAP (section 4.1) for astrocytes and Iba1 for microglia. Specifically, there were significantly increased GFAP immunoreactive astrocytes at 72 hours post-injury with persistence up to 7 days post-injury. Cortical microglial activation was seen up to 7 days post injury (39).

On the other hand, Williams et al (2007) developed an in vivo pTBI model simulating the damage resulting from a penetrating bullet round by inserting an inflatable penetrating probe into the right frontal hemisphere of Sprague -Dawley rats (68). The Williams et al model

resulted in significantly increased GFAP immunoreactive astrocytes emerging 6 hours post-injury which peaked at 72 hours post-injury and peak microglial activation at 72 hours post-injury with resolution by day 7(68). Williams et al results are different to Cernak et al. Cernak et al suggests the difference may be explained by the methods of injury, namely a projectile induced trauma in Cernak et al model versus inflatable balloon in the Williams et al model. Interestingly, both studies did not count microglial numbers per unit area - another commonly used analysis to demonstrate microglial response to injury. Specifically, Robel et al 2011 found significantly increased microglial numbers surrounding stab wound injury site versus control in a pTBI stab wound model (71).

Bardehle et al 2013 studied, astrocytic responses to pTBI by localized stabbing of the somatosensory cortex in mice brain. Astrocytes became hypertrophic and had increased GFAP expression whilst also subsets of astrocytes polarized towards the lesion by extending long polarized processes towards the lesion (70). Interestingly, astrocytes post-injury extend processes towards the lesion and have been named as “palisading” or “polarized astrocytes” (138) . Astrocytic polarization towards the lesion has been considered a hallmark of the glial scar. Live in vivo imaging demonstrated that astrocytes near the vicinity of the injury orientate themselves towards the lesion and extend long processes (***figure 10***).

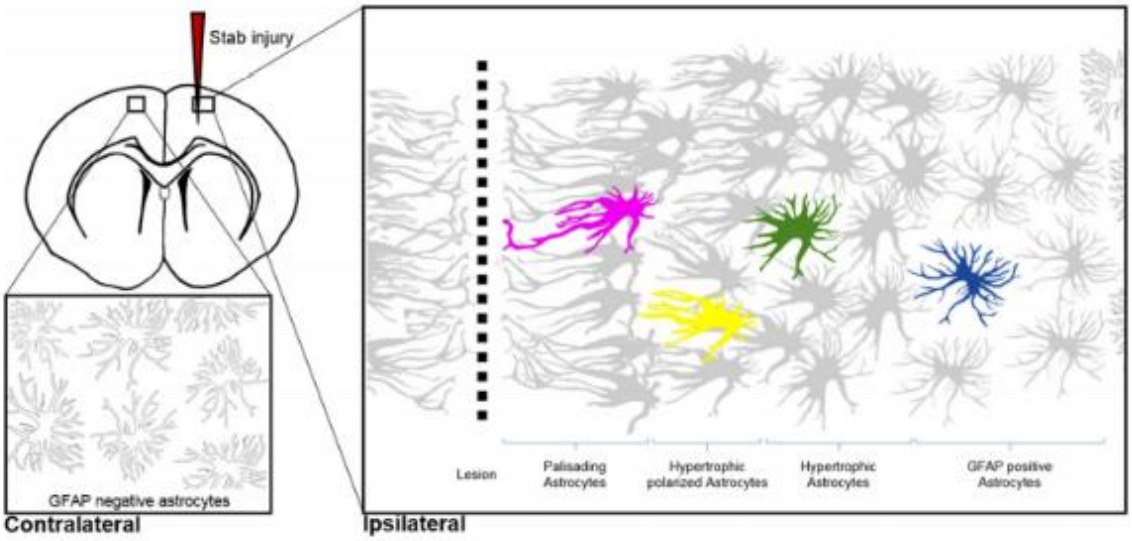

Figure 10: Palisading astrocytes respond to the lesion

In vivo astrocytes respond to pTBI by hypertrophic changes and a hallmark palisading astrocytic layer of cells closest to the lesion with decreasing process extension as distance from lesion increases.

Astrocytes posterior to the palisading layer, are also hypertrophic and orientate processes towards the lesion. As the distance from the lesion increases, the hypertrophic responses tend to decrease. Microglial responses to injury are rapid, often within minutes, whilst hypertrophic astrocytes and GFAP upregulation occurs 2-3 days post-injury with palisading astrocytes observed 1-week post-injury. Interestingly palisading astrocytes adjacent to the lesion vicinity retain their hypertrophic morphology permanently whilst hypertrophic astrocytes further away from the lesion site return to normal.

Zhao et al (2019) developed a rat pTBI model by creating a craniotomy in the left parietal bone and placing an impact tip on the dura inside the bone window (66). Subsequently, a 40g weight impactor was dropped from a height of 20 cm onto the impact tip. The lesion was then sutured and closed. The sham group received only a craniotomy without the injury. The results showed the increased presence of Iba1 positive reactive amoeboid microglia in ipsilateral lesioned rat brains 24 hours post-injury versus sham- where most microglia

adopted a ramified and processed morphology. Similarly, ramified astrocytes with fine filopodial processes and small cell bodies were seen in sham operated tissue, whilst hypertrophic reactive astrocytes with large cell bodies and extended processes were seen around sites of lesion. Analysis with ImageJ software demonstrated that microglia and astrocytes in lesioned tissue had significantly increased expression of Iba1 and GFAP immunoreactivity respectively. Interestingly, it was also noted that glial reactions occurred in remote parts of the uninjured tissue as well as lesioned tissue. Microparticles- a kind of extracellular vesicle are released from glial cells and dying cells and have been postulated as a potential reason as to why glial reactions are seen in remote uninjured regions of the brain. Extraction and addition of microglial-derived microparticles have shown to propagate neuroinflammation and activate resident microglia, highlighting that glial cell responses can be widespread (66).

Evaluation of rodent pTBI models

Rodents are significantly cheaper and more accessible than larger animals to most laboratories. Specifically, mice offer several advantages over rats: the ability to use knockout and transgenic mice and the significantly lower costs associated with housing, maintaining and purchasing mice versus rats. In addition, rodent brains mimic the neuroanatomical proportions seen within human brains. Finally, the majority of existing rodent pTBI models allow researchers to focus on cellular responses to pTBI, in particular the glial cell responses.

However even small animal pTBI models are low throughput versus in vitro cell culture-based systems. Secondly, the models are technically challenging and require significant training and are subject to Home Office regulations and obtaining the relevant licenses. Thirdly, injury methods are very invasive and pose significant ethical considerations. Finally, specialist equipment is required to reproducibly introduce injuries (***figure 9***) adding to the expense and accessibility only some laboratories may have.

1.5.4 The use of organotypic brain slice cultures as in vitro pTBI models

Organotypic brain slices are thin slices of brain tissue which are maintained in culture for extended periods typically greater than 7 days (139–141). Currently, very few studies have used organotypic slice cultures as models for pTBI. Krings et al (2016) subjected organotypic hippocampal slice cultures to trauma through dropping a metal stylus under stereomicroscopic control from a height of 7mm (142). This is a well-established method for reliably introducing lesions into organotypic slice cultures. In this study the efficacy of desflurane in neuroprotection post-pTBI was evaluated through trauma intensity measures (trauma intensity was assessed by measuring propodium iodide uptake by damaged cells). No pathological pTBI features such as the glial scar were assessed in this study. Weightman et al (2014) developed an in vitro spinal cord slice model where injury was reliably introduced with a scalpel. Post-lesion astrocytes became hypertrophic and intensely expressed GFAP significantly higher in the first 100 microns of the lesion. Furthermore, microglia infiltrated the lesion, with numbers peaking at day 5 post-injury. It was also noted that the microglia in the lesions had amoeboid morphologies versus ramified microglia seen in control samples (143).

Evaluation of organotypic brain slice pTBI models

Generally, brain slices are able to maintain neuronal function and synaptic circuity whilst also preserving brain architecture (141). Also, unlike in vivo systems, brain slices allow good experimental access and control. Furthermore, brain slices can recover from the trauma of excision before further experiments (139). Finally, brain slices allow for the study of interaction of many cell types including neurons, astrocytes, OPCs and microglia.

However, there are considerable limitations with organotypic brain slice models. Firstly, brain slice models are still moderate throughput and although brain slice preparation is relatively facile, the current penetrating lesioning methodologies are challenging versus cell culture based in vitro models which often involve scratching confluent cultures with sterile pipette tips/needles (70,71,139,144,145). Secondly, such models have a finite length of viability as

they are maintained in vitro. Thirdly, to prepare brain slices the intact brain is sectioned and thus this process of sectioning may contribute to cellular activation seen in response to injury, in addition to the presence of increased numbers of dead cells. Finally, organotypic brain slices still require the use of animals and thus only contribute the Reduction and Refinement of animal models and not the Replacement of animal models.

1.5.5 In vitro models could provide many solutions to the limitations posed by current in vivo pTBI models

In vitro pTBI models offer many advantages over in vivo systems. Firstly, the majority are facile, high throughput, easily reproducible and allow monitoring of single cell responses using standard and widely available microscopy methods.

The most basic in vitro models utilize immortalized cell lines. Immortalized cell lines are widely used as they are easy to procure, widely available, well characterized, inexpensive and relatively robust. However immortalized cell lines have been known to suffer from disruption of contact dependency and poor adhesion (140). Furthermore, many cells are resistant to cell death, prone to cryptic contamination and have an increased risk of cellular aneuploidy (146).

Disassociated primary cultures offer another system to study pTBI features. Most models utilize a monoculture format. Etienne-Manneville et al (2006) demonstrated that a confluent astrocytic (mono) culture on a glass coverslip can be scratched with a 2 µl micropipette tip to produce a 300 µm lesion. Post-lesioning, hallmark astrocytic polarization and process extension towards the lesion site “analogous to palisading astroglia in traumatic brain injury” was seen (147). Furthermore, Nishio et al (2005) showed that when a confluent astrocyte monoculture is scratched, cells at the lesion edge increased expression of intermediate filaments such as GFAP. In addition to this, astrocytes at the edge of the lesion became polarized with unidirectional processes and migrated to fill the lesion area (148). This shows that in vivo reactive astrogliosis seen in response to pTBI in vivo can be reliably replicated in vitro.

The major disadvantages of using monocultures however is that they are overly simplistic and do not replicate the complexity of multiple cell types which are present within the CNS. Liddlelow et al (2017) showed that classically activated neuroinflammatory microglial release of IL-1 alpha , tumor necrosis factor (TNF) and C1q in response to neuroinflammation can induce A1 reactive astrocytes both in vivo and in vitro (64). Specifically, absence of a microglial and OPC component means such models lack inter-glial communication such as microglial dependent-astrocytic activation, a key initiation step for glial scar formation. Thus ideally, a good model should contain all of the neural cell types.

Finally, co-cultures, allow the presence of multiple glial cell types. This enables intercellular cross talk and provides a more complex model than overly simplistic monocultures. Commonly used co-cultures include astrocyte-neuron and astrocyte-microglia models (149). However, currently there seems to be very little literature describing an injury model application of these co-cultures. Perhaps this is due to the difficulty and time required to create stoichiometrically defined neural co-cultures in the first instance.

More recently, researchers have developed and refined brain-on-a-chip models to simulate TBI. These models are 3D cell-cultures which attempt to model the physiological responses of the brain in a microfluidic environment (140). Currently, these models allow pathology to be created on a chip and a large number of chemicals can be screened to evaluate positive physiological effectiveness. TBI has previously been modelled by applying pneumatic pressure through a deformable plate upon which the cultures had been placed, leading to a strain injury (140). Here, axonal injury and biochemical changes along with mitochondrial membrane potentials were studied (140). Although such models have inherent advantages over in vivo alternatives including being higher-throughput and providing a more ethically viable alternative, these models tend to be very expensive to establish(140). In addition, the ability to replicate pTBI on a chip is currently limited. Also, brain-on-a-chip models only contribute the Reduction and Refinement of animal models and not the Replacement of animal models and thus more ethically viable alternatives need to be considered.

1.5.6 Reduction, Replacement and Refinement of animal models

There are several disadvantages of cell-culture based models: cells can behave differently, in vivo versus in vitro and the dissection process used to harvest cells is intrinsically injurious in nature. However, cell culture based in vitro models are facile and high throughput, with the possibility of large numbers of technical replicates to be easily and simultaneously obtained for experimental reproducibility. Currently, there are very few if any in vitro cell-culture based multi-glial pTBI models which are capable of biomaterial testing, and thus it is vital for researchers to develop these models in the future.

Despite the inherent limitations of in vivo models, in vitro alternatives cannot outright replace such models, as rigorous animal testing will always be required prior to human trials. However, in line with the Reduction, Replacement and Refinement (3R's) of animal models initiative, such in vitro models can reduce unnecessary animal experimentation in the early stages of research and development, and provide researchers with detailed solutions prior to vigorous animal testing (***figure 11***) (150).

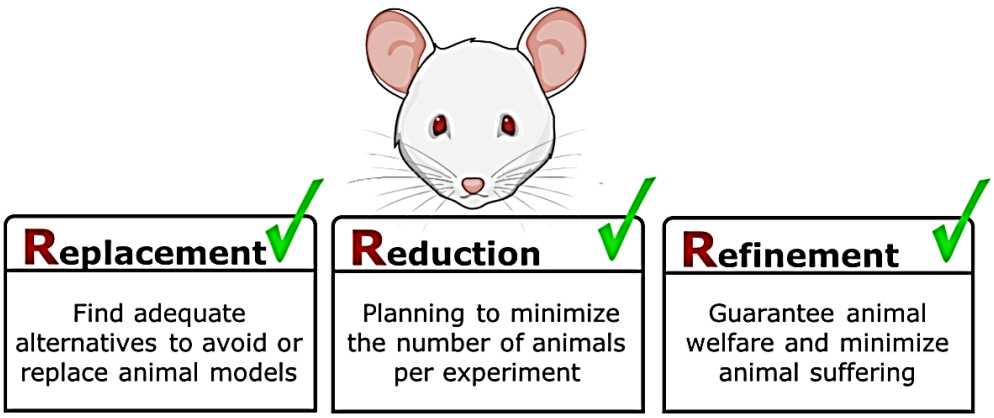

Figure 11: A schematic displaying the principles of the Replacement, Reduction and Refinement (3R's) of animal models initiative (150)

Furthermore, such models allow key regenerative biomaterials/strategies to be identified, which can then be trialled in more complex animal models (150).

1.5.7 Current models used to test biomaterials in pTBI

Current methods predominately focus on in vivo biomaterial testing. For example, electro spun nanofiber scaffolds were implanted into the lesioned brains of male Wistar rats (151) (53). The results showed there was no significant inflammation from either microglia or astrocytes, furthermore the scaffold supported neurite infiltration. Similarly, Xiong et al implanted a type 1 collagen scaffold embedded with human marrow stromal cells into an in vivo TBI model and found a significantly increased cell viability versus cells transplanted into culture medium alone (151,152). Although, biomaterial testing in vivo is plentiful the same advantages and disadvantages of these models apply as discussed previously (section 1.5.6). Thus in vitro models could offer invaluable insight and accessibility into studying the regenerative capability of biomaterials. Weightman et al described an in vitro biomaterial testing application for spinal cord injury and is one of the only described injury in vitro biomaterial testbeds (143). The model consists of organotypic spinal cord slices cultured in vivo, which can be reliably injured with a scalpel, the efficacy of nanofibers was then tested by placing the nanofiber meshes over the lesions and alignment of astrocytes neurites was determined. The results showed that in injury states, astrocytes became hypertrophic whilst also expressing GFAP in the first 100 microns adjacent to the lesion versus tissue further away. These pathological hallmarks are analogous to the glial scar. Interestingly, poly-D-lysine coated laminin nanofiber implantation resulted in increased alignment of astrocytes and polarization of long thin processes towards the material. On the other hand, uncoated nanofibers behaved similarly to control samples without nanofibers as “no evidence of astrocyte attachment and alignment was observed”. Although, this model allows for key astrocytic-biomaterial interactions, there is one key disadvantage. Firstly, the fact that the control samples did not exhibit astrocytic polarization and a palisading astrocytic layer was not formed, highlights that the astrocytes in this model react morphologically differently to other pTBI models where the palisading astrocytic morphology in response to injury has been extensively characterized. Astrocytic process extension and entangulation has been

associated as a key step in forming a glial scar barrier. Furthermore, extensive microglial attachment to the nanofibers was noted.

Although, the Weightman et al model is a progressive step towards in vitro biomaterial testing applications in neurological injury, organotypic slice cultures have inherent disadvantages (section 1.5.4). Thus, currently there is a critical need for cell culture based in-vitro TBI model which can support biomaterial testing. Such a model if possible, should be novel, high-throughput, facile, contain the major the glial cell types and once injured should be neuropathomimetic to pTBI.

Thus, in order to facilitate the development of such a model, the following objectives have been devised:

1.5.8 Objectives

1. Develop an in vitro injury pTBI model, capable of supporting biomaterial implantation to assess regenerative strategies.
2. Characterize the glial responses to injury and determine whether such a model can simulate in vivo pTBI glial responses.

More detailed and specific objectives are listed under the corresponding experimental chapters.

Chapter 2
Materials and Methods

2.1 Materials

Primary cell cultures: All culture grade plastics were from Thermo Fisher Scientific (Loughborough, UK). Media components included Dulbecco's Modified Eagle Medium, Neurobasal-A Medium, Foetal bovine serum (FBS), penicillin-streptomycin solution, B27 supplement, sodium pyruvate and glutaMAX-I. Media, including media supplements and reagents except where stated were from Thermo Fisher Scientific (Loughborough, UK), and Sigma-Aldrich (Dorset, UK).

Biomaterial implantation experiments: Neurosurgical biomaterial DuraGen Plus™ was from Integra LifeSciences (New Jersey, USA). The Mcllwain tissue chopper was from The Mickle laboratory engineering co. Ltd (Guilford, UK). Paraformaldehyde (PFA) was from Thermo Fisher Scientific (Loughborough, UK).

Antibodies for immunocytochemistry (ICC): Primary antibodies were anti-glial fibrillary acidic protein (GFAP), from DakoCytomation (Ely, UK), anti-Iba1and biotin-conjugated lectin from Thermo Fisher Scientific, anti-NG2 from Milipore (Massachusetts, USA), purified anti-neuron-specific class III beta-tubulin (Tuj1) from Biolegend (California, USA), anti-A2B5 from Sigma-Aldrich (Dorset, UK).

Secondary antibodies were, Fluorescein isothiocyanate (FITC)-conjugated donkey anti-mouse, -rabbit, -goat and cyanine 3 (Cy3) donkey anti-mouse, and -goat, which were all from Stratech Scientific (Suffolk, UK). FITC-conjugated anti-biotin secondary antibody was also from Stratech Scientific (Suffolk, UK). Vectashield mounting medium containing 4′,6-diamidino-2-phenylindole (DAPI) was from Vector laboratories Inc (Peterborough, UK). Normal donkey serum (NDS) was from Stratech Scientific (Suffolk, UK) and Triton X-100 was from Sigma-Aldrich (Dorset, UK).

Cells and biomaterial histological staining experiments: Haematoxylin and Eosin (H&E) staining kit was from Sigma-Aldrich (Dorset, UK). 3,3'-diaminobenzidine (DAB) Substrate Kit, Peroxidase (HRP), with Nickel (SK-4100) was from Vector Laboratories. Picrosirius red solution was from Sigma-Aldrich (Dorset, UK).

2.2 General Protocols

2.2.1 Coverslip preparation

Coverslips were washed with ethanol 70% and added to 24 well plates where they were coated with poly-D-lysine for 20 minutes and washed with distilled water (2x washed, 5 minutes/wash).

2.2.2 Cell fixation

4% PFA in phosphate buffered saline (PBS) solution was prepared prior to fixation and added to the 24 well plates. The cells were fixed at room temperature for 20 minutes, then washed three times with PBS. For micro-mixed glial (Model 1- mixed-glial cultures seeded into a micro-well format) experiments, the cells were fixed at days 14,15 and 21 in vitro, (see 3.3.2, for further details). For neuron-glia (model 2) experiments, the cells were fixed at day 14in vitro (see 3.39, for further details).

2.2.3 Immunocytochemistry

Post-fixation cells were incubated with normal donkey serum in PBS with 0.3% Triton X-100 for 30 minutes before the primary antibodies Tuj1 1:250, GFAP 1:500, Iba1 1:500, Lectin 1:500 and NG2 1:500 were incubated with the cells overnight at 4°C (***table 2***).

Cell type immunolabelled	Primary antibodies and labelling molecules (species of origin)	Secondary antibodies
Neurons	TUJ1(mouse)	CY3 Donkey anti-mouse
Astrocytes	GFAP (rabbit)	FITC Donkey anti-rabbit
Microglia	Iba1 (goat)	CY3 Donkey anti-goat
	Lectin (*Lycopersicon esculentum)*	FITC-conjugated anti-biotin
OPCs	A2B5 (mouse)	CY3 Donkey anti-mouse
	NG2 (rabbit)	FITC Donkey anti-rabbit

Table 2: Antibodies used to detect various neural cell types

The following day primary antibodies were removed, and samples were washed thrice with PBS, and incubated with NDS for a further 30 minutes at room temperature. FITC 1:200 and Cy3 1:200 secondary antibodies diluted in NDS were added to the wells and incubated for 2 hours. The cells were then washed three times with PBS.

2.2.4 Coverslip mounting

Coverslips in 24 well plates were carefully lifted up with a 21g needle and carried with fine forceps onto a drop of DAPI mounting medium on a glass slide. The coverslips were then sealed with nail varnish along the edges.

2.3 Preparation of mixed-glial cultures

The mixed-glial cultures have traditionally been established as bulk cultures. Here disassociated cerebral cortices are seeded into T175/T75 culture flasks. In this thesis, the term “macro-mixed glial culture” will be used to refer to the traditional bulk mixed-glial culture format, whilst the term “micro-mixed glial culture” will be used to refer to the mixed-glial culture seeded into a 24 well micro-well format. The term “neuron-glia” model is used to describe an adaptation of the micro-mixed glial model established with neuronal medium versus D10 medium. Animal care and use was according to the Animal (Scientific Procedures) Act of 1986 (UK) with approval by the local ethics committee.

2.3.1 Preparation of macro-mixed glial cultures (bulk cultures)

Primary mixed glial cultures were prepared according to the Mccarthy and de Vellis protocol (153). For this, eight to twelve CD1 mouse pups per litter at postnatal day 1-3 (P1-P3), were anaesthetized using pentobarbitone via intraperitoneal injection. The mouse pups were then decapitated, and each brain was then dissected out of the skull and placed in PBS on ice. Under a laminar hood the brains were transferred to a fresh petri dish containing PBS and onto a sterile hand towel. The olfactory bulbs, cerebellum, medulla and midbrain were removed from the brain using curved forceps, leaving the only the cerebral cortex. The cerebral cortex was subsequently rolled along the hand towel to remove the meninges. The cortices were then transferred into 35mm petri dishes and mechanically dissociated with a sterile scalpel. 2ml of PBS was added to the dissociated cortices, the suspension was then transferred into a universal tube where the tissue was triturated 40 times with a plastic Pasteur. The suspension was further triturated thrice each by using syringes attached to a 21g and 23g hypodermic needle and placed through a 70-micron and 40-micron strainer.

The filtrate was then centrifuged at 1000 rpm for 4 minutes. The supernatant was removed, and the pellet was loosened by agitating the universal tube and diluted in1ml of the cells suspension was diluted with Dulbecco’s Modified Eagle Medium containing an additional 10% foetal bovine serum, 2 mM, glutaMAX-I, 1 mM sodium pyruvate, 50 µg/ml streptomycin

and penicillin (D10). A cell count was performed by mixing 10 µl cells with 40 µl of 0.4% trypan blue and adding this to a Neubauer chamber. The cells suspension was then seeded on to pre-prepared poly-D-lysine coated T175 flasks, at a fixed concentration of 0.83 x10^5 cells/ml. After seeding, cultures were left in an incubator 37°C in 5% CO_2 95% humidified air. The cultures were only removed from the incubator for medium replacement; at 1 day post-seeding 100% of the medium was changed (300 µl of D10), then every 2/3 days, 50% medium changes with D10 (150 µl of D10). Prior to medium replacement the cultures were imaged under a light microscope (section 2.3.1) within the same culture room to track culture development and confluency. The macro-mixed glial cultures (mixed-glial cultures established as bulk cultures in T175 culture flasks) were conducted in parallel to the micro-mixed glial cultures to determine whether there were any noticeable differences in terms of culture development and confluency versus the micro-mixed glial cultures (see 3.3.2 for details).

2.3.2 Preparation of micro-mixed glial cultures

The mixed-glial cultures were prepared according to the protocol in section 2.3.1, except the cells suspension was seeded on to pre-prepared poly-D-lysine coated coverslips in a 24 well plate at a fixed concentration of 0.83 x10^5 cells/ml in addition to T175 culture flasks. After seeding, cultures were left in an incubator (37ºC, 5% CO_2, 95% humidified air). The cultures were only removed from the incubator for medium replacement; at 1 day post-seeding 100% of the medium was changed (300 µl of D10), then every 2/3 days, 50% medium was changed with D10 (150 µl of D10). Prior to medium replacement the cultures were imaged under a light microscope (section 2.3.1) within the same culture room to track culture progress. Here, both bulk (macro) mixed-glial cultures and micro-mixed glial cultures were imaged in parallel, to document culture development, including the confluency of astrocytic-like morphologies forming an astrocytic bed layer and the presence of microglial/OPC- like morphologies developing on top. The bulk cultures were established in parallel to determine whether, seeding the mixed-glial suspension in a micro-well format altered the development and confluency of the cultures. At day 14, when the cultures became confluent, they were

fixed in PFA (section 2.22), and single immunocytochemistry was performed (section 2.2.3) to label astrocytes with GFAP, microglia with Iba1/lectin and OPCs with NG2/A2B5 (***figure 12***).

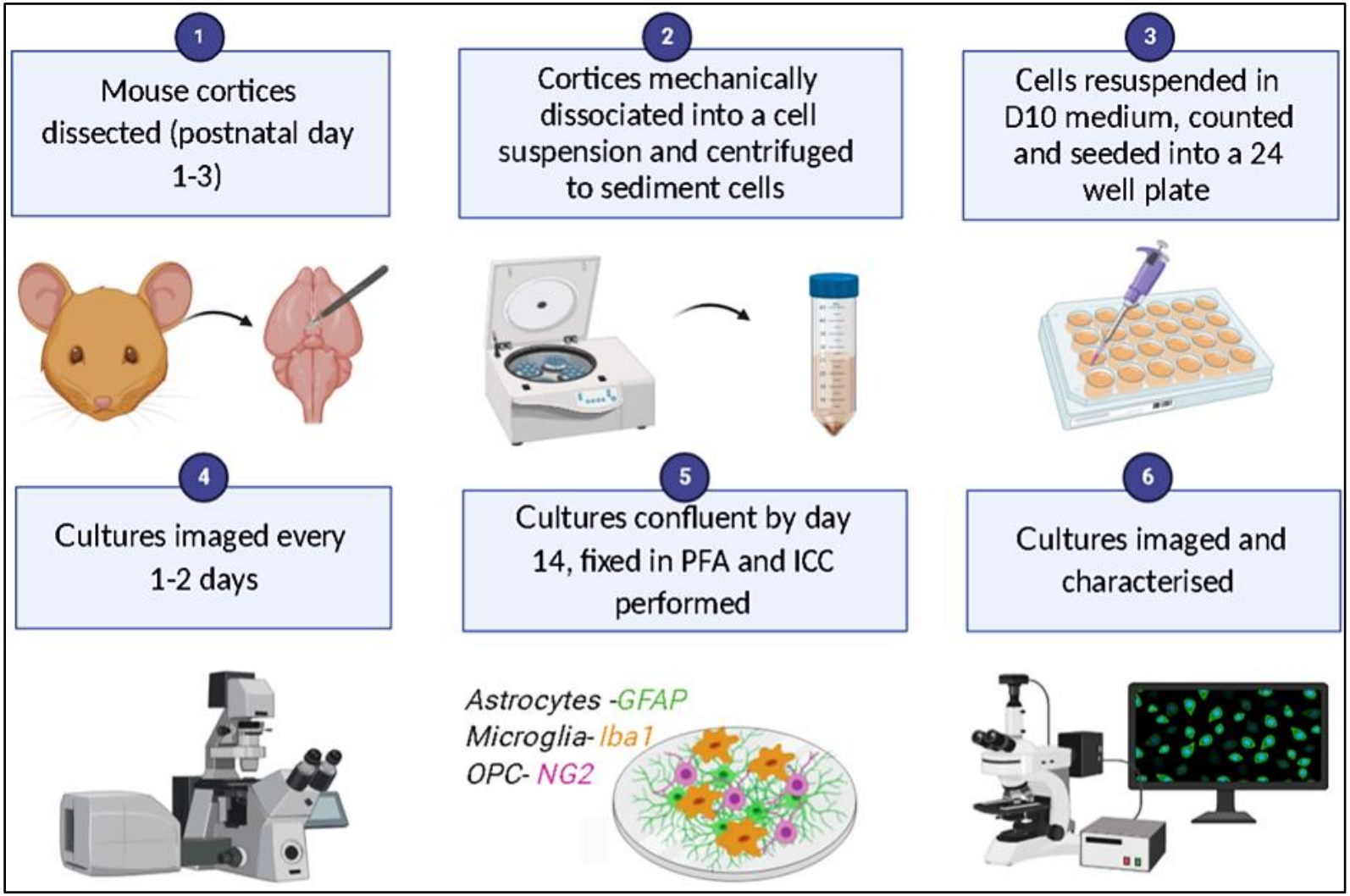

Figure 12: A schematic showing the protocol undertaken to establish the micro-mixed glial model (Model 1)

2.3.3 Establishment of an injury paradigm in Model 1:

By day 14, Model 1 was confluent and 24 well plates which contained the cultures were placed in the laminar flow hood. A sterile P200 pipette tip was scraped across the coverslip from one corner of the coverslip to the other to create a transection injury. Note, it is crucial that one applies the tip perpendicularly to the glass coverslip and not angled to ensure the full diameter of the pipette tip is in contact with the culture, enabling the creation of a lesion with lesion edges at a consistent distance apart and removal of adhered cells along the whole lesion. Post-lesioning, the D10 medium was discarded to remove cellular debris and fresh medium re-added to the wells. The remaining cultures were re-incubated (37^{o}C, 5% $CO_{2,}$ 95% humidified air).

To identify the lesion margins including measurement of the lesion width (section 2.4.2), the cultures were fixed in PFA immediately post-lesioning and ICC performed to label the astrocytes with GFAP and DAPI ***(figure 13)***.

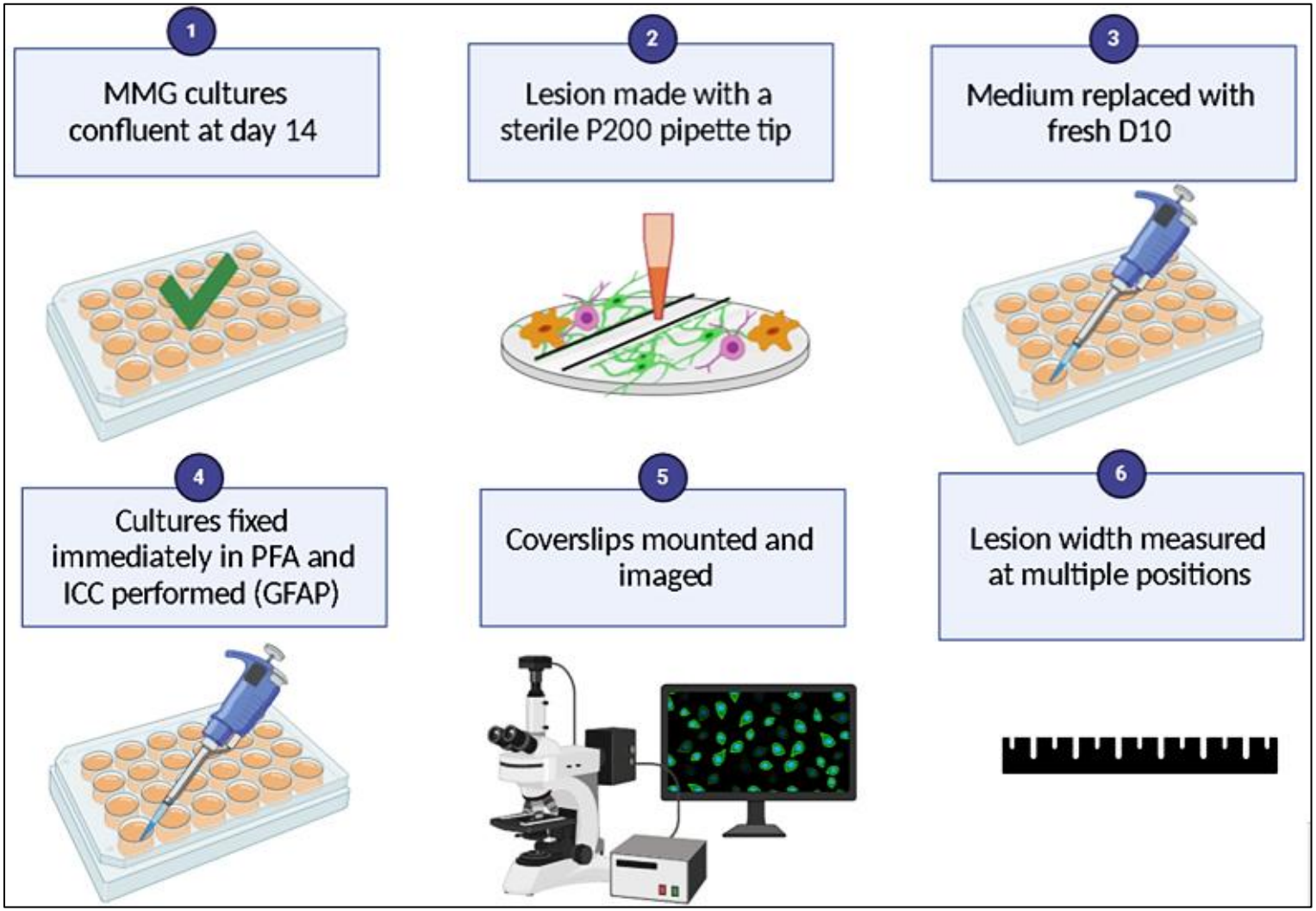

Figure 13: A schematic showing the steps taken in order to establish a lesion in Model 1

2.3.4 DuraGen Plus™ preparation

DuraGen Plus™ was supplied in sterile packaging as a 10 x 12.5 x 2 cm dry, square, piece of material. Using a sterile scalpel, under a laminar hood, a 5 x 5 x 20 mm piece was isolated. This was placed in a petri-dish and 3 drops of PBS from a plastic Pasteur was added onto the biomaterial. The DuraGen Plus™ absorbed the PBS. This helped to adhere the biomaterial with the petri-dish enabling the biomaterial to remain in-situ whilst chopping. The McIlwain tissue chopper was then set to chop the DuraGen Plus™ at a thickness of 250 microns, here parallel cuts were made slicing the biomaterial at the pre-set thickness. The DuraGen Plus™ was then placed onto a petri dish which had a pre-measured grid with sub-mm dimensions and ca 800 x 1200 x 250 µm pieces were then prepared using a sterile scalpel.

2.3.5 Establishing a protocol for implanting a DuraGen Plus™ sheet into the lesion

The penetrating lesion was made in cultures in accordance to section 3.3.3. The cultures were then re-incubated for 2 hours. After 2 hours, the cultures were brought into a laminar flow hood which contained a dissection microscope. The medium was then removed completely and a pre-prepared DuraGen Plus™ sheet (section 2.2.6) was inserted using fine forceps under microscopic guidance at 12.5x magnification, into the lesion. Note it is vital to add the biomaterial in the absence of medium, since this promotes biomaterial adherence to the glass coverslips. Attempts to implant the biomaterial in media results in the biomaterial floating. Once the DuraGen Plus™ was implanted into the lesion, 200 µl of fresh D10 is then slowly added to the wells. The cultures were then incubated (37°C, 5% CO_2, 95% humidified air), with 50% medium changes every 2 days. The cultures were fixed at 1 day and 7 days post-lesion. ICC was performed to label astrocytes (GFAP), microglia (Iba1), and OPCs (NG2). There were 3 experimental groups *(i)* lesioned *(ii)* unlesioned *(iii)* DuraGen Plus™ treated lesions. All three groups underwent the same subsequent protocol steps ***(figure 14)***.

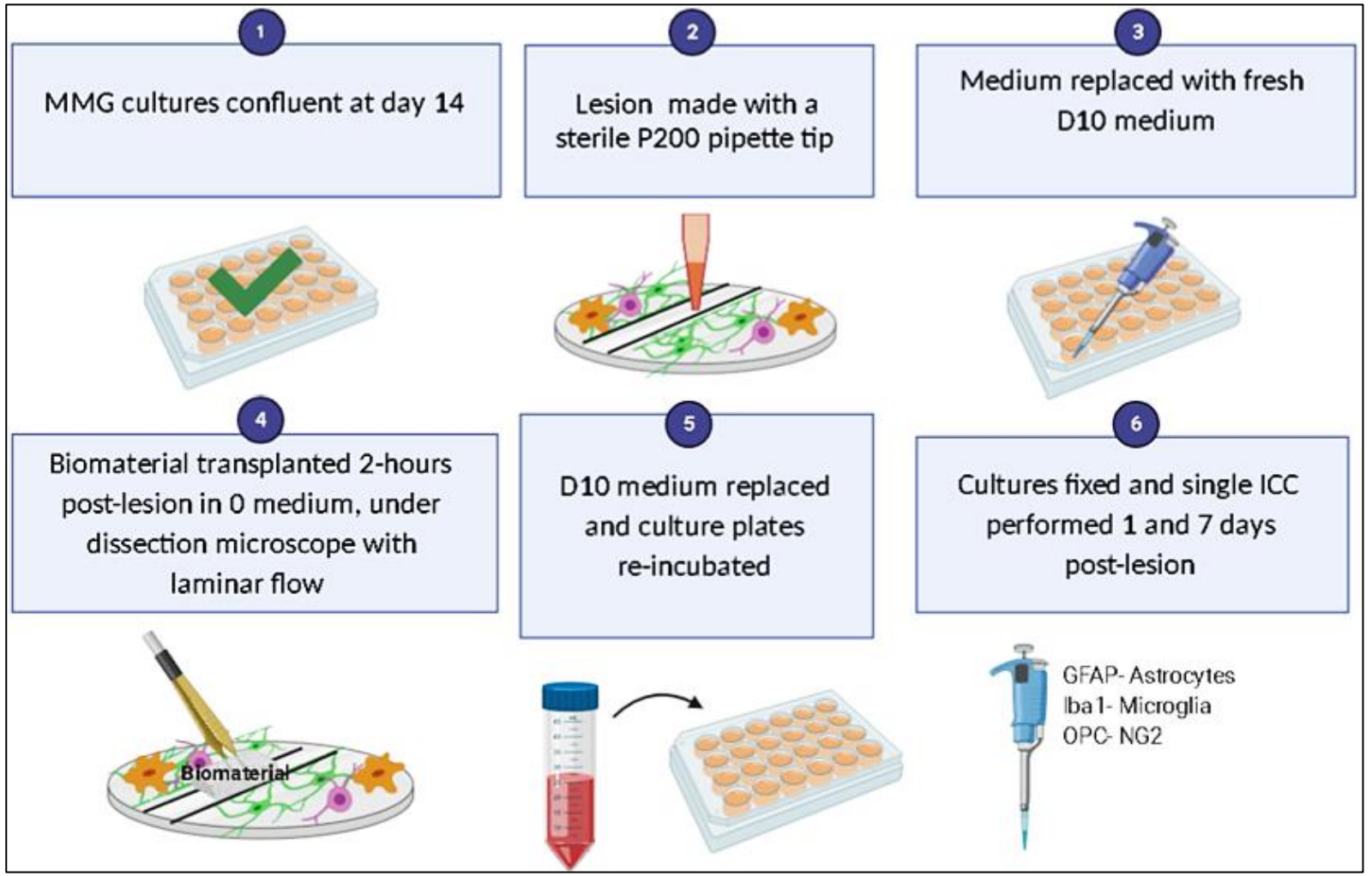

Figure 14: A schematic showing the steps taken in order to implant a biomaterial into the lesion

2.3.6 Pilot study to develop a model (Model 2) containing neurons and the major glial cell types

Model 1 lacks a neuronal component and thus an effort was made to develop a model which contained all of the neural cell types. Here, the same protocol was followed in section 3.3.2 to establish a micro-mixed glial culture with two main differences: (i) Model 2 was established and fed with neuronal medium (96% Neurobasal A, 2 mM Glutamax-I, 2% B27 and penicillin/streptomycin), (ii) the cells were seeded at a higher density of 4 x 10^5 cells/ml. After seeding, the cultures were fed every 2/3 days with neuronal medium (50% change). The cultures were only removed from the incubator for feeding and for observation of the culture including development, confluency, and assessment of the cell morphologies. By day 14 these cultures were deemed confluent and fixed in 4% PFA (section 2.2.2). ICC was performed in accordance to the protocols set out in section 2.2.3, to label neurons (Tuj1), astrocytes (GFAP), microglia (Iba1) and OPCs (NG2). The glass coverslips containing the samples were mounted onto glass slides (section 2.2.4) and imaged under a fluorescence microscope (section 2.3.1). 3 random separate fields (imaged initially on the DAPI field in three separate regions) of x400 magnification images were taken for each stain were taken. Since this was a pilot study, the images were used to determine whether Model 2 contains all of the neural cells and a visual assessment without quantitative or statistical methods was performed to determine a rough estimation of the proportions of each cell type within the model *(**figure 15**)*.

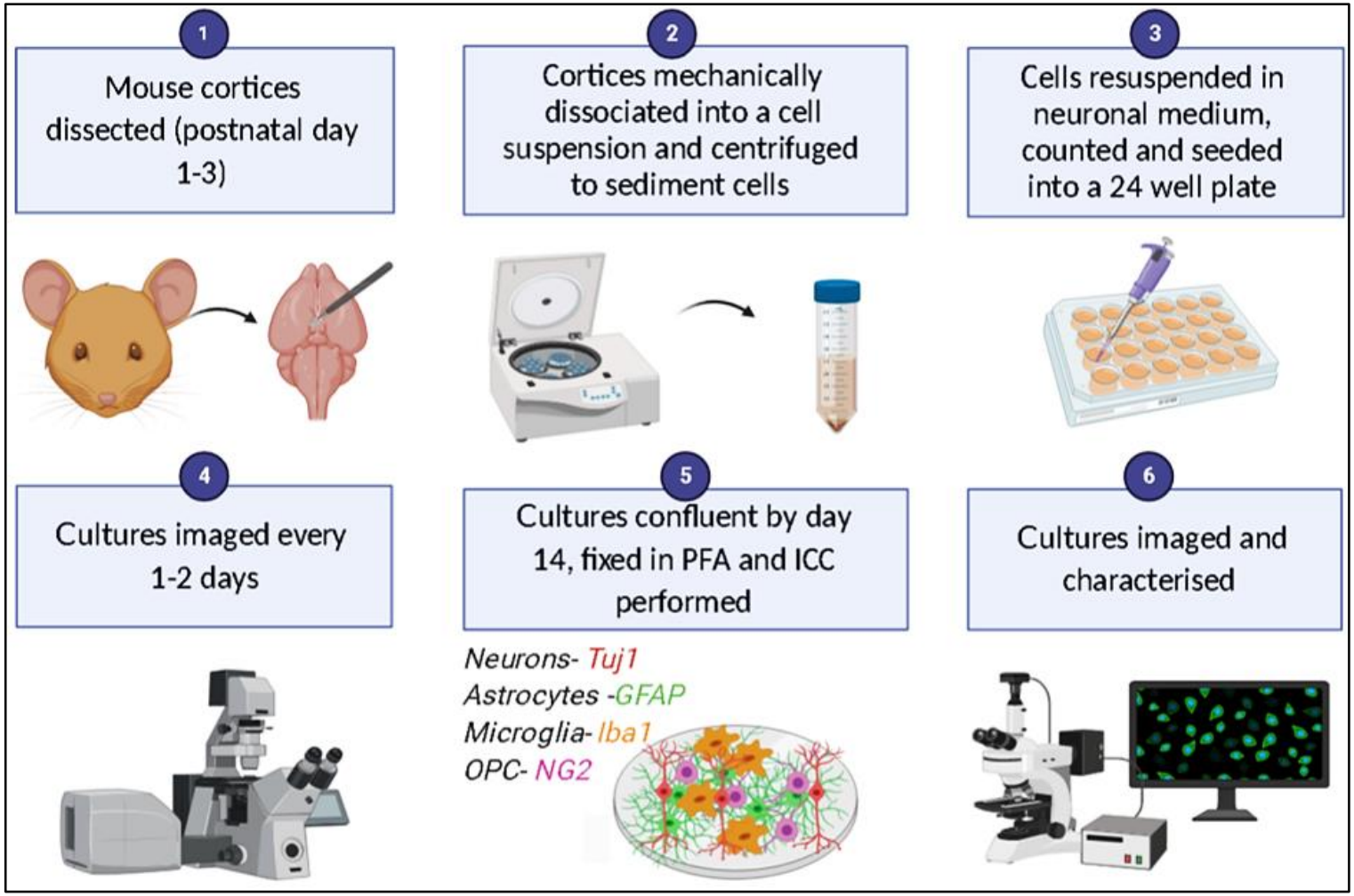

Figure 15: A schematic showing the protocol undertaken to establish the neuronal- glia model (Model 2)

2.4 Imaging

2.4.1 Light microscopy

A Motic AE31E phase contrast microscope, with Moticam 3Plus camera and software was used for phase image characterization of the macro-mixed glial cultures (bulk cultures) and micro-mixed glial cultures. Light microscopy was also used for cell and biomaterial histological staining experiments to visualize the lesion at 0 hours post-lesion and after biomaterial addition at 2 hours post-lesioning. Fluorescence microscopy was used for all other experiments unless otherwise stated.

2.4.2 Polarizing light microscopy

A Nikon Eclipse LV100N fitted with a digital camera was used to visualize the birefringence of collagen fibres in DuraGen Plus™ (See 3.3.6 for experimental details).

2.4.3 Fluorescence microscopy

Fluorescence microscopy was used to characterize both the micro-mixed glial model and neuronal-glia model at day 14, after immunostaining. Fluorescence microscopy was also used to assess cellular responses to lesions and biomaterials at 0 hours post-lesion, 1 day post-lesion and 7 days post-lesion. The analysis of each experimental condition was conducted using fluorescence images captured at low magnification on an AxioScope A1 microscope fitted with an Axiocam ICc1 digital camera, utilising Axiovision imaging software by Carl Zeiss Microimaging, Gmbh (Germany).

2.5 Analyses

2.5.1 Characterizing the glial cell proportions in the micro-mixed glial model at day 14

P1-P3 mice derived micro-mixed glial cultures at day 14 in vitro were fixed in 4% PFA and stained for GFAP, Iba1, NG2 and DAPI. Fluorescence micrographs were taken and merged using Axiocam software and all analyses were performed using ImageJ software (NIH USA). Culture characterization for $GFAP^+$, $Iba1^+$, $NG2^+$ cultures at day 14 was quantified from fluorescent images taken from three random fields (3 separate regions of the coverslip using DAPI only channels first) per coverslip with at least 100 nuclei assessed from each experiment. Each nucleus was counted as positive or negative for GFAP, Iba1 or NG2, and thus a total proportion of positive cells was determined.

2.5.2 Evaluation of the lesion width at 0 hours post-lesion

P1-P3 mice derived micro-mixed glial cultures, lesioned after 15 days in vitro were fixed in 4% PFA immediately after lesioning (section 3.3.3). To assess the reproducibility of the lesioning technique (section 3.3.3), the diameter of the lesion was assessed across four litters (1 lesion per litter). Here, fluorescence micrographs of GFAP stained lesions at 0 hours post-lesion were taken by obtaining low magnification x100 (x10 objective) images of the lesion. The total length of the visible lesion (where both corresponding edges of the lesion edge could be visualized) was measured and divided by ten, providing ten points at which measurements were taken from one lesion edge to the other (perpendicular to the direction of the lesion, with all measures being parallel to each other). 10 measurements per lesion per culture were averaged to create a graph displaying the average lesion width per culture, (*n=4*). Quantification was carried out using ImageJ analysis software (NIH USA).

2.5.3 GFAP optical density fold-change measurements

P1-P3 mice derived micro-mixed glial cultures, lesioned after 15 days in vitro were fixed in 4% PFA at 1 and 7 days post-lesion and stained for GFAP and DAPI. Low magnification x100 GFAP images of the lesion edge were obtained and converted to grayscale. A

superimposed rectangle (aligned with lesion edge) of sufficient width to measure 500 µm from the lesion edge was placed on the image; then measures at 10 equally distanced points along rectangle length were taken. The ten points which marked the beginning of optical density profiles were generated using ImageJ software and extended 500 microns perpendicularly into the culture (***figure 16***).

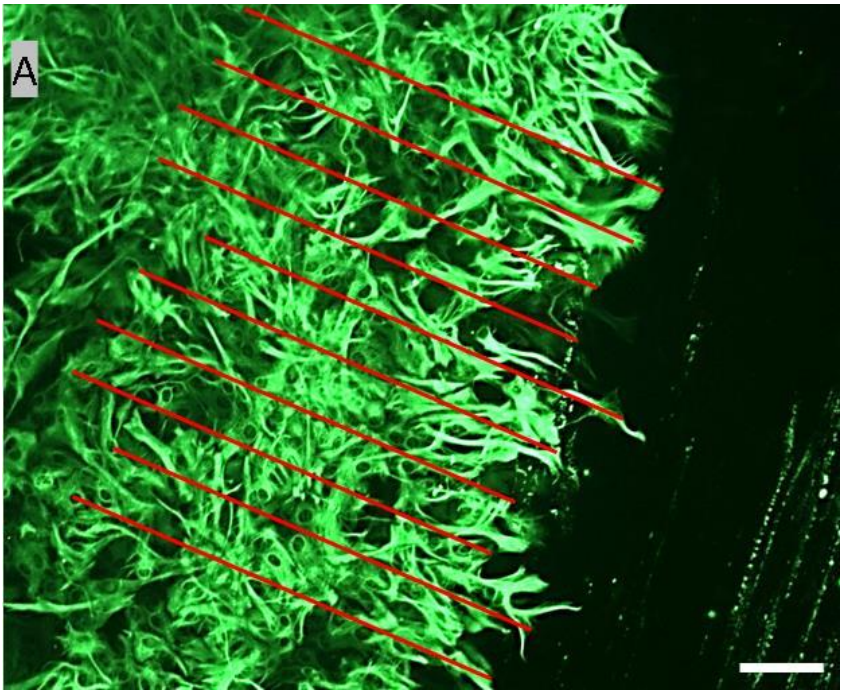

Figure 16: Optical density analysis in GFAP$^+$ cultures

A: *Representative fluorescent micrograph of GFAP$^+$ cultures 1 day post-lesion. A superimposed rectangle (aligned with lesion edge) of sufficient width to measure 500 µm from lesion edge was placed on the image; then measures at 10 equally distanced points along rectangle length were taken. Here, parallel lines extending 500 microns into the culture measured the optical densities across the length of the line. Optical density values were obtained along each of the indicated red lines, and also within unstained regions of the lesion, to provide background values. Scale bar: 100 microns.*

The ten measurements were averaged to form a single profile for each lesion, for 3 separate litters. Within each lesion, an area devoid of staining was identified and measured to give

background optical density values. A single corrected optical density profile from the astrocytic edge of each lesion was produced by subtracting the background optical density values.

For DuraGen Plus™ treated experiments, P1-P3 mice derived micro-mixed glial cultures, were lesioned and had DuraGen Plus™ implanted after 15 days in vitro were fixed in 4% PFA at 1 and 7 days post-lesion and stained for GFAP and DAPI treated experiments. Low magnification x100 GFAP images of the lesion edge were obtained and converted to grayscale. Only the astrocytes in direct contact with the biomaterial were analysed and deemed useable. This was determined by DAPI-GFAP double merged images, here the DAPI was able to highlight the location of the DuraGen Plus™ insert (***figure 22e, figure 28 b/d***). A superimposed rectangle (aligned with lesion edge) of sufficient width to measure 500 µm from lesion edge was placed on the image; then measures at 10 equally distanced points along rectangle length were taken. The ten measurements were averaged to form a single profile for each lesion which was then averaged across lesions from 3 separate litters. A separate region within each lesion devoid of staining was identified to give background optical density staining. A single corrected optical density profile from the astrocytic edge of each lesion was produced by subtracting the background optical density values.

For controls, P1-P3 mice derived micro-mixed glial cultures, were fixed in 4% PFA at day 15 and day 21 in vitro and stained for GFAP and DAPI. Low magnification x100 GFAP images were taken from 3 random fields and converted to grayscale images. The middle of the image was determined, and the height of the image measured and divided by ten providing points which marked the beginning of optical density profiles and extended 500 microns perpendicularly into the culture. The ten measurements were averaged to form a single profile for each lesion which was then averaged across lesions from 3 separate litters.

To quantify the optical density fold change, the single optical density values were grouped in distance away from the astrocytic edge 0-100 microns, 101-200 microns, 201-300 microns 301-400 microns, 401-500 microns. The optical density fold change was then calculated by

dividing the optical density value at 401-500 microns away from the astrocytic edge in each image by all of the other data groups per experiment. For controls all group values were divided by the control 401-500 microns values. This was done to normalise the optical density fold change measurements taking microscope exposure settings out of the equation, each image thus acting as its own control. Quantification was carried out using ImageJ analysis software (NIH USA).

2.5.4 Directionality analyses

To characterize the palisading astrocytic morphologies seen at the lesion edge in response to injury, the directionality analysis on ImageJ was attempted. This analysis is used to infer the orientation of structures present in an image. Images without any orientation are expected to give a flat graph with no peaks, whereas a greater proportion of features sharing an orientation will produce a peak at that orientation. For example, in ***figure 17*** the image on the right of the leaf displays projections in two main orientations; the leaf blades in the direction ca 60^{o} and -60^{o}. The corresponding histogram on the left displays this by showing a double peak curved graph with a peak at these angles and thus indicating that this image has directionality.

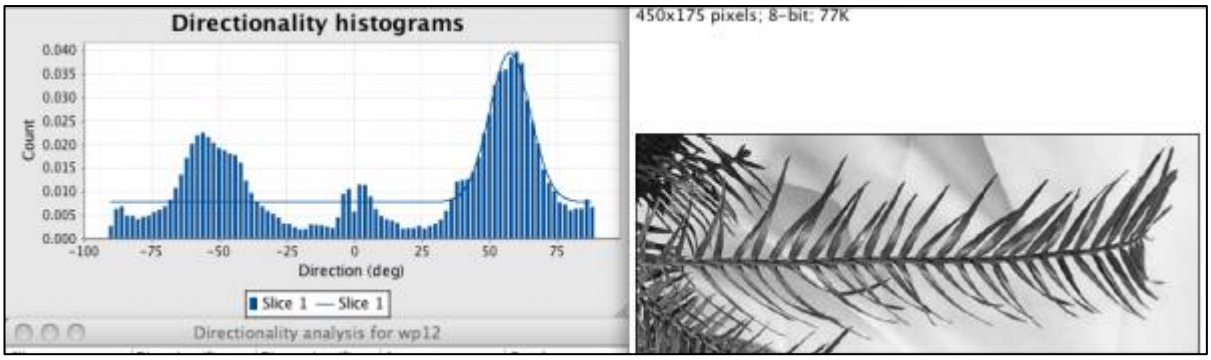

Figure 17: The principles of the directionality analysis

A histogram displaying the preferred orientation of the input image. Note how the leaf has projections ca 60^{o}and -60^{0}, which is displayed as two peaks on the histogram on the left.

Thus, given that astrocytes in Model 1 displayed palisading morphologies with long thin processes, this methodology was used to characterize such responses.

During 2.4.3, the same grayscale converted fluorescent GFAP micrographs were analysed for directionality. Here, the directionality was assessed in peri-lesional astrocytes (0-100 microns away from the astrocytic edge) and distal astrocytes (401-500 microns away from the astrocytic edge). Since the lesions were often imaged at an angle (***figure 12a***), the images were rotated to make the lesion straight at 0^{o} and a standard sized 100-micron wide box was placed in the peri-lesional area and distal area. For biomaterial treated coverslips only astrocytes associated with the biomaterial was analysed. This was determined by DAPI-GFAP double merged images, where the DAPI was able to highlight the DuraGen Plus^{TM} location (***figure 22e, figure 28b/d***). The directionality plugin on ImageJ was then used to generate a graph. The data per experimental condition was averaged across 3 litters to generate a single graph of directionality per experimental condition.

2.5.5 Cell infiltration into the lesion/biomaterial per unit area

P1-P3 mice derived micro-mixed glial cultures, lesioned after 15 days in vitro were fixed in 4% PFA at 1 and 7 days post-lesion and stained for Iba1, NG2 and DAPI. Low magnification x100 images of the lesion were obtained and the numbers of $Iba1^{+}$/ $NG2^{+}$ cells were counted (only when immunostaining was clearly associated with DAPI staining) within each lesion using a standard size grid overlaid onto each image. The total number of $Iba1^{+}$/ $NG2^{+}$ cells per unit area were then averaged at each time point.

For DuraGen Plus^{TM}, treated experiments, P1-P3 mice derived micro-mixed glial cultures, were lesioned and had DuraGen Plus^{TM} implanted after 15 days in vitro were fixed in 4% PFA at 1 and 7 days post-lesion and stained for Iba1, NG2 and DAPI. Low magnification x100 images of the DuraGen Plus^{TM} were obtained and the numbers of $Iba1^{+}$/ $NG2^{+}$ cells were counted (only when immunostaining was clearly associated with DAPI staining) within each biomaterial. The total area of the DuraGen Plus^{TM} was measured by drawing around

the biomaterial and used to generate the total number of $Iba1^+$/ $NG2^+$ cells per unit area, which was then averaged at each time point. Quantification was carried out using ImageJ analysis software (NIH USA).

2.5.6 Microglial and OPC morphological analyses

During analyses described in 2.4.5, as cells were counted, they were semi-quantitatively grouped for lesion only coverslips as either ramified (1 process or more) or amoeboid (no processes), the same criteria was applied for biomaterial treated coverslips (***figure 30a-b insets***). For lesion only coverslips OPCs were classified as ramified (3 or more processes) or bipolar/unipolar/unprocessed (2 processes or less) (***figure 33a-b insets***). The total number of cells with a morphological characteristic was then averaged at each time point.

2.5.7 Statistical analysis

GraphPad Prism v5.0 was used for all the statistical analyses performed. All quoted values are expressed as mean ± standard error of the mean (SEM) unless stated otherwise. Data was analysed by a one-way analysis of variance (*ANOVA*) with Tukey's post-hoc analysis. In all cases, the number of experiments (*n*) refers to the number of individual cultures derived from separate mice litters.

Chapter 3

Establishing a technical method to develop an in vitro multi-glial TBI model to evaluate cellular responses to biomaterial implantation

3.1 Introduction

Currently, the evaluation of hydrogel-based regenerative strategies is reliant on live in vivo animal TBI models (126). These models have considerable limitations (see section 1.5.1) (143). Pathomimetic in vitro TBI model alternatives, allow key biomaterials to be identified, whilst also preventing unnecessary animal experimentation and wasting valuable resources directly testing in vivo; an initiative in line with the Reduction, Replacement and Refinement of animal experimentation (the 3R's principles) (see section 1.5.6) (154).

An ideal in vitro TBI model used to assess biomaterial based regenerative strategies must be: *(i)* neuropathomimetic to TBI *(ii)* capable of supporting biomaterial implantation into lesion sites *(iii)* facile *(iv)* high throughput. Currently, there is no such in vitro TBI model, hence this chapter aims to establish this model.

In order to develop this model, a variety of in vitro culture systems could potentially be used. Organotypic slice cultures as pTBI models have previously been described in detail (see section 1.5.4). These models are neuromimetic and have been used to test biomaterials in vitro. However, as they are technically challenging and moderate throughput, such models are not widely accessible. On the other hand, whilst immortalized cell line-based models are high throughput and facile (see section 1.5.5) these models are unreliable due to the risk of cryptic contamination and resistance to cell death (140,146).

Primary cultures from dissociated brain tissue have been used as high throughput TBI models. A variety of models with differing injury mechanisms exist; transection, compression, barotrauma, acceleration/deceleration induced neurotrauma, hydrodynamic models and cell-stretch models. However, in the context of pTBI only transection models can simulate distinct areas of lesion "representative" of in vivo pTBI models (140). Furthermore, to assess the regenerative potential of biomaterials, a distinct lesion is essential to allow effective biomaterial implantation into the lesion sites, replicating current in vivo biomaterial testing.

In vitro transection models involve lesioning confluent cultures with objects such as plastic pipettes, stylets and blades. Although, these models contain distinct lesion sites, they have

not yet been adapted to support biomaterial implantation. The advantages and disadvantages of these models is required to understand which models are suitable for biomaterial implantation.

Previously, researchers have lesioned confluent astrocytic monocultures to mimic pTBI pathology (147). However, these models are not neuromimetic, specifically the lack of a microglial component means these models lack the primary immunocompetent immune cell of the CNS, which drives glial scar formation (64). More complex in vitro pTBI transection models include neural co-culture systems. Here, bulk cultures/cell lines are used to derive isolated neural cell populations, which are reseeded into 24 well plates. Astrocytes are most-commonly cultured with microglia and neurons (155). Furthermore, neurons and glial cells have also been co-cultured (155). There are considerable disadvantages with such co-culturing methodologies however; neural cell populations in different bulk cultures are often not cultured together in the same kind of media throughout the same experiment, which can influence cellular protein expression and behaviour (156). In addition, establishing stoichiometrically defined cell ratios in these models for reproducible and characterizable models is lengthy, and non-facile. In an attempt to exclude the effects of differing media/culture formats, researchers have grown mouse cortices as neurospheres and seeded single cells directly onto glass coverslips which differentiate into neurons, astrocytes and oligodendrocytes after 8 days (156). Although such a result shows promise, the lack of a microglial cell population is a limitation of this model. Thus, primary cultures which contain all of the glial cells need to be investigated for such application.

The mixed-glial culture system, originally developed by Mccarthy and de Vellis, over 3 decades ago, has been cited in more than 2,500 research papers (153). This protocol is widely used to derive individual glial cell populations from a bulk culture. Here, dissociated cortices are seeded into culture flasks and astrocytes form a confluent bed layer with microglial and OPC cells appearing on top. Once confluent, sequential shaking on rotary shakers can be used to derive high purity isolated glial cell populations. The original Mccarthy and de Vellis protocol derived cultures from rat brains, recently Schlidge et al 2013

has proven mice brain derived cultures also stratify in the same way and can be used to derive high purity isolated glial cell populations (157). Furthermore, mice cultures are considerably more economical to procure, maintain and house. Secondly, the ability to use transgenic/knockout mice provides increased experimental possibilities versus rat cultures. As a mouse mixed-glial culture contains all of the glial cell types which are the main determinants of responses to biomaterials and injury (see section 1.5.5), this chapter aims to adapt this mixed-glial culture into a micro-well format and introduce a lesion capable of supporting biomaterial implantation. Perhaps one disadvantage of such a model is that the lack of a neuronal component means axotomy and neuronal mediated microglial/astrocytic responses cannot be simulated. Thus, this chapter also intends to develop a high throughput primary culture system which contains all of the neural cell types: i.e. incorporating neurons.

3.1.1 Identifying a suitable biomaterial to implant into lesions to assess regenerative strategies

Collagen hydrogel matrices have been shown to provide therapeutic benefits in pTBI (see section 1.4.4). The major disadvantages of current studies, however, is that predominantly laboratory grade hydrogels unapproved for human use have been investigated. DuraGen Plus™, is a clinically approved collagen hydrogel and has been discussed in detail in section 1.4.5. Early studies have shown that DuraGen Plus™ is a biomimetic matrix, which supports the survival of neural cells, as well as possessing neuroprotective and neuroregenerative properties (128,129). Currently, there is no study which has investigated the regenerative potential of DuraGen Plus™ in pTBI and thus provides a novel objective.

3.1.2 Current methods to visualize collagen biomaterials in the CNS following biomaterial implantation

Distinguishing collagen biomaterials from surrounding tissue in vivo is challenging. Thus, researchers often have to rely on post-mortem analysis to determine the location of the biomaterials (113,114). In vitro models allow continuous biomaterial monitoring and can allow researchers to determine live cell-biomaterial interactions.

Polarizing light microscopy has been previously used to visualize the collagen within tissue sections (158). The dense network of parallel collagen fibres allows birefringence to be detected under polarizing light microscopy, thus this could be a useful tool to detect collagen biomaterials. Although fluorescent ICC forms a staple in visualizing cells, there are considerable disadvantages as when compared to histological methods of staining: samples tend to fade over time and require careful storage in dark and cool conditions. Secondly, fluorescent microscopes tend to be costly and may not be accessible to laboratories in poorer countries with limited resources and funding, whilst light microscopes are considerably cheaper. Picrosirius red is an example of a popular histological stain which has been used to stain collagen within tissue sections (159). In addition, studies have also demonstrated the efficacy of picrosirius red in staining collagen hydrogels (159). However, currently there are no protocols which enable researchers to double histological stain for both biomaterials and cells to study cell-biomaterial interactions, thus providing a novel aim for this chapter. There are considerable foreseeable challenges with such a protocol; histological stains such as picrosirius red, typically involve protocols which involve incubating the stains with samples for extended periods followed by acid washes, dehydration and subsequent mounting. Whilst such protocols are suitable for robust and durable tissue sections, they may be too harsh for cellular application. Secondly, a histological stain must either stain the cells/biomaterial only, but not both, so cells and biomaterial can be distinguished based on colour.

3.2 Objectives

I. Determine if the mixed-glial culture model can be utilized in a micro-well (24 well plate) format to develop an in vitro model containing the major glial cell types: astrocytes, microglia and OPCs (Model 1).

II. Establish a traumatic penetrating injury paradigm in Model 1.

III. Establish a protocol for implanting a DuraGen Plus™ sheet into the lesion site.

IV. Establish a double histological staining protocol whereby neural cells and DuraGen Plus™ can be distinguished based on colour using simple light microscopy.

V. Conduct a pilot study to develop a model containing neurons and the major glial cell types (Model 2).

3.3 Experimental procedures

Quantification methodologies for chapters 3 and 4 are set out under Materials and Methods: section 2.5

3.3.1 Reagents and equipment

All reagents and equipment are listed in section 2.1.

3.3.2 Development of a double histological staining protocol to distinguish neural cells and DuraGen Plus™ under light microscopy

3.3.3 Polarizing light microscopy to study DuraGen Plus ™

A pre-prepared piece of DuraGen Plus™ (section 2.3.4) was imaged under a polarizing light microscope (section 2.4.2) to determine if the biomaterial construct displayed birefringence. Here, the DuraGen Plus™ was placed under the microscope and imaged without the use of the polarizer i.e. simple light microscopy. To determine birefringence, counterpart images were taken of the DuraGen Plus™ when the polarizer was rotated.

3.3.4 H&E staining of cells

To determine whether the common histological stains H&E are suitable for a double histological cell-biomaterial staining protocol, each stain in turn was added to a pre-prepared piece of DuraGen Plus™ (section 2.3.4) to determine whether these histological stains do NOT stain DuraGen Plus™ and thus suitable for this protocol.

A plastic Pasteur was used to add a single drop off haematoxylin (10mg/ml) onto the DuraGen Plus™ for 30 seconds. Tap water was added to cover the DuraGen Plus™ for 1 minute and discarded. 0.3% acetic acid ethanol was added for 1 minute and discarded. Tap water was added for 1 minute and discarded. 70% ethanol was added for a further 1 minute discarded. 90% ethanol was added and discarded. Finally, the DuraGen Plus™ was mounted in Dibutylpthalate Polystyrene Xylene (DPX) onto a glass coverslip on a glass slide. Images of the DuraGen Plus™ were taken on a light microscope (section 2.4.1) to determine whether haematoxylin had stained the biomaterial.

A plastic Pasteur was used to add a single drop of eosin (0.25% eosin Y) onto the DuraGen Plus™ for 30 seconds. 90% ethanol was added to cover the DuraGen Plus™ for 1 minute and discarded. Likewise, 100% ethanol was added to cover the DuraGen Plus™ for 1 minute and discarded. Xylene was added for 2 minutes and the DuraGen Plus™ was subsequently mounted in DPX onto a glass coverslip on a glass slide. Images of DuraGen Plus™ were taken on a light microscope (section 2.4.1) to determine whether eosin stained the biomaterial.

3.3.5 The cell-biomaterial double histological staining protocol

To distinguish cells and biomaterials in differing coloured stains, a double histological staining protocol was developed. Here, fixed culture plates containing astrocytes were stained with GFAP-DAB to determine whether astrocytes could be immunolabelled. To determine whether this protocol could be combined with the collagen dye picrosirius red (PS red), fixed 7 days post-lesion biomaterial implanted cultures underwent the following protocol:

The sample was incubated with 5% NDS-0.3%Triton X100 PBS blocker for 30 minutes. The solution was removed and 1:500 GFAP in 5% NDS-0.3%Triton X100 PBS blocker was added and placed in a 4^{o}c fridge overnight. The solution was discarded, and the samples washed 3x in PBS (5 minutes/wash). The PBS was removed, and the samples incubated with 1:200 secondary biotinylated antibody in 5% NDS-0.3%Triton X100 PBS blocker for 2 hours. The solution was discarded, and the samples washed 3x in PBS (5 minutes/wash). The VECTASTAIN ABC© reagent was added for 30 minutes. The solution was discarded, and the samples washed 3x in PBS (5 minutes/wash). The peroxidase substrate (1:500 DAB diluted into PBS with either 1:1000 0.3% hydrogen peroxide (brown deposits) or 1:1000 nickel (black deposits) was added under a fume hood and the samples are brought immediately to a light microscope (section 2.4.1). As soon as the peroxidase/nickel label was added, the astrocytes began to change colour immediately and thus after ten minutes when the astrocytes had completely stained through the

peroxidase substrate was removed, and the samples washed 3x in tap water. A plastic Pasteur pipette was used to submerge the sample in picrosirius red 0.1% for 5 minutes. The solution was discarded, and the samples washed 3x in PBS (5 minutes/wash). Please note that traditionally, acetic acid 0.5% is used to wash off PS red solution. However, it was noted that PBS was effective and had less risk of damaging the delicate adhered cells on the glass coverslips. The samples were mounted (section 2.2.4) onto a glass coverslip and imaged under a light microscope (section 2.4.1). A combination of low magnification and high magnification images were obtained to display whether this protocol successfully labelled cells and biomaterial in contrasting colours (***figure 18***).

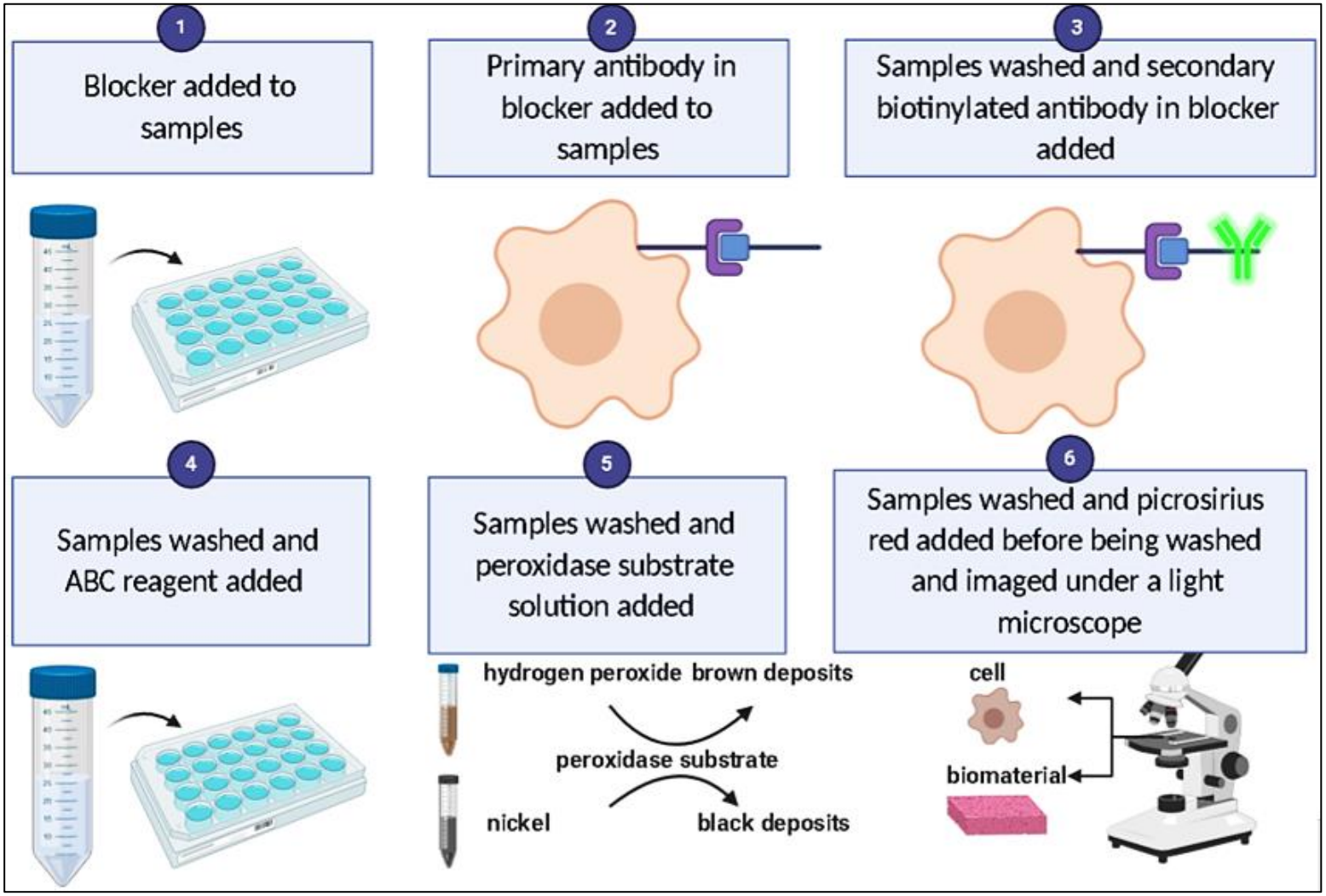

Figure 18: A schematic showing the DAB-PS red protocol

3.4 Results

3.4.1 Mixed-glial cultures show similar stratification in bulk and micro-well formats

Mixed-glial cultures established in micro-well (micro-mixed glial) formats developed and stratified similar to bulk (macro-mixed glial) formats (***figure 19***). Across both formats the cells suspension adhered to the culture plastics. Within the first 2 days, the cultures recovered from the dissection process and numerous rounded cells with no distinct identifiable glial cell morphologies were present (***figure 19a***). From days 3 onwards, although some debris was still present, some cellular morphologies were now adherent. In addition, there were cells with astrocyte-like morphologies (***figure 19b***). From day 5, there were distinct colonies of cells with flat, polygonal, morphologies characteristic of astrocytes (***figure 19c***). Here, little cellular debris was seen surrounding these colonies as compared to the rest of the culture. At day 7 astrocyte like morphologies had proliferated and formed an astrocytic bed layer like morphology which increases in confluency (***figure 19d-e***). By day 14, there were cells with clear microglia like (phase bright cells with rounded/triangular cell bodies) and OPC-like morphologies (phase dark cells with bipolar/branched processes and oval cell bodies) on top of a confluent astrocytic bed layer like morphologies (***figure 19f***).

Macro-mixed glial culture

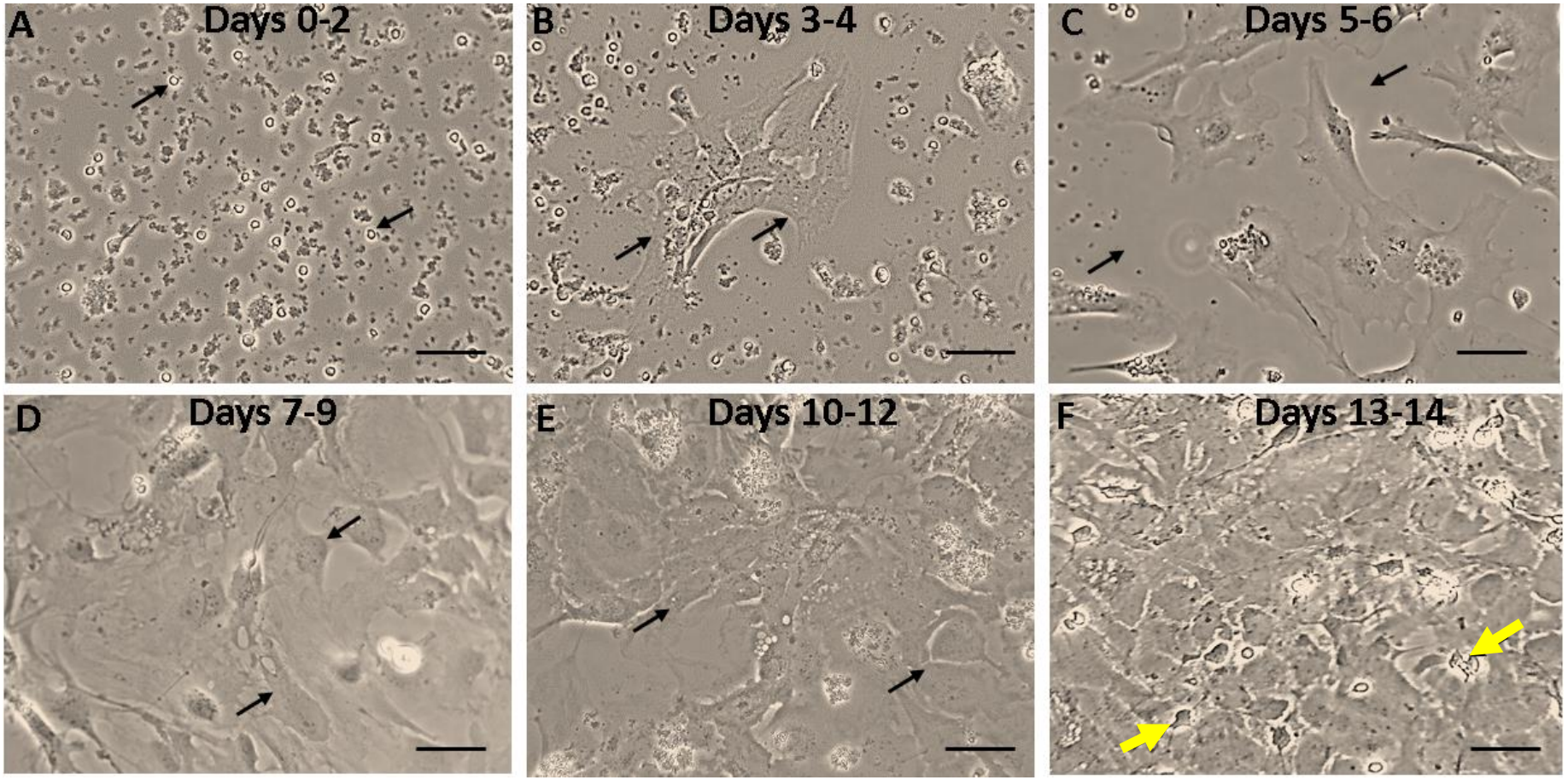

Micro-mixed glial culture

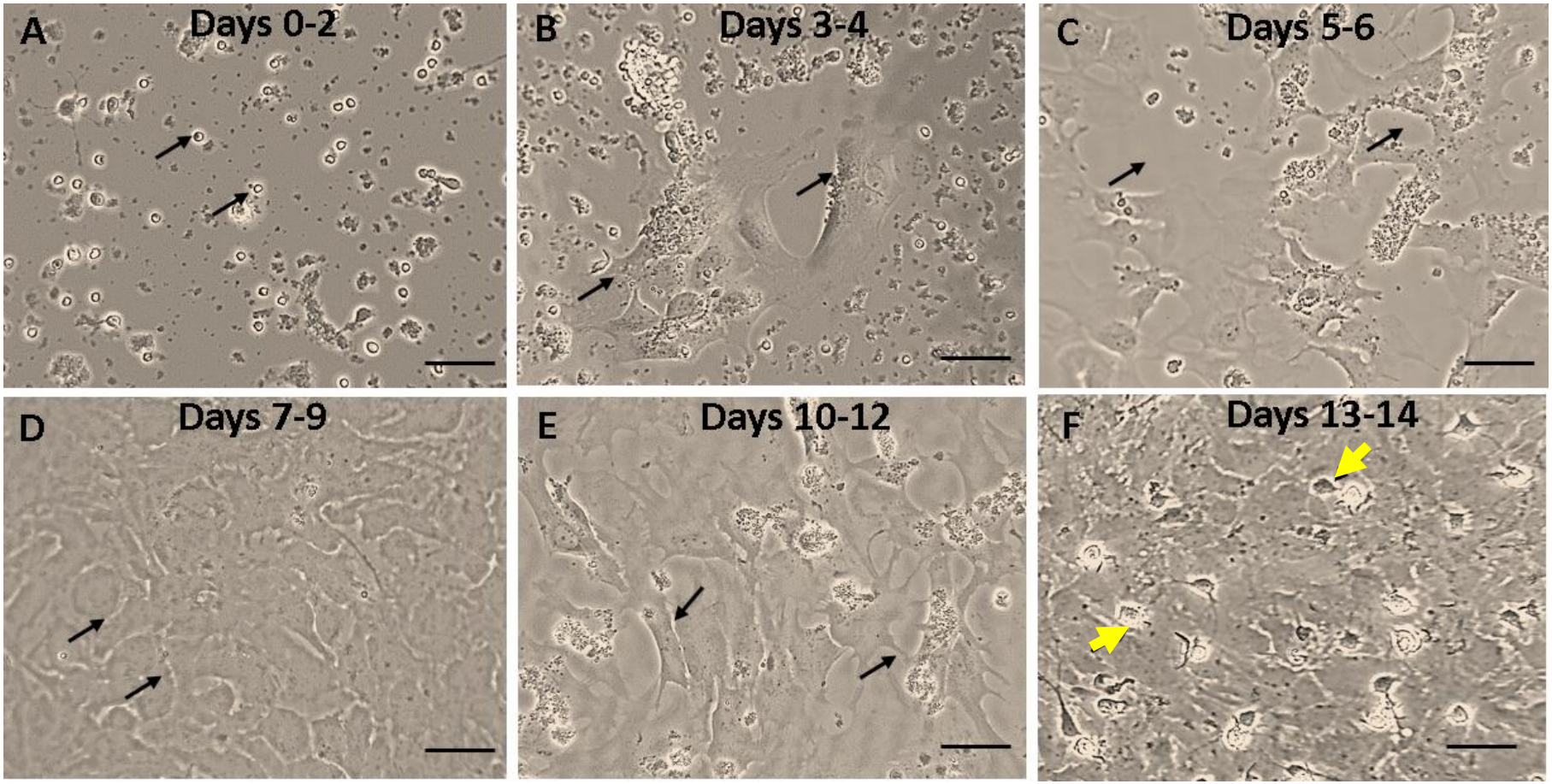

Figure 19: Phase contrast micrographs showed similar maturation and stratification of macro and micro-mixed glial cultures

A: *Representative phase contrast micrographs of days 0-2 in culture. The arrows show rounded cells and cellular debris with no distinct morphologies identifiable at this timepoint.* ***B:*** *Representative phase contrast micrographs of days 3-4 in culture. Cell debris was still present, but some cells were now adherent. The arrows show cells with astrocytic morphologies were evident.* ***C:*** *Representative phase contrast micrographs of days 5-7 in culture. The arrows show decreased cellular debris surrounding associated cell colonies.* ***D/E:*** *Representative phase contrast micrographs of days 7-12 in culture. The arrows show increasing confluency of astrocytic bed layer like morphologies (phase-dark flattened cells).* ***F:*** *Representative phase contrast micrographs of days 13-14 in culture. The culture was confluent. The arrows show OPC and microglial like morphologies can be identified on top of the astrocyte bed layer like morphologies. Scale bars: 100 microns.*

3.4.2 Lectin and A2B5 resulted in non-specific staining of the astrocytic bed layer

To characterize the micro-mixed glial culture, lectin and A2B5 were initially used to immunolabel microglia and OPCs respectively. Both antibody stains were deemed unsuitable for use since lectin non-specifically punctate stained astrocytic bed layer like morphologies (***figure 20a***) whilst A2B5 stained cells with clear astrocyte like morphologies (***figure 20b***). Thus, lectin and A2B5 staining was discontinued, and Iba1/NG2 antibody stains were trialled (***figure 20***).

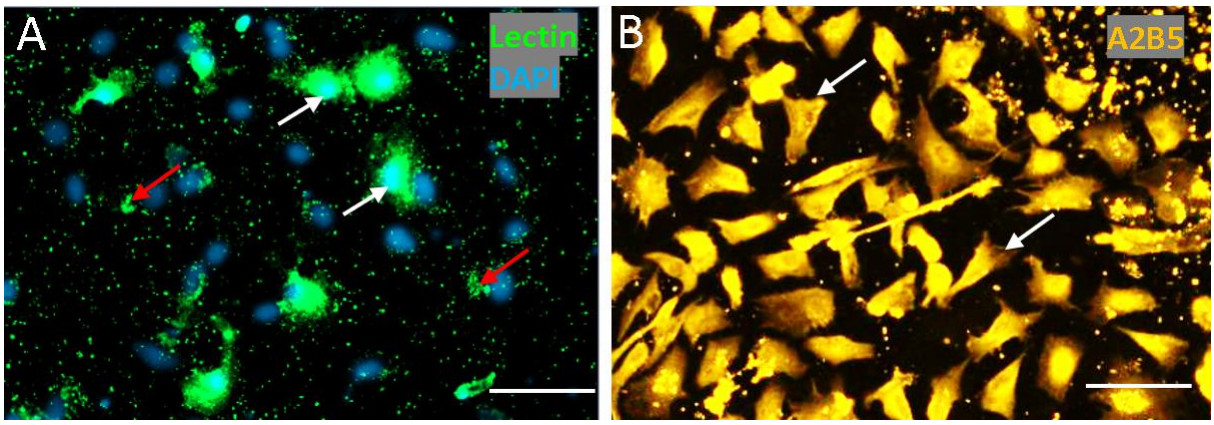

Figure 20: Lectin immunostaining resulted in artefacts while A2B5 staining was found to be non-specific

A: *Representative fluorescence micrographs of lectin$^+$ cells. The white arrows show that these lectin$^+$ cells displayed typical microglial morphologies. The red arrows show significant punctate staining of astrocytic bed layer like morphologies.* ***B:*** *Representative fluorescence micrographs of A2B5$^+$ cells. The white arrows show non-specific staining of cells with clear astrocyte like morphologies. Scale bars: 100 microns.*

3.4.3 Astrocytes represented the predominant glial cell type in Model 1

The micro-mixed glial cultures were characterized at day 14 to determine the presence of all of the glial cell types including their representative proportions within the cultures. The results showed that GFAP$^+$ cells had consistent astrocytic morphologies which clearly formed a confluent astrocytic bed layer (***figure 21a***). Furthermore, Iba1$^+$ cells showed consistent microglial morphologies and unlike lectin, did not result in punctate staining of the astrocytic bed layer (***figure 21b***). Similarly, NG2$^+$ cells showed consistent OPC morphologies and unlike A2B5 did not label astrocytes (***figure 21c***). With regards to glial cell proportions within the cultures: astrocytes were found to be the most numerous glial cell type (82.6 ± 5.2%) whilst microglia (9.3 ± 3.6%) and OPCs (6.7 ± 2.1%) were present in smaller numbers and represented the minority glial cell types (***figure 21d***).

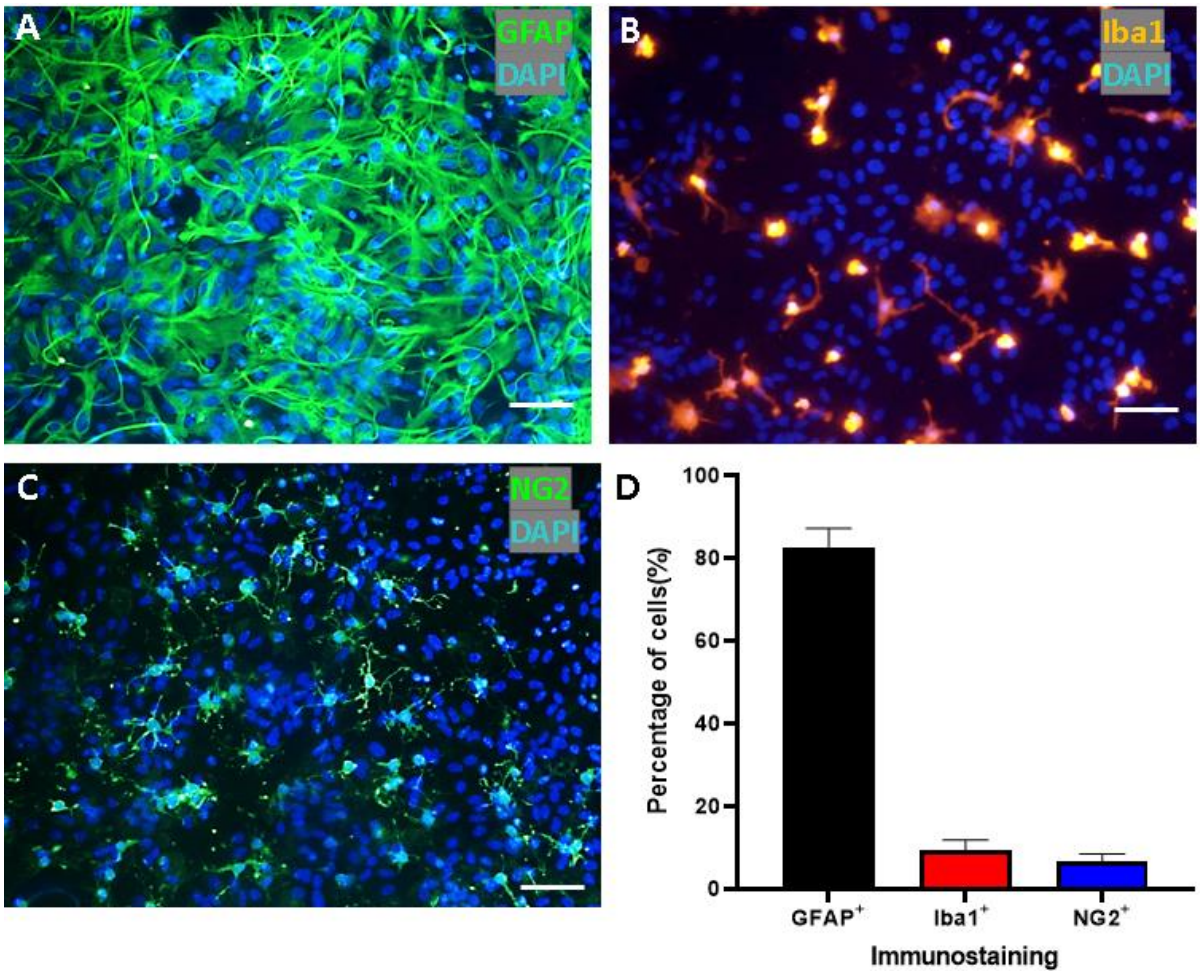

Figure 21: Characterisation of cellular composition in Model 1 at day 14

***A**: Representative fluorescent micrographs of GFAP$^+$ astrocytes at day 14. Here, astrocytes had formed a dense confluent astrocytic bed layer. **B:** Representative fluorescent micrographs of Iba1$^+$ cells consistent with microglial morphologies. **C:** Representative fluorescent micrographs of NG2$^+$ cells consistent with OPC morphologies. **D:** The graph shows the percentage of cells in the cultures at day 14. Here, astrocytes clearly represent the majority glial cell type. Scale bars: 100 microns, (n=4).*

3.4.4 A reproducible and distinct penetrating lesion was introduced in Model 1

A transecting lection was introduced into Model 1 according to the methods set out in section 2.3.3. At 0 hours post-lesion a reproducible and well-defined lesion was introduced (3.4.4) with very little cellular debris within the lesion (***figure 22a-b)***. The lesion area was observed to be largely devoid of remnants of cell debris from the injury process (***figure 22a-b***). Furthermore, $GFAP^+$ cultures demonstrated that a consistent and clear area negative for GFAP was consistent with the lesion (***figure 22b***). In addition, corresponding DAPI micrographs showed a distinct area devoid of nuclei consistent with the lesion (***figure 22b***). Furthermore, the astrocytic edges (lesion edges) could clearly be identified on either side of the lesion (***figure 22a-b***). The lesion width was measured according to the quantification methodology set out in section 2.5.2. Briefly, 10 measurements were obtained per-lesion, measuring the distance from one side of the astrocytic edge to the other. The average lesion width across all 4 cultures was 949 ± 26 µm (***Figure 22c***). The average lesion widths from 4 independent cultures showed that the lesion protocol resulted in consistent, reproducible and defined lesions within the cultures.

3.4.5 DuraGen Plus™ was successfully implanted into the lesion site

Model 1 was adapted to support DuraGen Plus™ implantation into the lesion (***figure 22d***). At 2 hours post-lesion, a pre-prepared DuraGen Plus™ insert (section 2.3.5) was introduced into the lesion under microscopic guidance and imaged under light microscopy. Here, phase contrast images show that a DuraGen Plus™ sheet can be accurately placed abutting the lesion margins allowing for cell-biomaterial interactions to be imaged (***figure 23d***). Under phase microscopy the DuraGen Plus™ sheet appeared to be dark grey/black in colour in contrast to the light grey coloured lesion margins. After 7 days post-lesion DuraGen Plus™ showed a blue silhouette and can be accurately identified under the DAPI microscopic channel with clear nuclei identifiable within the DuraGen Plus™ at this timepoint (***figure 22e***). This indicated two things; DuraGen Plus™ inserts could be implanted into the lesion and

remained within the lesion until later time points. Secondly nuclei, within the DuraGen Plus™ indicated cellular infiltration into the biomaterial.

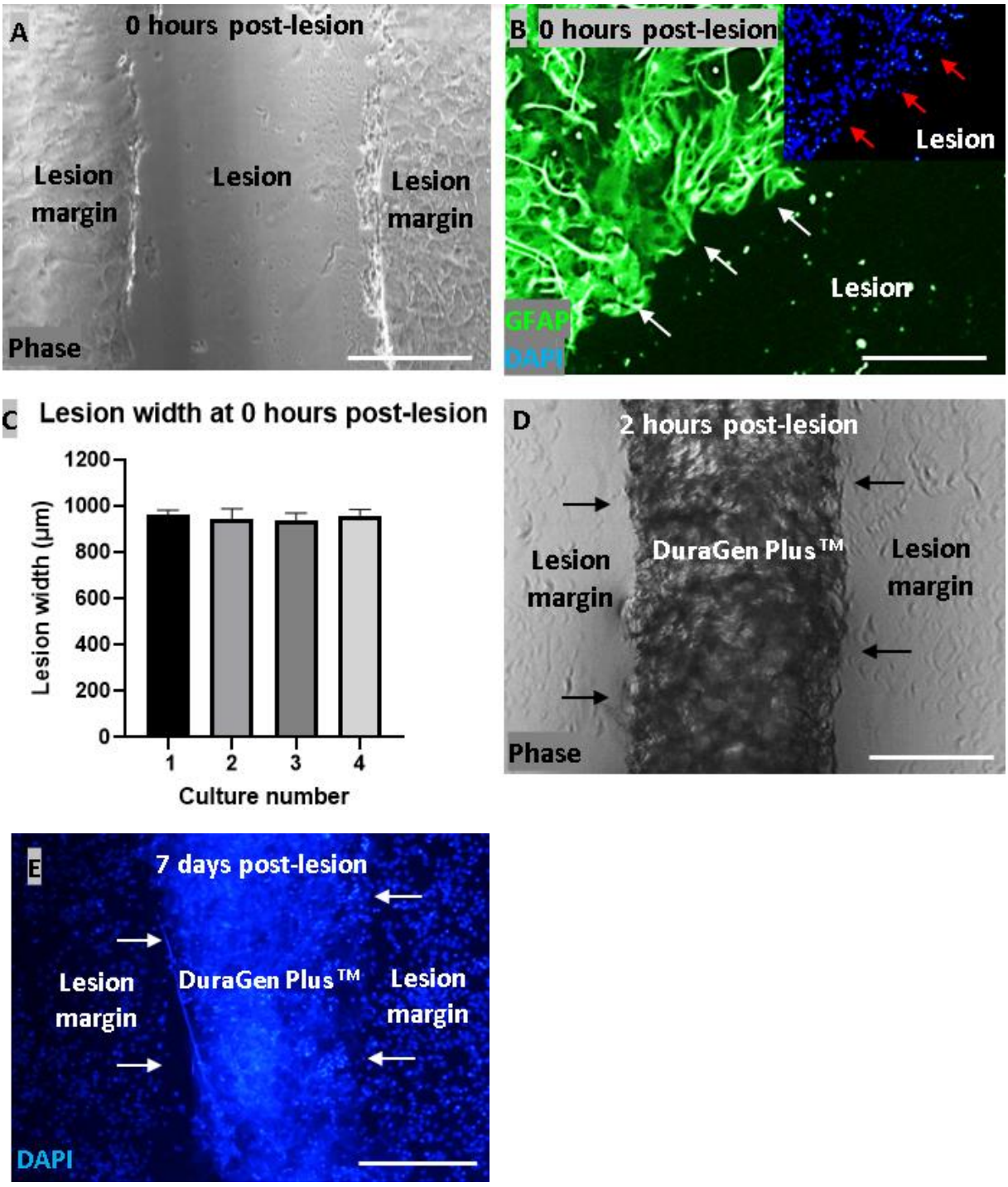

Figure 22: DuraGen Plus™ inserts were implanted into a well-defined lesion

A: *Representative phase micrograph showing a distinct lesion immediately after injury.* **B:** *Representative fluorescence GFAP$^+$ micrograph of a lesion at 0 hours post-lesion. Note the lesion margin (top left), with relatively straight edges showing that a reliable and consistent lesion was introduced.* ***Inset:*** *Counterpart DAPI micrograph at 0 hours post-lesion. Note the extremely limited amount of DAPI or GFAP staining between the lesion margins and lack of nuclei within the lesion.* ***C:*** *The graph shows that the lesion width across 4 independent cultures was consistent and thus reproducible lesions were introduced.* ***D:*** *The biomaterial was implanted into the lesion site 2 hours post-lesion. The arrows show that the biomaterial was placed abutting the lesion margin.* ***E:*** *Representative phase micrograph showing DAPI staining 7 days post biomaterial implantation. The white arrows show that the biomaterial remained in-situ, with nuclei within the biomaterial suggesting cellular infiltration into the biomaterial. Scale bars: A, D, E: 500 microns, B:300 microns, (n=10).*

3.4.6 DuraGen Plus™ did not show consistent birefringence under polarizing light microscopy

To determine the suitability of polarizing light microscopy to detect birefringence in DuraGen Plus™, the methodology in section 3.3.2 was followed. Under light microscopy, DuraGen Plus™ appeared to look dark grey with a mosaic like structure consistent with that of a 3D collagen biomaterial (***figure 23a-b***). Under polarizing light microscopy, it was evident that DuraGen Plus™ displayed small pockets of birefringence (***figure 23a-b***). On visual assessment only around 5% of the total biomaterial displayed birefringence and thus did not exhibit birefringence throughout, indicating that polarizing light microscopy cannot be used to detect the exact size and shape of the implanted DuraGen Plus™ (***figure 23***).

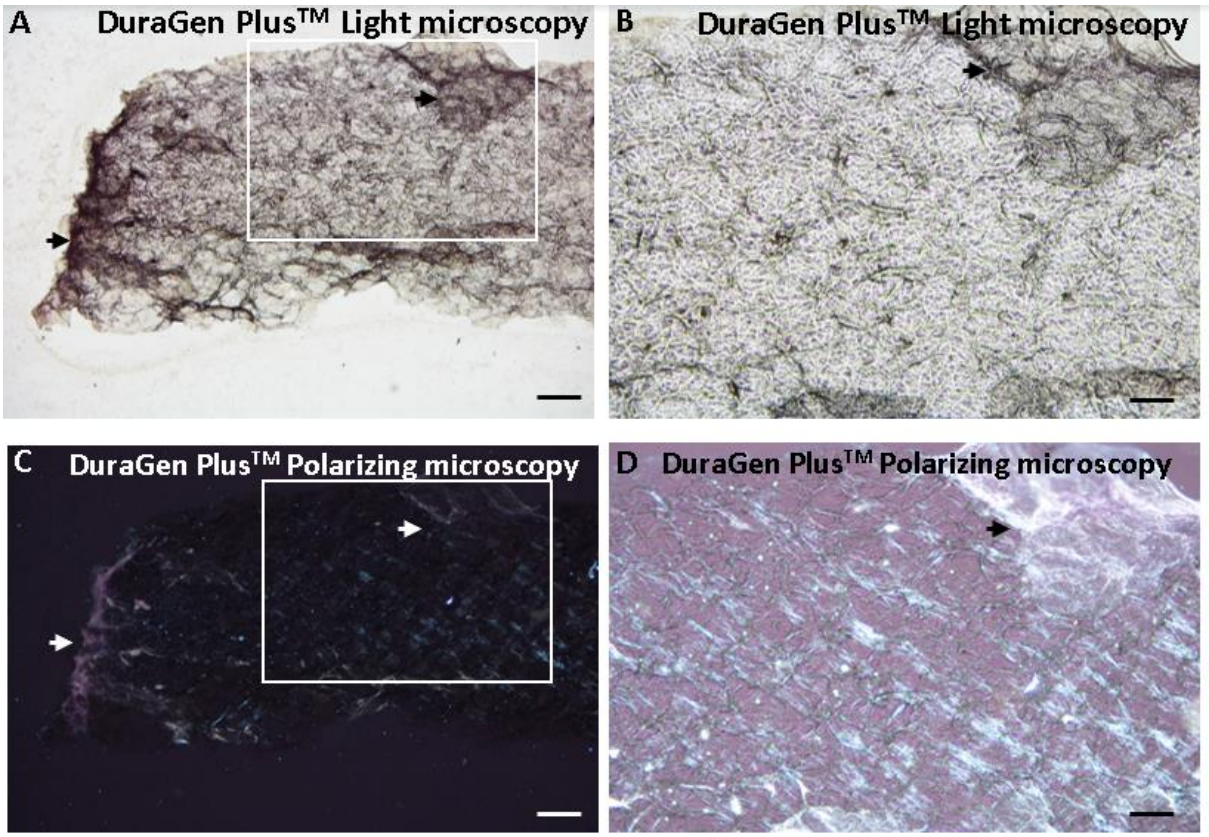

Figure 23: DuraGen Plus™ displayed minimal birefringence under polarizing light microscopy

A/B: *DuraGen Plus™ under light microscopy.* ***C/D:*** *Corresponding high magnification inset imaging showing areas of DuraGen Plus™ where birefringence was detected. Scale bars A/C: 100 microns, B/D: 25 microns.*

3.4.7 H&E intensely stained DuraGen Plus™

H&E were trialled to determine whether these stains could be incorporated into a double histological cell-biomaterial stain. DuraGen Plus™ was intensely stained by both H&E (***figure 24a-b***). Specifically, haematoxylin stained all the DuraGen Plus ™ black/brown, with varying intensities of staining throughout different sections of the biomaterial (***figure 24b***). On the other hand, eosin produced consistent and diffuse red staining throughout the whole thickness of DuraGen Plus™ (***figure 24a***). This indicated that H&E would be unsuitable to use a stain to distinguish biomaterial from cells.

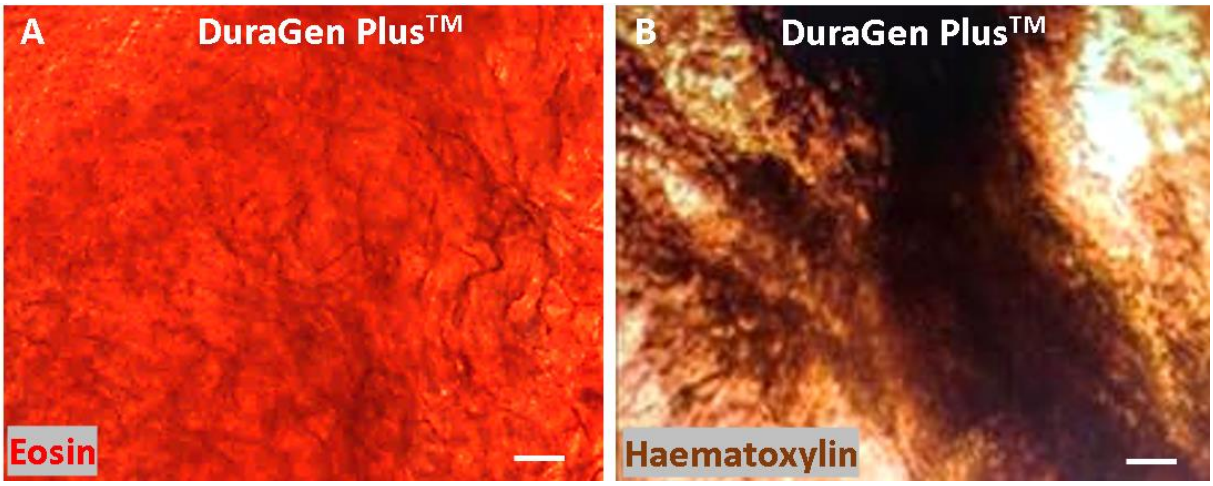

Figure 24: H&E staining of DuraGen Plus™

A: *Eosin stained DuraGen Plus™ in a diffuse red/pink colour.* ***B:*** *Haematoxylin stained DuraGen Plus™ brown/black. Scale bars: 50 microns.*

3.4.8 The double histological staining protocol distinguished astrocytes and DuraGen Plus™ under light microscopy

The DAB-GFAP staining protocol was used to determine whether astrocytes could be effectively immunolabelled. Here, DAB-GFAP$^+$ cells had clear astrocytic morphologies and appeared dark brown under light microscopy due to hydrogen peroxide deposits *(**figure 25a-b**)*. The DAB-PS red protocol was used determine whether DuraGen Plus™ and astrocytes could be co-immunolabelled. Here the confluent astrocytic bed layer was clearly labelled with black deposits (nickel) and could be seen in contrast to the diffuse and intensely red stained DuraGen Plus™. The biomaterial was stained red/pink whilst cells were stained brown (hydrogen peroxide staining) or black (nickel staining) (***figure 25c-d***). Since this protocol successfully distinguished astrocytes and DuraGen Plus™ it was evident that at 7 days post-lesion the astrocytes had infiltrated the biomaterial (***figure 25c-d***). Thus, the DAB-PS red protocol effectively distinguished biomaterial from cells.

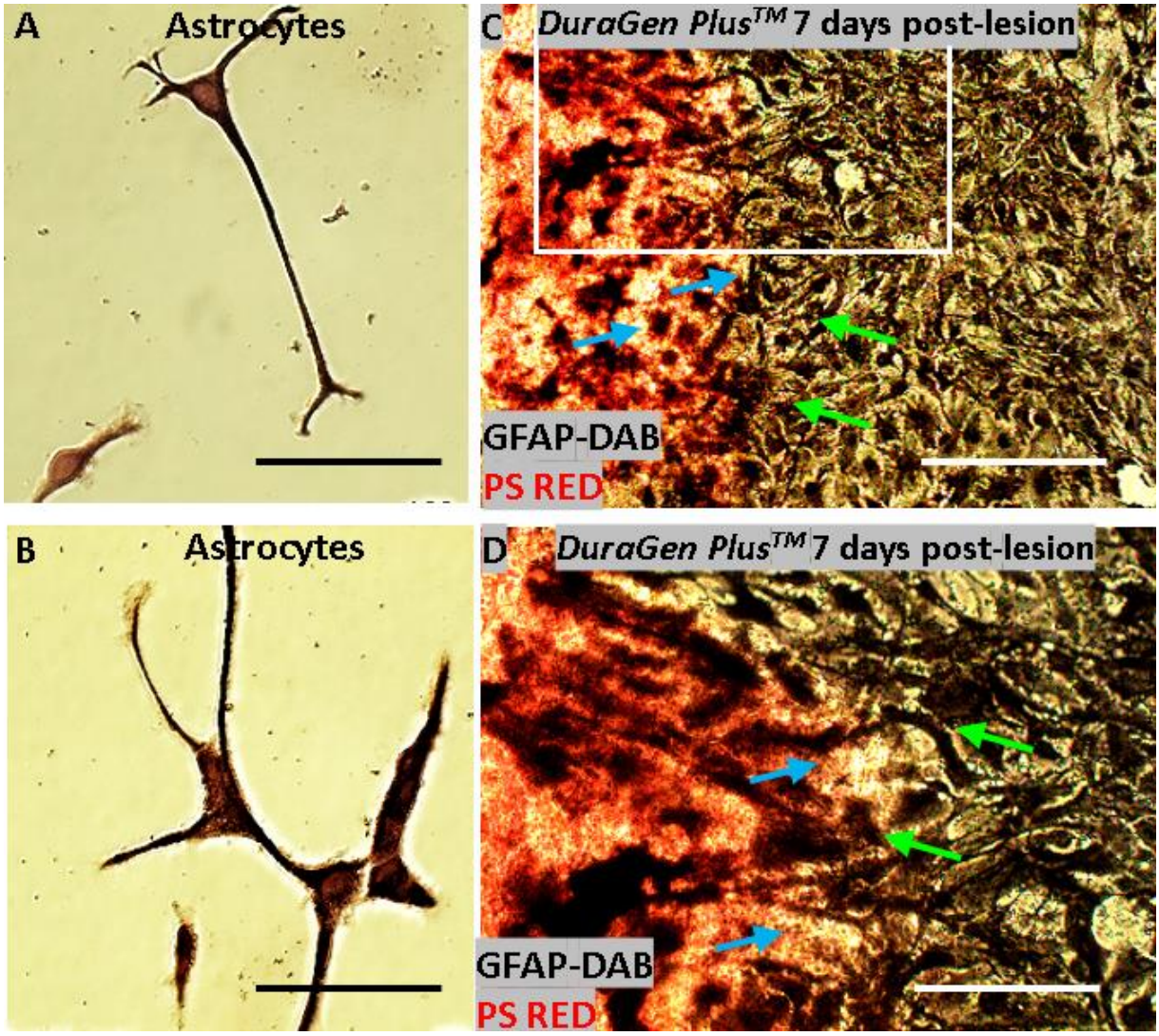

Figure 25: Astrocytes and DuraGen Plus™ were distinguished via the DAB-PS red protocol

A/B: *Brown astrocytes labelled with GFAP-DAB and hydrogen peroxide. The cells were clearly stained and show morphologies associated with astrocytes****. C/D:*** *Black astrocytes (green arrows) labelled with GFAP-DAB and nickel contrast against the red stained (blue arrows) DuraGen Plus™. Moreover, at 7 days post-lesion the astrocytes infiltrated the DuraGen Plus™. A/B: Scale bars: A/B: 25 microns, C: 100 microns, D: 40 microns.*

3.4.9 Pilot data indicated that Model 2 contained all the major neural cell types

The development of an in vitro model containing all of the neural cell types was attempted by establishing mixed-glial cultures in neuronal medium. The pilot data showed that Tuj1 could be used to label neurons within the culture. Two neuronal morphologies were seen; classical long processed neurons ***(figure 26a***, white arrows) and rounded/clumped neurons (***figure 26a***, green arrows). Iba1^{+} cells were consistent with microglial morphologies. Similarly, GFAP^{+} cells were consistent with astrocyte morphologies. In contrast with Model 1 a confluent astrocytic bed layer was not formed. Also, NG2^{+} cells had morphologies consistent with ramified OPCs. On visual assessment it was deemed that the percentage of cell types represented was approximately: neurons 30% (***figure 26a)***, astrocytes 60% ***(figure 26c)***, microglia 5% ***(figure 26b)***, OPCs 5% ***(figure 26d)*** of cells within the culture.

Note: The preliminary evidence supporting the development of Model 2 is provided above. Due to the COVID-19 pandemic and subsequent university shutdown, further datasets could not be generated to validate this finding.

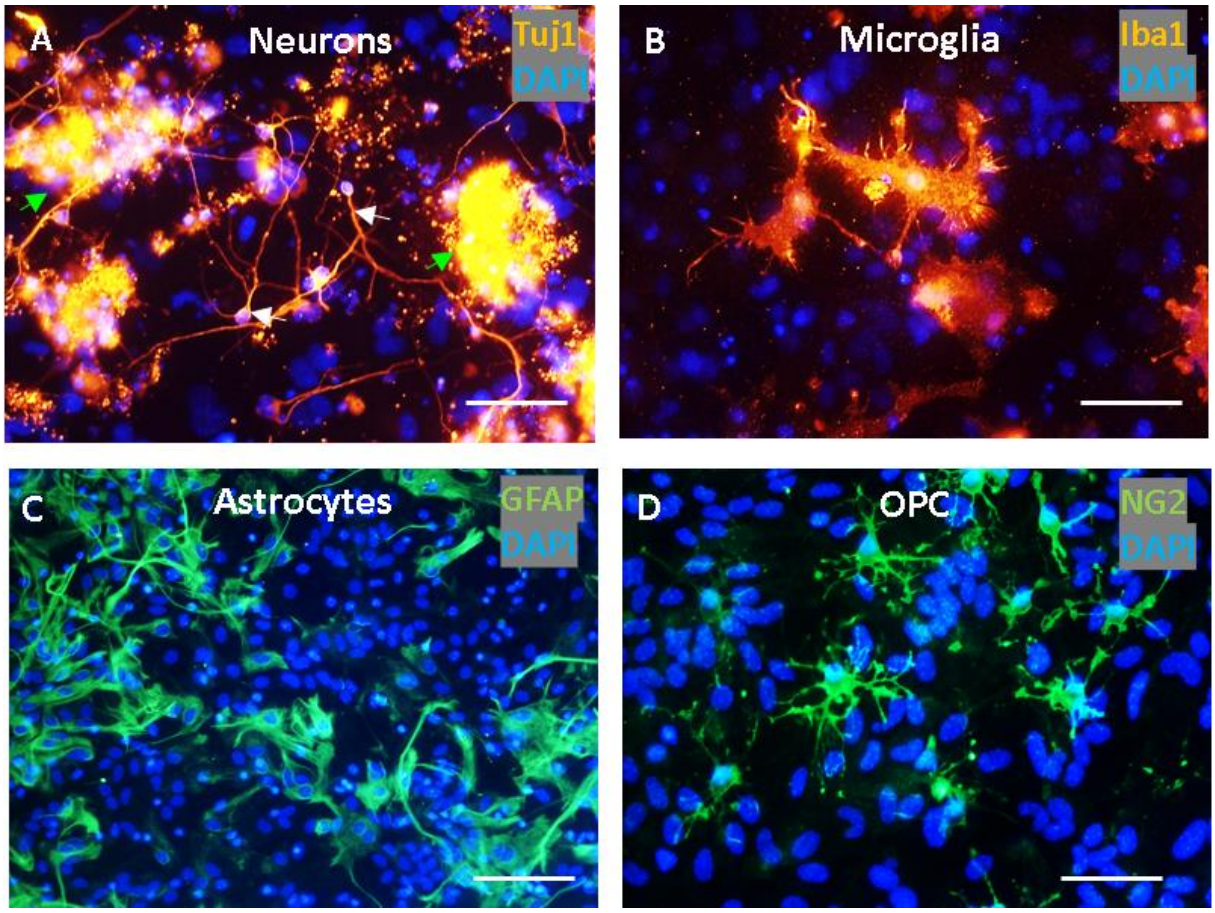

Figure 26: Neuronal medium supported the growth of all neural cell types

A-D: *Representative fluorescence micrographs showing the presence of Tuj1^{+}cells consistent with neuronal morphologies. Note how both rounded (green arrows) and processed neurons (white arrows) were present.* ***B:*** *Representative fluorescence micrographs showing the presence of Iba1^{+} cells consistent with microglial morphologies.* ***C:*** *Representative fluorescence micrographs showing the presence of GFAP+ cells consistent with astrocyte morphologies. Note how the astrocytes were not confluent in this culture.* ***D:*** *Representative fluorescence micrograph showing NG2^{+}cells consistent with ramified OPC morphologies. Scale bars: A, B, D: 50 microns, C: 150 microns. (Pilot data, n=1).*

3.5 Discussion

3.5.1 Successful establishment of a high throughput, multi-glial, in vitro pTBI model

I have developed a novel, high throughput, in vitro injury model capable of supporting implantation of a clinical grade biomaterial into the lesion site, to evaluate cell-biomaterial interactions. As discussed previously, current in vitro models typically use simplistic monocultures containing one glial cell type. This study modifies the original and widely used mixed-glial protocol to culture cells in a micro-well format, allowing high throughput studies on all the glial cell types together, rather than deriving high purity fractions of each individual cell type.

Model 1 develops and stratifies in a very similar manner to the traditional bulk mixed-glial culture. Consistent with previous studies utilising bulk mixed-glial cultures, I found that in Model 1, astrocytes formed a confluent bed layer and represented the majority cell type (>80%) within the culture, followed by microglia and OPCs (153,157). Interestingly, astrocytes also represent the largest population of glia in the CNS, thus indicating that Model 1is neuromimetic with respect to astrocytic representation (160).

With regards to immunolabelling of cells, GFAP, Iba1 and NG2 was successful in labelling astrocytes, microglia and OPCs respectively. Iba1 was chosen preferentially to lectin as lectin seemed to have non-specific, punctate staining of the astrocytic bed layer making it difficult to identify microglia based on the immunostaining alone. Similarly, NG2 was used in preference to A2B5, since A2B5 non-specifically stained all of the cells within the culture, including cells which had clear astrocyte like morphologies. Chen et al (2007) mentions that mouse OPCs do not share all of the cell surface antigens with their rat counterparts such as A2B5 and thus could provide an explanation for this unexpected finding (161).

In addition to this model being high throughput, this model is also facile versus current astrocytic monocultures/neural co-cultures. Simplistic astrocytic monoculture models can take 3-4 weeks to develop, since bulk mixed-glial cultures need to be established prior to isolation and re-seeding of astrocytes (147). In this study, Model 1 is fully confluent and

stratified by day 14. Model 1 is also seeded at a low seeding density of 0.83 x 10^5 cells/ml whilst the astrocytic monoculture models are seeded at high seeding densities (>4 x 10^5 cells/ml), essentially meaning more tissue is needed to generate the same number of coverslips per culture, thus making such models lower throughput overall (147,157).

Furthermore, Model 1 can be processed for live-cell imaging to allow real-time cellular responses to injury and biomaterials in addition to high resolution electron microscopy. I have previously noted that Model 1 can survive up to 38 days in vitro. One criticism of Model 1 is that post-natal tissue tends to be more plastic and pro-regeneration versus adult CNS, thus introducing lesions within the cultures at later time points may provide responses more representative of the adult CNS. Also, Model 1 provides an ideal platform to add additional immune cell types such as peripheral macrophages (56,81,162–165). Like microglia, peripheral macrophages also respond to injury and infiltrate the lesion core of the glial scar. In addition, like microglia, evidence suggests that peripheral macrophages may be beneficial for repair and regeneration post-injury. Thus, adding peripheral macrophages makes Model 1 more neuropathomimetic to in vivo pTBI responses.

3.5.2 A reproducible lesion was introduced into Model 1

I have shown that a transection lesion which mimics the lesion track in pTBI can be introduced in a reliable and facile format. Specifically, I report similar and consistent lesion widths across 4 independent cultures. Researchers have previously used transection methods in in vitro models to mimic in vivo pTBI injury (140). The pipette tip induced lesions in this model resulted in lesions with little remaining intra-lesional cellular debris, and clearly identifiable astrocytic edges. Furthermore, unlike needle/scalpel based lesioning techniques, our lesion did not scratch the glass coverslip. This is an important consideration since glass fragments could influence glial responses whilst the depth and consistency of the scratch could alter the lesion environment along the length of the scratch which could elicit different glial responses.

3.5.3 Biomaterial implantation capabilities in Model 1

To the best of our knowledge, this is the first time an in vitro pTBI model has been adapted to support biomaterial implantation into the lesion within a micro-well format. This chapter has demonstrated a successful protocol for implanting DuraGen Plus™ – a neurosurgical grade biomaterial, within a described lesion. This protocol provides troubleshooting solutions to the inherent difficulties with such a concept i.e. ensuring DuraGen Plus™ remains within the lesion and does not drift upon addition of media. Although DuraGen Plus™ was selected to establish this protocol, additional biomaterials could also be implanted into the lesion to screen regenerative strategies. Furthermore, nanoparticles could be injected into the large, well-defined lesion in Model 1 and thus Model 1 could also be used to test the utility and neural cell responses to nanoparticle additions (section 5.1.2).

3.5.4 Polarizing light microscopy is unsuitable to visualize DuraGen Plus™

Imaging of biomaterials can be challenging, especially within a biological environment, and represents a major challenge for the field of tissue engineering. Polarizing light microscopy has previously been successfully used to visualize collagen containing tissue sections (158). This study showed that DuraGen Plus™ would be unsuitable to visualize under polarizing microscopy due to the lack of consistent birefringence. Two possible explanations include: collagen biomaterials contain disorganized collagen fibres versus the organized parallel collagen fibres found in tissue sections, as a result only microenvironments containing pockets of parallel collagen fibres show birefringence as demonstrated in this study. This could be due to setting the collagen in a mould versus natural collagen production present within tissues. Secondly, generally tissue sections have a greater density of parallel collagen fibres versus the collagen fibres within DuraGen Plus™ and thus shows a more intense birefringence signal.

3.5.5 Successful development of a double histological staining protocol

To the best of our knowledge, this is the first time a double histological staining protocol has been developed which stains cells and collagen biomaterials in different colours allowing clear and distinct visualization of cell-biomaterial responses. In order to develop this protocol common histological staining methods such as H&E were trialled and deemed unsuitable, due to biomaterial staining, thus meaning neither cells nor biomaterials can be distinguished based on colour alone. I have shown that the DAB-PS red protocol allows researchers to counterstain black/brown coloured cells with red coloured biomaterial. This novel protocol offers many advantages to current fluorescent microscopy methods; collagen-specific staining within the biomaterial provides definitive evidence for the presence of the biomaterial versus reliance on auto-fluorescence. In addition, biomaterials which can be histologically stained are cheaper to use, as they do not require specialized dark storage conditions and samples do not fade with time -a major dilemma with fluorescently labelled samples. Furthermore, this protocol is accessible to remote laboratories with basic facilities since because basic light microscopes can be used to image the cell-biomaterial interactions without the need for complex and expensive fluorescent microscopes. Also, this protocol can be modified to support the use of additional dyes and histological stains. Masson's Trichome is a collagen dye which has been widely used to stain tissue sections previously, and thus could be used as a replacement/in addition to picrosirius red.

CSPGs have previously been described (section 1.2.2) as regeneration inhibitors and are present within the glial scar, thus the identification and characterization of such molecules through staining could provide important clues about the glial scar within Model 1. Finally, Model 1 has the capability to study detailed cell-biomaterial interactions and microglial dependent biomaterial biodegradation through live in vitro imaging, a type of microscopy very difficult to utilize in vivo. Although sufficient data was not gathered to evidence this in the thesis due to the COVID-19 pandemic, I have taken the first steps to characterize these cell-biomaterial interactions through time-lapse microscopy.

3.5.6 Promising evidence in favour of a complete neural cell pTBI model

Perhaps one limitation of Model 1 is that the model lacks a neuronal component. This means that axotomy and subsequent glial responses to axonal damage cannot be simulated (the neuronal responses in pTBI has been discussed in detail 1.3.9). In light of this limitation, the first steps have been taken to develop a novel, facile, high throughput injury model which contains all of the major neural cell types. I have shown through a pilot experiment, that the mixed-glial culture system can be established by replacing the D10 medium with a neuronal medium, which supported cultures containing neurons, astrocytes, microglia and OPCs. Although the pilot results seem promising, further experiments and testing is required to replicate this finding and adapt the model to support both a lesion and the capability of biomaterial implantation into the lesion to assess regenerative strategies.

Chapter 4

Characterizing injury responses in the micro-mixed glial injury model (Model 1)

4.1 Introduction

Reactive gliosis is the main glial response to pTBI (see section 1.3.8) (61). Specifically, both reactive microgliosis and astrogliosis have key roles in glial scar formation. Researchers have previously characterised glial responses to traumatic injury through a range of differing methodologies. It is important to simulate some of these responses in order to assess the safety and efficacy of biomaterials intended to treat pTBI.

4.1.1 Methodologies to quantify reactive microgliosis

The glial scar has been described anatomically as two distinct zones; the lesion core and the astrocytic zone (46,65,68). To characterise reactive microgliosis, researchers have previously quantified microglial infiltration into the lesion (66). In addition, researchers have determined whether microglia show stereotypical signs of activation, i.e. amoeboid M1 microglia (see section 1.3.4 for a detailed explanation of the different microglial activation states).

Weightman et al (2014), characterized microglial infiltration into a transecting lesion in organotypic spinal cord slices by counting the number of lectin positive cells within the lesion site of each slice, using a standard size grid overlaid onto each image (143). The total number of microglia per unit area were then quantified at each time point. This methodology provides a facile, yet robust and reliable method to quantify microglial cell density in the lesion areas. Furthermore, Weightman et al found that microglia in the lesion displayed “activated morphologies”, which appeared to be consistent with amoeboid morphologies. Microglia further away from the lesion were ramified characteristic of unactivated morphologies, though these cell responses were not quantified.

Williams et al (2007), determined inflammatory leukocyte infiltration into the lesion in a rat penetrating ballistic brain injury model through morphological H&E staining and it was noted that “large macrophage-like cells“were present. Furthermore, Williams et al, found that in response to injury, microglia became highly ramified and positive for OX-18 (68). In peri-lesional areas, microglia exhibited “immunoreactive processes” and bushy morphologies.

There are considerable limitations with this study. Firstly H&E is a non-specific histological stain and thus the cells within the lesion cannot be accurately identified as microglia, perhaps ICC methods such as Iba1/lectin staining could have been used which would provide stronger evidence in favour of microglial infiltration. Secondly, in contrast to the current literature, Williams et al found that in response to injury microglia increased in ramification. Although this shows that microglial responses can vary according to culture type, and mechanism of injury, amoeboid immunoreactive microglia are typically associated with injury responses. Furthermore, both Weightman et al, and Williams et al did not quantify any morphological changes and thus definitive changes with any statistical significance cannot be determined.

Cernak et al (2014), characterized reactive microgliosis in a mouse pTBI model through Iba1 image densitometry (39). Here, the staining intensity per pixel is characterized. Such a methodology is limited, as one cannot determine whether any changes are due to changes in microglial number, shape or size, rather an overall readout of how bright an image is given. Thus, quantifying both the microglial number and morphology separately could provide stronger evidence of microgliosis.

4.1.2 Methodologies to quantify reactive astrogliosis

Resting and processed astrocytes respond to injury by undergoing reactive astrogliosis (62). Here, astrocytes become reactive and hypertrophic and upregulate intermediate filament proteins such as GFAP. Morphologically, palisading astrocytes have been considered as a hallmark of the glial scar. Here, astrocytes align and extend long thin processes towards the lesion, eventually the thin processes entangle. ICC and histological methods of staining typically show reactive astrocytes with increased staining intensity versus non-lesioned astrocytes. Currently, researchers aim to quantify the increased staining intensity through a variety of methodologies.

Cernak et al (2014) characterized reactive astrogliosis in the peri-lesional area by quantifying the image densitometry of GFAP staining intensity across timepoints (1 day, 3 days and 7

days post-lesion). This methodology allows GFAP immunoreactivity to be measured across conditions and timepoints. There are considerable limitations however, with regards to determining the effect of GFAP immunoreactivity when the biomaterial is added; here cells contacting the biomaterial needs to be compared to distal cells not in contact with the biomaterial. As a result, the image densitometry methodology is unsuitable when quantifying the GFAP immunoreactivity change in responses to biomaterial addition.

Weightman et al (2014) characterized reactive astrogliosis by determining GFAP optical density in organotypic spinal cord slices 0-350 microns away from the lesion edges (143). Optical density measures were then averaged and grouped for every 100 microns away from the lesion edge. The groups were then compared across conditions. The Weightman et al study provides a useful methodology to compare the change in GFAP immunoreactivity within each lesion. Furthermore, this methodology is useful for Model 1 since it determines whether biomaterial addition has any effect on GFAP immunoreactivity, since comparisons between the astrocytes at the edge of the lesion in contact with the biomaterial and distal astrocytes can be made.

Furthermore, as mentioned previously in response to injury astrocytes undergo marked morphological changes. Most studies currently do not quantify these morphological changes, rather comment on the morphologies. For instance, Weightman et al noted that in the peri-lesional area reactive astrogliosis was noted by astrocytes possessing hypertrophic soma and thick processes, whilst astrocytes distal to the lesion were found to have “normal polygonal” morphologies.

Bardehle et al (2013) is one of the few studies which has quantified astrocytic morphologies in response to traumatic injury (70). Bardehle et al determined that in response to an in vivo stab injury, astrocytes within 300 microns of the stab wound became palisading astrocytes with polarizing astrocytic morphologies and marked process extension towards the lesion site. Thus, in order to quantify this response, astrocytic processes were measured and compared to the astrocytic processes at 0 days post lesion. Bardehele et al found processes

extended up to 111 microns in length and astrocytes at 3-5 days post-lesion had a 3-fold greater length of processes versus astrocytes at 0 days post-lesion. However, there are inherent difficulties when applying this methodology to Model 1. In Model 1, the dense network of extended intertwined astrocytic processes makes counting, drawing and measuring such cells on analysis platforms such as ImageJ challenging and inaccurate, as each process must be linked to the corresponding astrocytic soma. Thus, a more generalised form of analysis which provides data on the overall morphological astrocytic changes is required.

4.1.3 Methodologies to quantify OPC responses to traumatic injury

The lesion core of the glial scar primarily contains fibroblasts, microglia and OPCs (***figure 6***). Previous studies have demonstrated that much like microglia, OPCs become activated, proliferate and infiltrate the lesion and peri-lesional area (79,81,83). Specifically, oligodendrocytes are highly susceptible to neural damage and depend on OPC differentiation and maturation to replace lost oligodendrocytes. Thus, characterizing this infiltration is crucial. Hampton et al characterized OPC infiltration into the peri-lesional area in a cortical stab wound injury model (82). Here, NG2 positive cells were counted only where a cell body and nucleus could be identified. Cell counts were recorded in 0.01mm^2 standardized squares, which were placed adjacent to the lesion core. Buffo et al determined OPC infiltration into the peri-lesional area of a cortical stab wound by counting the number of Olig2 positive cells in a 200,000-micron^2 standardised grid, placed at the edge of the lesion (83). The values were then then expressed as cells/mm^2 to allow comparisons across experimental groups (83). The methodology described here is similar to the methodology used by Weightman et al to determine microglial infiltration and provides an unbiased method to characterize cellular infiltration.

4.2 Aims and objectives

The establishment of novel, high throughput, multi-glial in vitro model capable of supporting biomaterial implantation has been described in chapter 3. This chapter aims to characterize the glial responses to injury/biomaterial implantation and determine whether such a model is pathomimetic to pTBI. The specific objectives for this chapter are as follows:

I. Characterize the astrocytic, microglial and OPC responses to the lesion in Model 1.
II. Characterize the astrocytic, microglial and OPC responses to the DuraGen Plus™ insert within the lesion site in Model 1.

4.3 Results

4.3.1 Peri-lesional astrocytes upregulated GFAP immunoreactivity in response to injury

It was anticipated that any upregulation of GFAP near the lesion would be evident as being elevated compared to more distal regions. GFAP immunoreactivity was measured in peri-lesional astrocytes (astrocytes within the first 100 microns of the astrocytic edge) and more distal astrocytes (101-500 microns away from the astrocytic edge). All data were normalised to the values for 401-500 microns (this region is hereafter referred to as the 'distal lesion astrocytes'), within the same micrograph, and so expressed as fold-change versus 401-500 microns. Uninjured control cultures showed no significant differences in GFAP immunoreactivity across 10 adjacent 100 micron regions of the culture (no lesion is present, so no astrocytic edge exists; 0 microns is an arbitrary location), indicating that there is little variation in GFAP intensity across control cultures (***figure 27a-b***). In response to injury, this study found a significant difference in the GFAP immunoreactivity fold-change between peri-lesional astrocytes at 1 day (1.58 ± 0.12 normalised optical density fold-change) and 7 days post-lesion (1.69 ± 0.25 normalised optical density fold-change) than distal astrocytes at either timepoint (1.00 ± 0.00 normalised optical density fold-change ; 401-500 microns; ***figure 27c***). Astrocytes at 101-200 microns, 201-300 microns, 301-400 microns away from the astrocytic edge at 1 and 7 days post-lesion also displayed a fold-change in GFAP immunoreactivity versus distal astrocytes, but no statistical significance was found ($p>0.05$, one-way *ANOVA* with Tukey's post-hoc analysis, n=3).

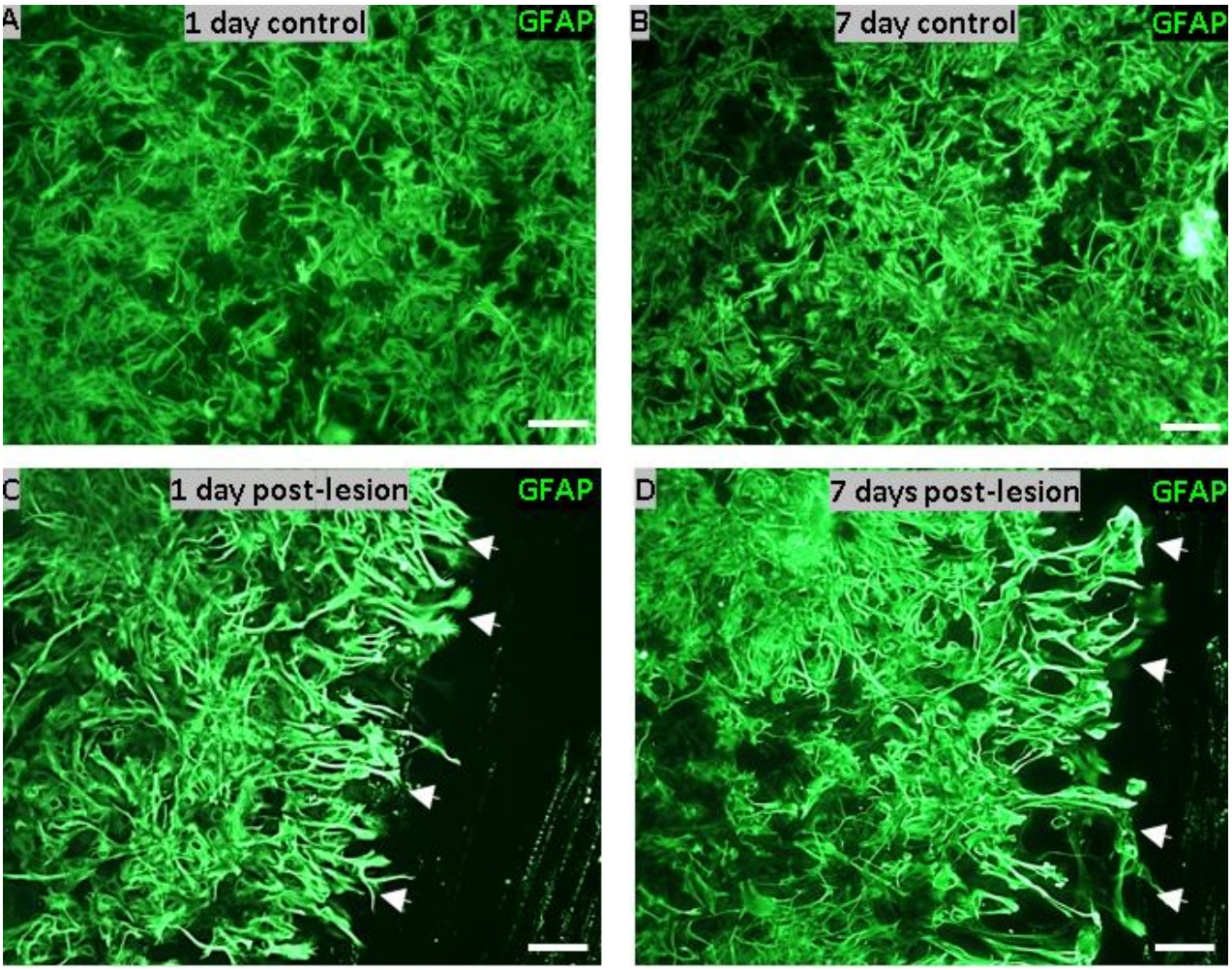
A
1 day control
GFAP
B
7 day control
GFAP
C
1 day post-lesion
GFAP
D
7 days post-lesion
GFAP

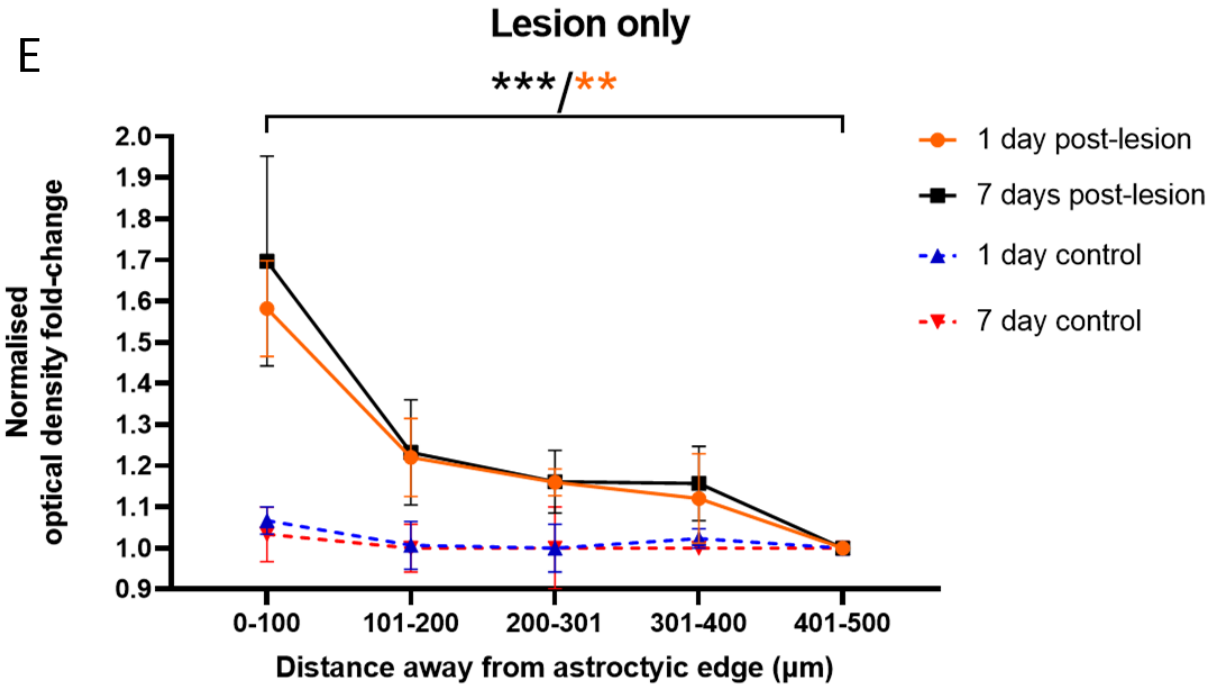
E
Lesion only
***/**
Normalised optical density fold-change
2.0
1.9
1.8
1.7
1.6
1.5
1.4
1.3
1.2
1.1
1.0
0.9
0-100
101-200
200-301
301-400
401-500
Distance away from astroctyic edge (µm)
1 day post-lesion
7 days post-lesion
1 day control
7 day control

Figure 27: GFAP immunoreactivity was elevated at the astrocytic edge

A-B: *Representative fluorescence micrographs at 1 day and 7 day GFAP positive control cultures.* ***C-D:*** *Representative fluorescence micrographs of lesioned GFAP positive cultures at 1 day and 7 day post lesion. The arrows indicate the marked morphological changes and GFAP immunoreactivity difference at the astrocytic edge.* ***E:*** *The graph shows that the fold change in normalised optical density is greater within 100 microns of the astrocytic edge, at both 1 day and 7 days post-lesion (versus 401-500 microns away from the astrocytic edge; 1 day post-lesion: **p<0.01, 7 day post-lesion: *** p <0.001, one-way ANOVA with Tukey's post-hoc analysis, n=3). Scale bars: 100 microns.*

4.3.2 DuraGen Plus™ implantation into the lesion did not attenuate scarring responses

The fold-change in GFAP immunoreactivity between peri-lesional astrocytes and distal astrocytes in DuraGen Plus™ treated cultures was compared to the fold-change in lesion only cultures (***figure 28e and figure 27e***) to determine astrocytic responses to DuraGen Plus™. Similar to the result described in 4.3.1, this study found a significant difference in GFAP immunoreactivity in DuraGen Plus™ treated astrocytes in the peri-lesional area at 1 day (1.48 ± 0.13 normalised optical density fold-change) and 7 days (1.51 ± 0.23 normalised optical density fold-change) post-lesion versus distal lesional astrocytes (1.00 ± 0.00 normalised optical density fold-change) (***figure 28e***). However, no significant difference in the fold-change GFAP immunoreactivity between peri-lesional astrocytes in lesion only cultures at 1 and 7 days post-lesion (1.58 ± 0.12 normalised optical density fold-change) / (1.69 ± 0.25 normalised optical density fold-change) and DuraGen Plus™ treated cultured at 1 and 7 days post-lesion (1.48 ± 0.13 normalised optical density fold-change) / (1.51 ± 0.23 normalised optical density fold-change), ($p>0.05$, one-way *ANOVA* with Tukey's post-hoc analysis, $n=3$). This result indicated that DuraGen Plus™ implantation into the lesion neither attenuates nor aggravates astrocytic scarring responses.

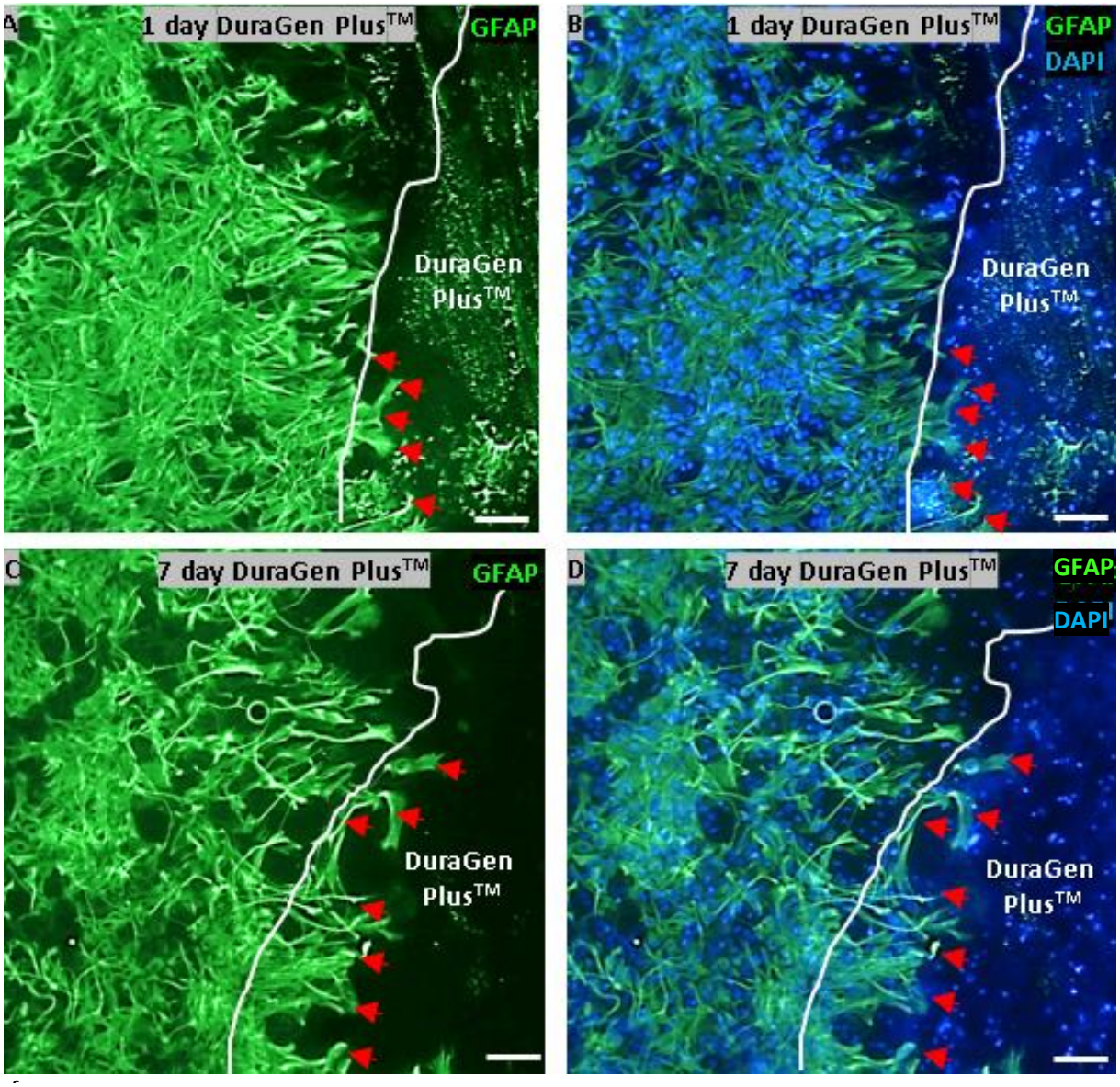

DuraGen Plus™ Treatment

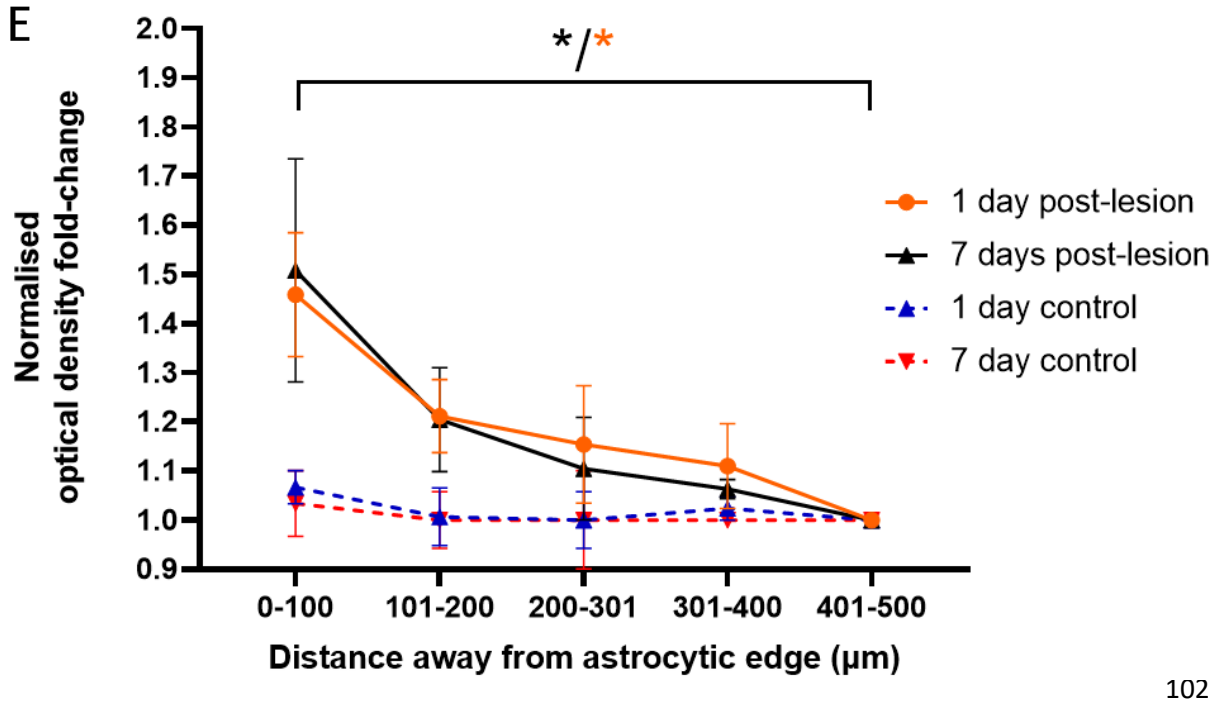

Figure 28: DuraGen Plus™ interfacing astrocytes upregulated GFAP immunoreactivity at the astrocytic edge

A-D: *Representative fluorescent micrographs showing DuraGen Plus™ treated lesions. The arrows indicate where the astrocytes have extended long processes and infiltrated the biomaterial.* ***C/D:*** *DAPI-GFAP double merged fluorescent micrographs provided to show DuraGen Plus™ location with respect to the astrocytic edge.* ***E:*** *The graph shows that the normalised fold-change in optical density is significant at both 1 day and 7 days post-lesion, between 0-100 microns away from the astrocytic edge and 401-500 microns away from the astrocytic edge (1 day post-lesion: *p<0.05, 7 days post-lesion: *p<0.05, one-way ANOVA with Tukey's post-hoc analysis, n=3). Scale bars: 100 microns.*

4.3.3 Astrocytes responded to injury by extending aligned processes perpendicular to the lesion

In response to injury astrocytes underwent marked morphological changes (***figures 27c/d, figure 28c/d***). Here astrocytes became hypertrophic and extended long processes towards the lesion/biomaterial indicating the formation of a palisading astrocytic zone. On visual assessment, astrocytes tended to extend long processes perpendicularly to the lesion. Due to the high density of intertwined processes, identifying and measuring individual astrocytic processes was deemed unreliable. Thus, a new form of analysis was attempted to determine whether the general astrocytic morphologies could be characterized (see section 2.5.4). The directionality analysis on ImageJ was used to determine whether astrocytes within an image displayed alignment. The images shown in ***figure 27c/d*** and ***figure 28a/c*** were analysed. The automated analysis plugin represents any alignment preference (directionality) by displaying a graph with peaks, the peak indicating the angle at which the alignment preference is identified. Whilst, no alignment preference (equal representation for every direction) is represented by a straight horizontal line with no peak.

Lesion only and biomaterial treated peri-lesional astrocytes were represented on the graph as a curve with a peak indicating an alignment preference, whereas distal lesional astrocytes were represented with a straight line indicating random alignment (***figure 29a-d***).

A

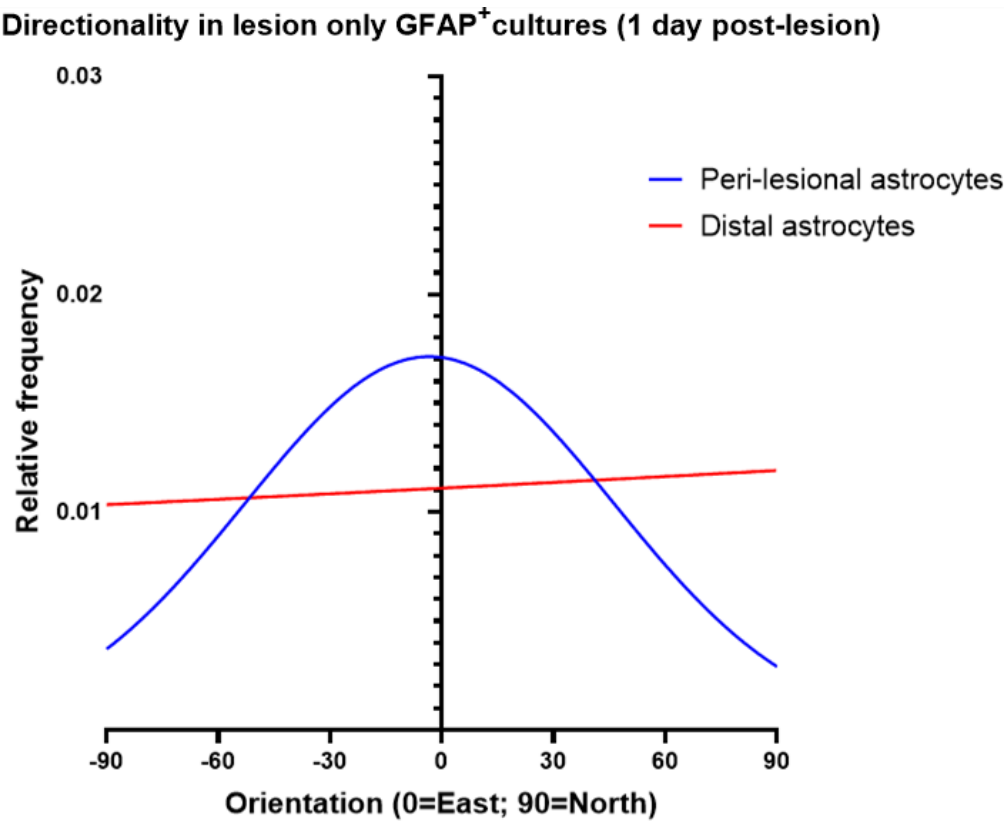
Directionality in lesion only GFAP+cultures (1 day post-lesion)
0.03
0.02
0.01
Relative frequency
Peri-lesional astrocytes
Distal astrocytes
-90
-60
-30
0
30
60
90
Orientation (0=East; 90=North)

B

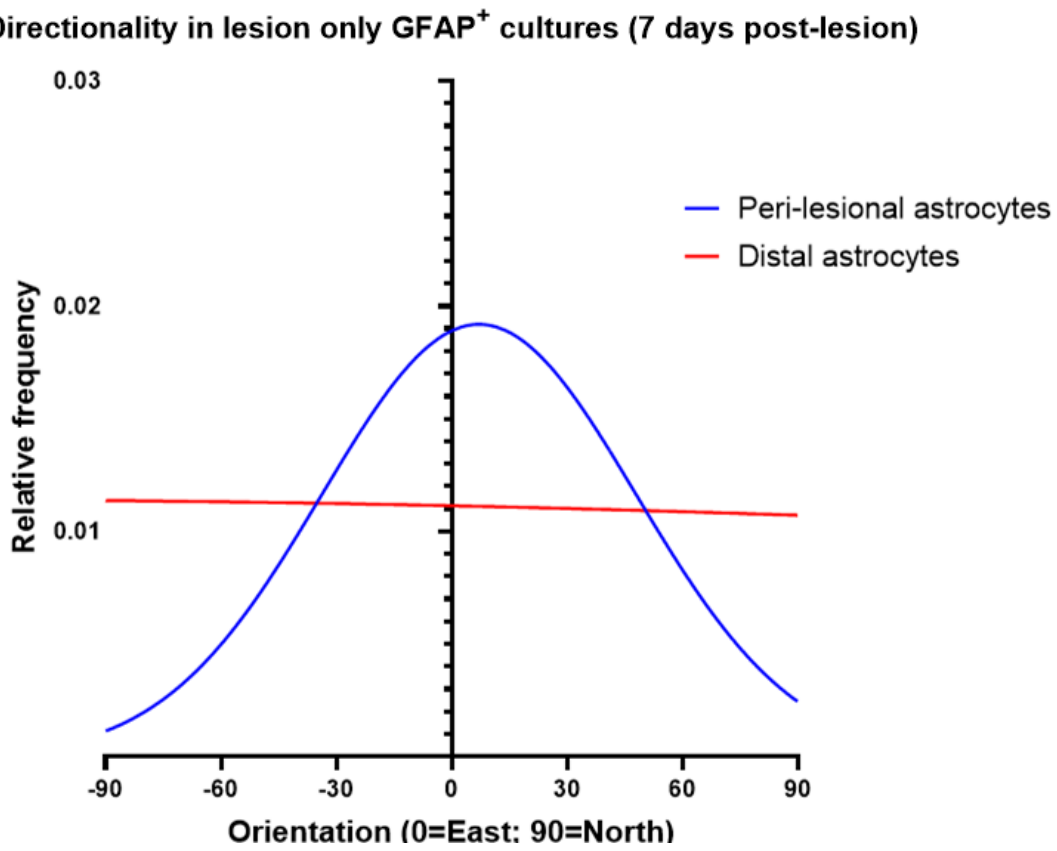
Directionality in lesion only GFAP+ cultures (7 days post-lesion)
0.03
0.02
0.01
Relative frequency
Peri-lesional astrocytes
Distal astrocytes
-90
-60
-30
0
30
60
90
Orientation (0=East; 90=North)

C Directionality in DuraGen Plus™ treated GFAP+ cultures (1 day post-lesion)

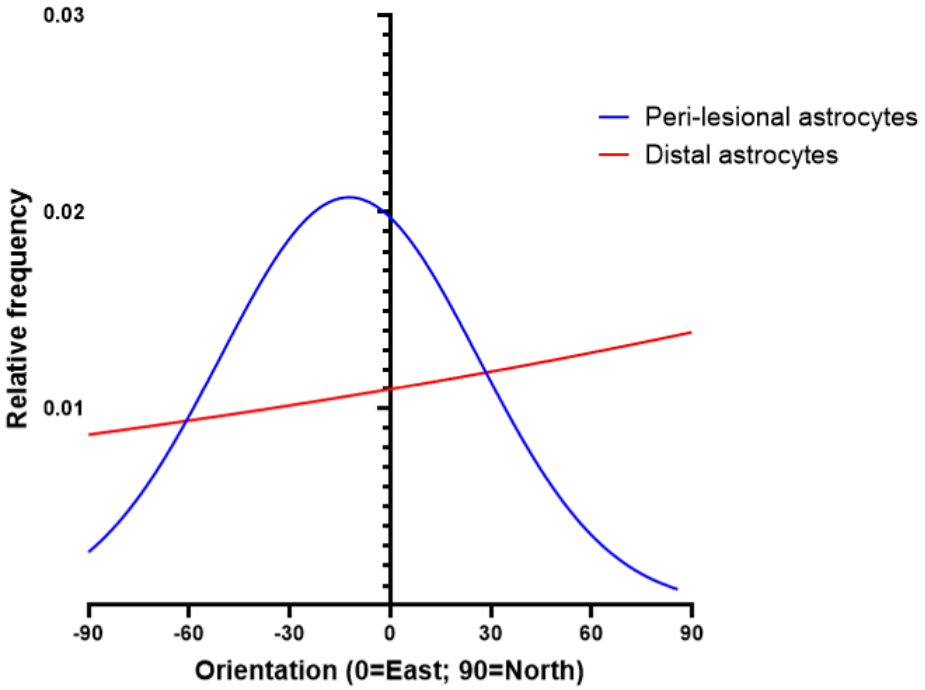

D Directionality in DuraGen Plus™ treated GFAP+ cultures (7 days post-lesion)

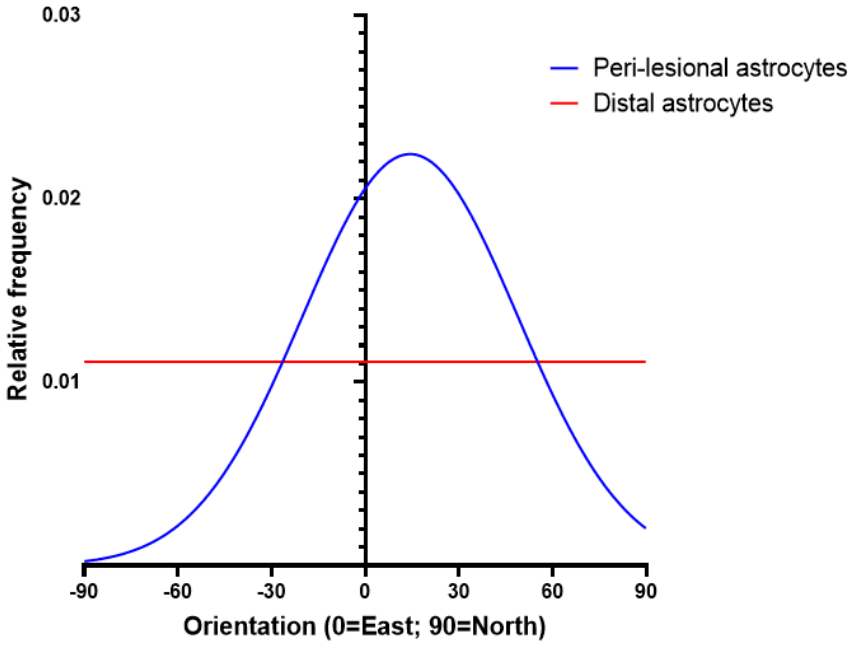

Figure 29: Images of peri-lesional astrocytes displayed an alignment preference towards the lesion versus images of distal astrocytes

A-D: *The graphs indicate that regardless of time-point and biomaterial addition, micrographs of astrocytes within the first 100 microns from the astrocytic edge display alignment which is indicated by a large peaked curve, whilst images of astrocytes 401-500 microns from the astrocytic edge display an even frequency across all orientations, and are represented by a straight line with no peak, (n=3).*

4.3.4 Microglia and OPCs infiltrated both the lesion and DuraGen Plus™

The number of microglia/OPCs per unit area was determined across time-points to determine whether these glial cell types infiltrated the lesion core in Model 1. Significantly greater numbers of microglia infiltrated the lesion core at 7 days post-lesion (82.04 ± 5.11 cells/mm^2) than 1 day post-lesion (37.48 ± 7.54 cells/mm^2; $p<0.05$, one-way *ANOVA* with Tukey's post-hoc analysis, *n=3*; ***figures 30a-b, figures32a***). Similarly, significantly greater numbers of OPCs infiltrated the lesion core at 7 days post-lesion (45.72 ± 9.08 cells/mm^2) than1 day post-lesion (1.65 ± 1.62 cells/mm^2) than, $p<0.05$, one-way *ANOVA* with Tukey's post-hoc analysis, *n=3*) (***figure 34a-c***).

The number of microglia per unit area within the DuraGen Plus™ was also determined to allow comparisons with the numbers of cells/unit area within the lesion core in lesion only cultures. Significantly greater numbers of microglia infiltrated the DuraGen Plus™ at 7 days post-lesion (132.41 ± 15.83 cells/mm^2) versus lesion only cultures at 7 days post-lesion (82.04 ± 5.11 cells/mm^2), $p<0.05$, one-way *ANOVA* with Tukey's post-hoc analysis, *n=3*) (***figures 31a-d,figures 32a***). Also, significantly more microglia infiltrated the DuraGen Plus™ at 7 days post-lesion (132.4 ± 15.83 cells/mm^2) versus 1 day post-lesion (55.35 ± 17.44 cells/mm^2) (***figures 31a-d, figures 32a***, $p<0.05$, one-way *ANOVA* with Tukey's post-hoc analysis, *n=3*). There was evidence to suggest that OPCs also infiltrated the DuraGen Plus™ and adopted rounded morphologies with very few processed cells (***figure 34a-d***).

4.3.5 Microglia predominately adopted amoeboid morphologies in the lesion and DuraGen Plus™

To determine microglial morphology within the lesion/DuraGen Plus™ microglia were classified as ramified or amoeboid (section 2.5.6). This study found that microglia infiltrating the lesion predominately had amoeboid morphologies at 1 day post-lesion (74.3 ± 5.5%) versus ramified morphologies (25.7 ± 5.5%) (***figure 30a-b, figure 32a***). Similarly, at 7 days post-lesion microglia predominately had amoeboid morphologies (70.3 ± 2.2%) versus ramified morphologies (29.7 ± 2.2%). Similarly, microglia predominately had amoeboid morphologies in the DuraGen Plus™ at 1 day post-lesion (79.8± 4.0%) versus ramified morphologies (20.2 ± 4.0%), ***(figure 31a-d, figure 32b***), $p<0.001$, one-way *ANOVA* with Tukey's post-hoc analysis test, *n=3*). At 7 days post-lesion microglia also predominately had amoeboid morphologies in the DuraGen Plus™ (76.4 ± 9.1%) versus ramified morphologies (23.6 ± 9.1%) (***figure 31a-d, figure 32b***), $p<0.001$, one-way *ANOVA* with Tukey's post-hoc analysis test, *n=3*).

4.3.6 OPCs adopted ramified morphologies in the lesion and evidence of rounded morphologies in DuraGen Plus™

On visual observation it was noted that the majority of OPCs seemed to have many processes within lesion only cultures, thus were classified as ramified (3 or more processes) or bipolar/unipolar/unprocessed (2 processes or less) (***figure 33a-b***). This study found that in lesion only cultures OPCs were predominately ramified (***figure 33d***) at both 1 day post lesion (79.6 ± 7.8%) and 7 days post-lesion (81.4 ± 5.4%), $p<0.001$, one-way *ANOVA* with Tukey's post-hoc analysis test, *n=3*).

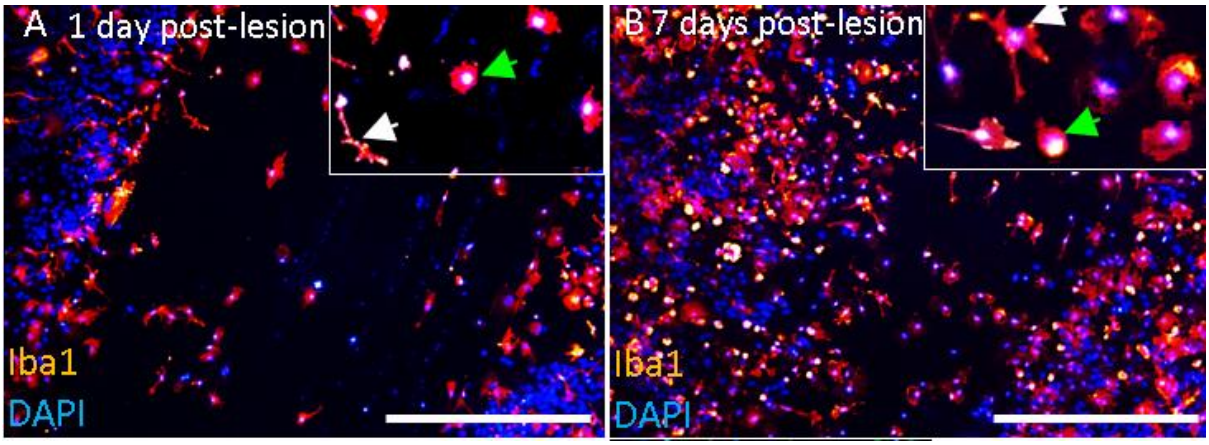

Figure 30: Increased microglia infiltrated the lesion core at 7 days post-lesions versus 1 day post-lesion

A: *Representative fluorescence micrographs showing early evidence of microglial infiltration at 1 day post-lesion.* ***B:*** *Representative fluorescence micrographs showing increased microglial infiltration at 7 days post-lesion. Note the inset images show that microglia are predominately amoeboid in morphology (green arrow) versus ramified (white arrow). Scale bars: 500 microns.*

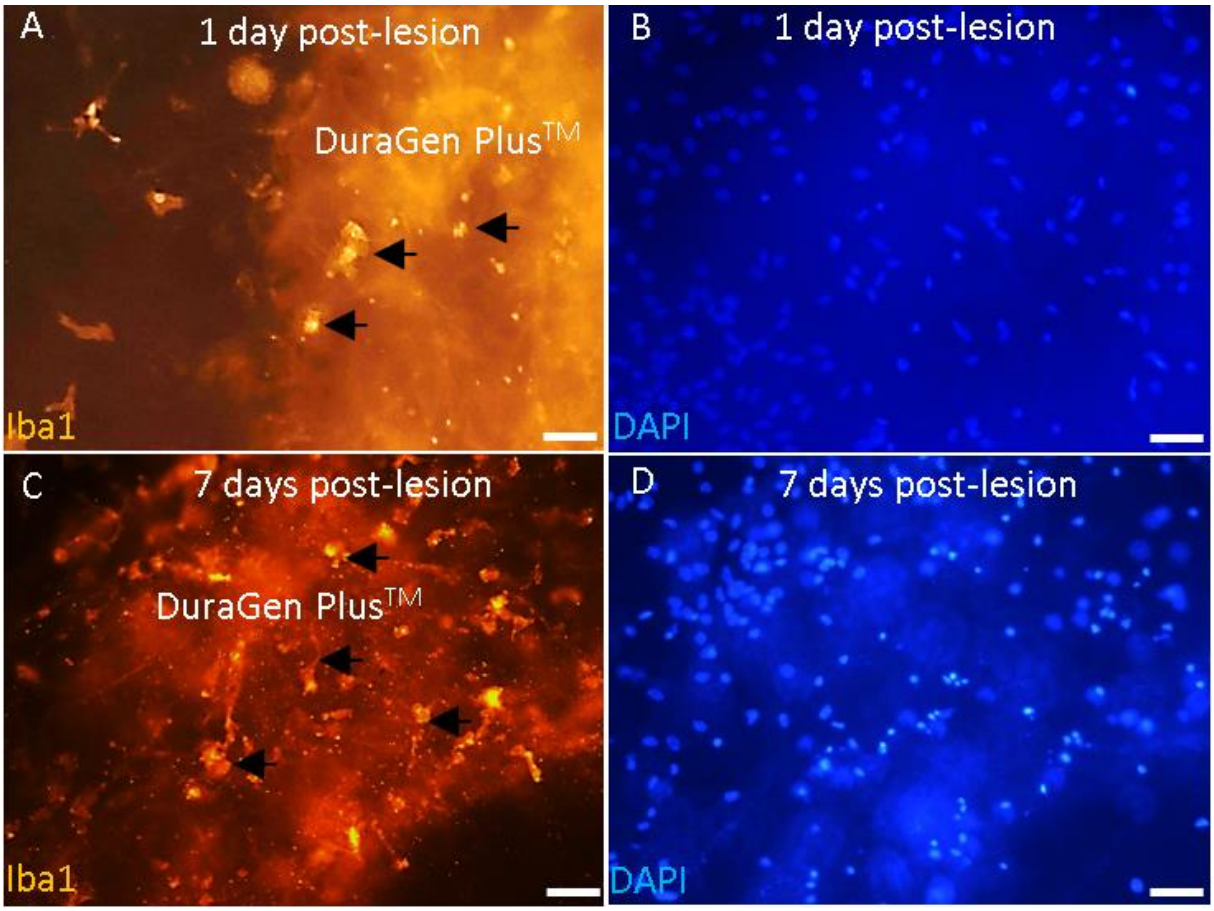

Figure 31: Increased microglia infiltrated the DuraGen Plus™ 7 days post-lesion compared to 1 day post-lesion.

A: *Representative fluorescence micrographs showing early evidence of microglial infiltration into the DuraGen Plus™ at 1 day post-lesion.* ***B:*** *DAPI counterpart for A.* ***C:*** *Representative fluorescence micrographs showing increased microglial infiltration into the DuraGen Plus™ at 7 days post-lesion.* ***D:*** *DAPI counterpart for C. Scale bars: 100 microns.*

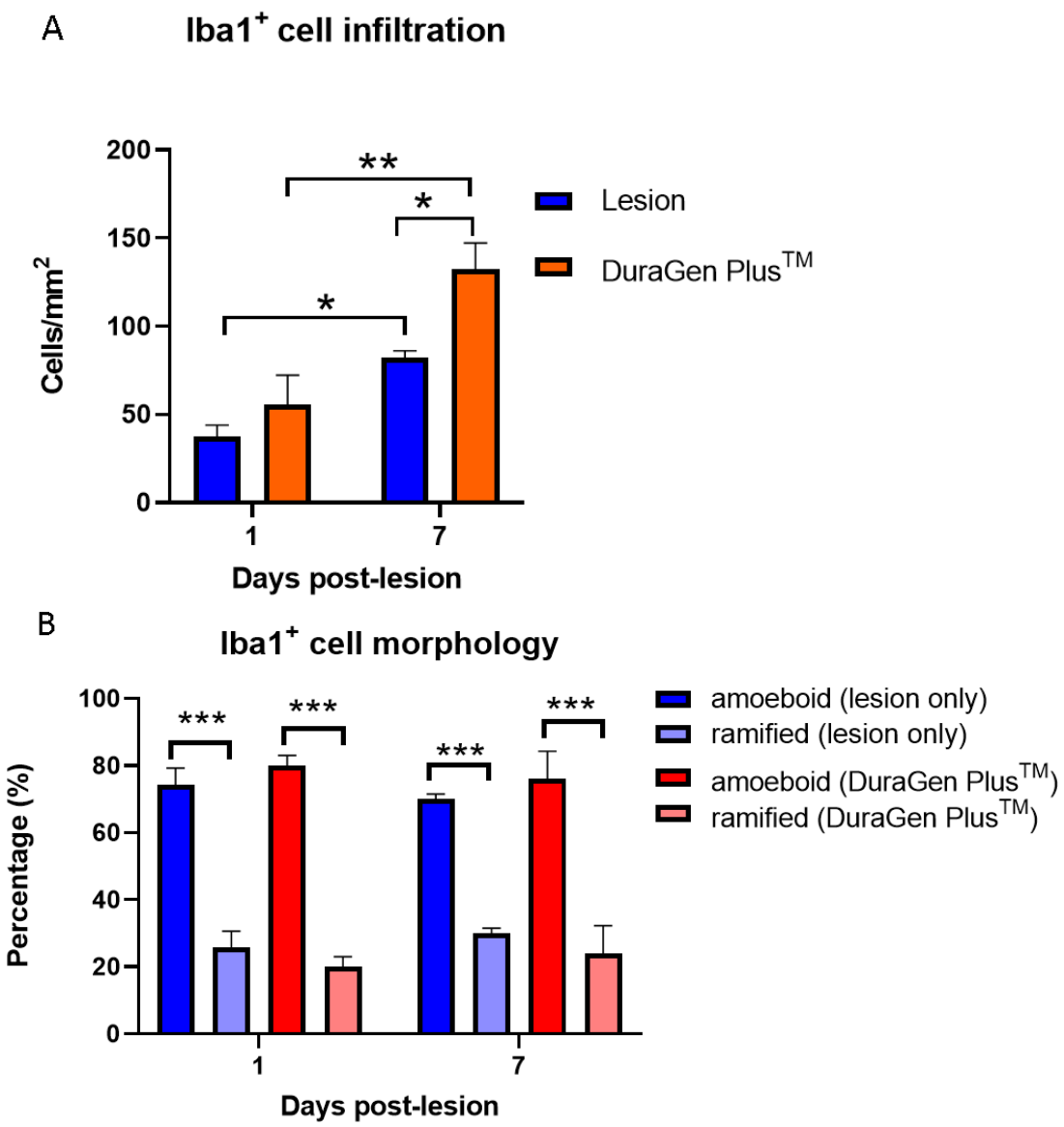

Figure 32: Iba1⁺cells infiltrated the lesion core and DuraGen Plus™

A: *The graphs shows significantly more Iba1+ cells in lesion only cultures at 7 day post lesion versus 1 day post lesion. Furthermore, there were significantly more Iba1⁺ cells in the DuraGen Plus™ at 7 days post-lesion versus 1 days post-lesion. Finally, there were significantly greater Iba1⁺ cell infiltration into DuraGen Plus™ versus lesion infiltration at 7 days post-lesion (*p<0.05; **p<0.01; one-way ANOVA with Tukey's post-hoc analysis, n=3).*

B: *The graph shows significantly more amoeboid Iba1+ cells in the lesion versus ramified at both 1 day and 7 days post-lesion. There were significantly more amoeboid cells in the DuraGen Plus™ insert at both 1 and 7 days post-lesion (***p<0.001, one-way ANOVA with Tukey's post-hoc analysis, n=3).*

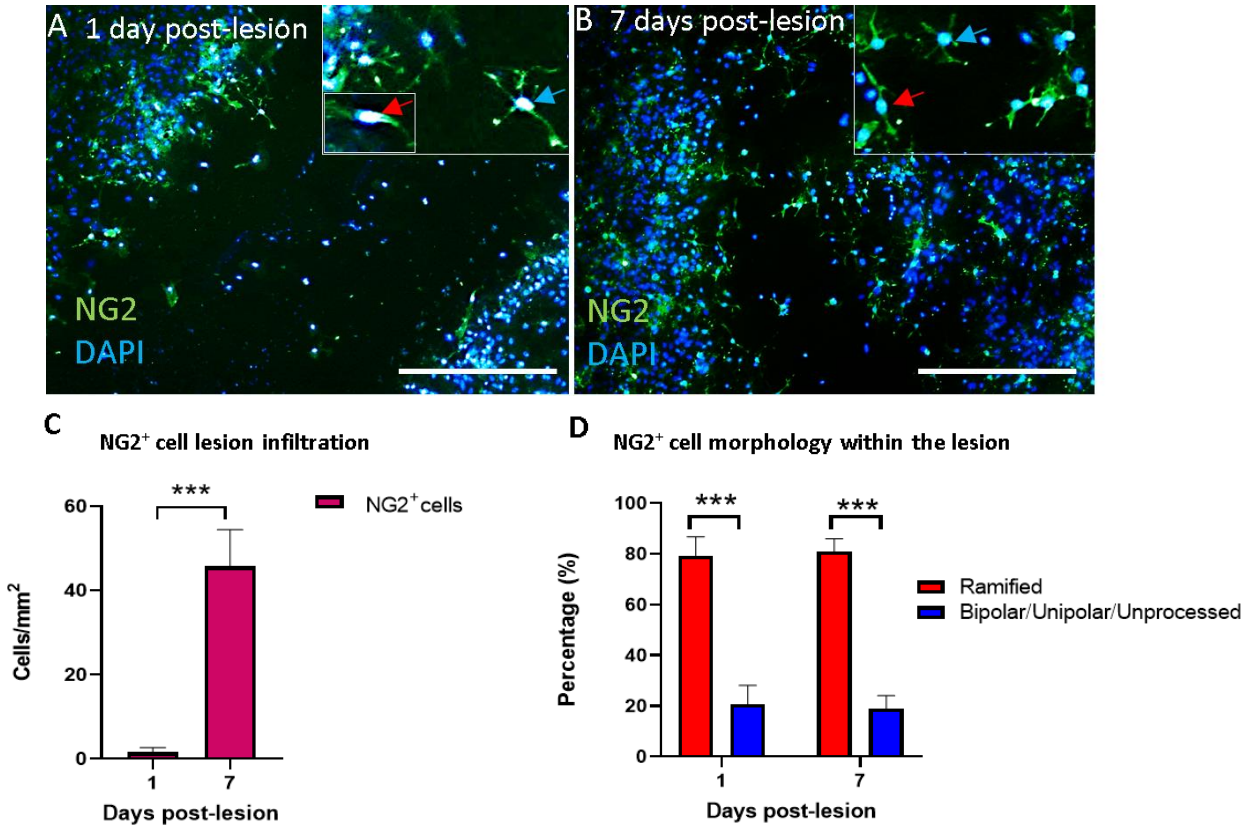

Figure 33: Increased OPCs infiltrated the lesion core at 7 days post-lesion versus 1 day post-lesion

A: *Representative fluorescence micrographs showing early evidence of OPC infiltration at 1 day post-lesion.* ***B:*** *Representative fluorescence micrographs showing increased OPC infiltration at 7 days post-lesion. The corresponding inset images show examples of ramified (blue arrow) and bipolar (red arrow) OPC morphologies.* ***C:*** *The graphs show significantly more NG2$^+$ cells within the lesion at 7 days post-lesion versus 1 day post-lesion.* ***D:*** *The graphs shows significantly more ramified cells in the lesion versus bipolar/unipolar/unprocessed cells in the lesion at both 1 and 7 days post-lesion. Scale bars: 500 microns. (p-value for *** = p<0.001 unless otherwise stated, one-way ANOVA with Tukey's post-hoc analysis, n=3).*

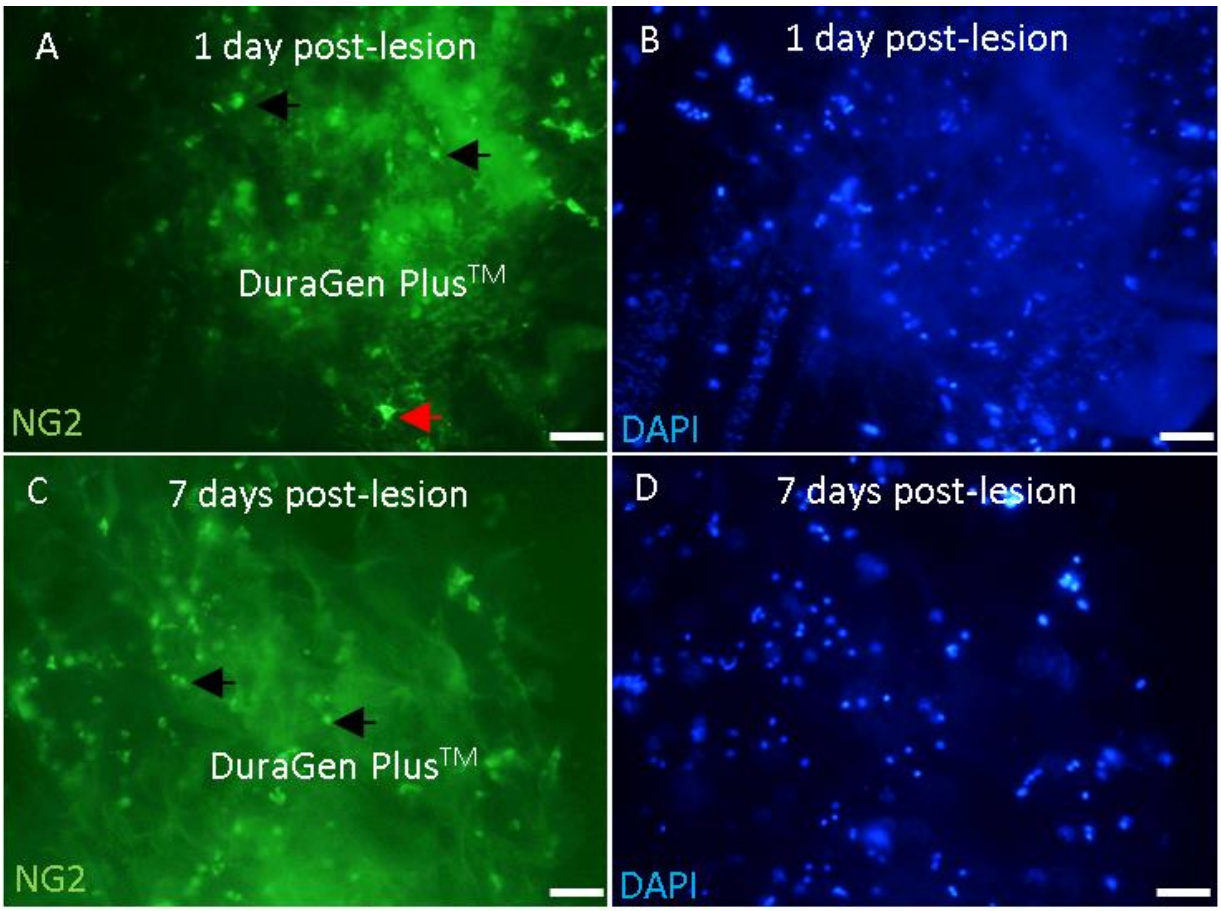

Figure 34: OPCs infiltrated the DuraGen Plus™ and adopted rounded morphologies

A: *Representative fluorescence micrographs showing rounded OPC morphologies in the DuraGen Plus™* at *1 day post-lesion.* ***B:*** *DAPI counterpart for A.* ***C:*** *Representative fluorescence micrographs showing predominately rounded OPC morphologies (black arrows) in the DuraGen Plus™ versus processed (red arrows) at 1 day post-lesion.* ***D:*** *DAPI counterpart for C. These images were deemed unsuitable for quantification, due to the difficulty in visualizing the cells. Scale bars: 75 microns.*

4.4 Discussion

I have developed a novel, facile, multi-glial injury model which can screen biomaterials for clinical applications. Experimental studies investigating regenerative strategies rely heavily on animal models, and biological replicates in double digit numbers are the norm. I consider that the in vitro Model 1 can contribute significantly to the Reduction and Refinement animal models. I have previously seeded mixed-glial cultures in 5 x 24 well plates at a concentration of 0.83 x 10^5 cells/ml derived from 8 P1-P3 mouse cortices, which became confluent by day 14 and were ready to support lesions/biomaterial implantation. This means 60 different biomaterials can be screened and directly compared to one another at any one time (in addition to 60 lesion only control coverslips). Thus, Model 1 is **high throughput** and can be used to screen multiple biomaterials at the same time prior to in vivo testing. Interestingly, mixed-glial cultures have previously been derived from human brain tissue (166). However, like rodent models, these cultures have predominately been established in bulk culture format. Ray et al has successfully cultured a human-neuronal glia model in vitro in a micro-well format (167). Here, neurons and glia could be observed from day 20 in vitro. Thus, like Model 1, human mixed-glial cultures have the potential to be established in a micro-well format. A human micro-mixed glial model has a major advantage; human cells, would provide a neuropathomimetic platform to human in vivo cellular responses. To develop the Ray et al model further, application of the lesion and biomaterial implantation protocols set out in this thesis could provide a human neuron-glia model to study the regenerative properties of relevant biomaterials.

If Model 1 is demonstrated to be pathomimetic for features of pTBI, Model 1 will provide a first-line screening system for promising regenerative therapies prior to animal experimentation. This study showed that peri-lesional astrocytes upregulated GFAP as compared to distal astrocytes in response to a transecting lesion both 1 day and 7 days post-lesioning. This finding is in-line with previous studies; GFAP upregulation in response to injury is considered a hallmark of the glial scar. The mouse pTBI model developed by Cernak et al (2014) showed that peak GFAP upregulation in response to injury was observed at 72

hours post-lesion with GFAP upregulation persisting 7 days post-injury (39). The finding of significantly increased GFAP upregulation at 1 days post-lesioning is expected from the literature on in vivo responses, as often cells react rapidly to injury. Specifically, the Williams et al rat pTBI model showed upregulated GFAP by 6 hours-post injury (68). The organotypic SCI model developed by Weightman and colleagues found significantly increased GFAP upregulation within the first 100 microns away from the lesion in response to transection, with fluorescent intensity measures decreasing as distance away from the lesion increases, a finding replicated by our study (143). The findings from the current study are therefore consistent with these observations.

Due to the distinct palisading astrocytic morphologies, potentially the upregulated GFAP could be explained due to greater GFAP localization within the outstretched astrocytic processes, whilst the overall amount of GFAP within the astrocytes remains constant. Since the optical density of GFAP was measured across 500 microns into the culture from the lesion edge, such a phenomenon would have already been taken into account and would not yield a difference in the normalised optical density fold-change as seen in Model 1.

Previously, studies have shown that astrocytes infiltrate biomaterials, and bridge the lesion (126). This study found that astrocytes infiltrated the DuraGen Plus™ and that there was no significant difference between the GFAP upregulation in peri-lesional astrocytes in lesion only and DuraGen Plus™ treated cultures. This indicated that DuraGen Plus™ neither disrupted nor aggravated glial scarring with respect to the astrocytic responses. Furthermore, this result showed that DuraGen Plus™ implantation into Model 1 did not damage the astrocytes and thus aggravate the reactive astrogliosis responses, providing evidence that the biomaterial implantation protocol is reliable.

There was a concern that astrocytic GFAP upregulation could be due to the intralesional cells being displaced on top of the peri-lesional cells, thus falsely elevating GFAP. Although this may be of concern within other culture systems there is very little to no evidence to suggest that this is the case within Model 1. Firstly, on a glass coverslip, PDL helps to

adhere cells to the glass coverslip. Within Model 1 upon lesioning it would be extremely unlikely that the cells would be displaced onto the peri-lesional area and adhere on top of the cells. It is much more likely that the lesioned cells float within the medium and are removed during the medium replacement step. Secondly, it is clear from figure 27 C and D, that astrocytes have clear palisading morphologies in the peri-lesional area, whilst control cells do not adopt these morphologies. If the cells did displace, then one would expect control like morphologies with no palisading activation within the peri-leisonal area, however this is not seen. In addition, it is clear that GFAP is upregulated within the palisading astrocytic processes and is localized here. If cell displacement did occur, one would not expect palisading astrocytic morphologies and certainly not expect black gaps between well-defined GFAP positive astrocytic processes. Finally, from figure 22b it is clear the numbers of nuclei at the edge of the lesion are similar throughout the coverslip (except within the lesion), thus if cells had displaced onto the lesion edge this would be associated with a greater concentration of DAPI positive nuclei accordingly.

I have shown that in response to injury, astrocytes underwent significant morphological changes. In particular, hypertrophy of astrocyte soma, extension of astrocytic processes and astrocytic alignment perpendicularly to the lesion. These astrocytic responses are analogous to the palisading astrocytes which are considered a hallmark of the glial scar in vivo (70,71). This study found that the general palisading astrocytic responses seen in Model 1 can be represented and quantified through a directionality analysis. There are however considerable limitations with this methodology. Indeed, this protocol enables researchers to broadly characterize palisading astrocytes, however it cannot provide nor compare the lengths of astrocytic processes across experimental conditions. Furthermore, comparisons across experimental conditions such as with DuraGen Plus™ treated cultures cannot be made since the graphs simply indicate whether an alignment is detected. One solution to this, is to perhaps obtain TEM images, of the palisading astrocytes, here individual astrocytes should be identifiable and thus the measurements of astrocytic processes extension can be viewed in context with the directionality analysis allowing cross condition analysis.

I have shown that microglia infiltrated the lesion core, as early as 1 day post-lesion with significantly more microglia infiltration at 7 days post-lesion. Furthermore, significantly more microglia within the lesions were morphologically amoeboid versus ramified. This finding is in line with the current literature; Cernak et al that cortical microglia remained activated up to 7 days post-injury, a finding replicated in a rat pTBI model, previously developed by Cernak and colleagues. Furthermore, Weightman et al (2014) found that microglia also infiltrated the lesion, with peak microglial levels detected at 5 days post-lesion and adopted amoeboid morphologies, a finding similar to ours. Evidence both for and against microglial infiltration into the lesion as an inhibitory step to regeneration exists in the current literature. Microglia have been implicated as inhibitors of axonal regeneration via the expression of inhibitory guidance molecules such as netrin-1 (143). However previous studies also indicate that initial microglial infiltration into the lesion helps to clear cellular debris which is inhibitory to axonal regeneration (15,53,65). Secondly, the microglial role in astrocytic activation has also been described as a key step in glial scar formation, preventing healthy cells to be exposed to inhibitory molecules and cellular debris within the lesion core (64).

Also, I have demonstrated that significantly more microglia infiltrated the DuraGen Plus ™ than the lesion after 7 days post-lesioning. Furthermore, in the DuraGen Plus ™ the microglia predominately had amoeboid morphologies versus ramified. This result shows that DuraGen Plus™ an ultrapure, FDA approved biomaterial which is branded as biocompatible, biodegradable and minimally immunogenic, may not be as ‘minimally immunogenic’ as is claimed by the company. Currently, little is known whether transient microglia infiltration into biomaterials is beneficial or detrimental. It is postulated that microglial infiltration into biomaterials and subsequent enzymatic breakdown of the hydrogels influence biodegradability. However further research such as high-level gene profiling studies is needed to determine whether microglial infiltration into the DuraGen Plus™ is beneficial or detrimental to repair.

I also demonstrated that OPCs infiltrated the lesion, with significantly more OPC infiltration 7 days post lesion versus 1 day post-lesion and adopted. Our study showed that very few

OPCs were in the lesion site at 1 day post-injury (81). This could potentially be explained by a loss in OPC number due to the toxic, acute lesion environment. In particular, proteolytic enzyme release from necrotic cells can damage cells. Furthermore, activated microglial release of free radicals, pro-inflammatory cytokines and glutamate has been shown to promote oligodendrocyte loss (81). Previously, studies have demonstrated that OPCs infiltrate the lesion and peri-lesional area, here OPCs can differentiate into oligodendrocytes to replaces dead cells (81). In addition, this study showed, that the cells in the lesion had ramified morphologies indicating that the lesion environment did not affect OPC maturation from 1 day post-lesion to 7 days post-lesion. The presence of OPCs in the biomaterial could be explained by OPCs preferentially migrating into a less toxic environment versus the lesion alone which contains some cellular debris. This may also be explained by a preference to infiltrate a softer biomaterial in comparison to a relatively hard glass coverslip. Interestingly, our study also showed that OPCs adopted rounded morphologies within the biomaterial. This is a surprising finding, however Russel et al previously demonstrated that OPCs incorporated into a PEG hydrogel adopted spheroid morphologies similar to the morphologies seen in this study and thus OPCs may be less likely to mature into oligodendrocytes within the DuraGen Plus™ than the lesion alone (168). One possible explanation is that DuraGen Plus™ is a relatively soft biomaterial. Previous studies have demonstrated that OPCs cultured inside soft hydrogels display “round morphologies with very few spreading processes” whilst OPCs on medium stiffness hydrogels resemble the processed OPCs seen within the host CNS (169).

One possible limitation of this model is that the cells which have been associated as infiltrating the biomaterial, may be underneath it and thus there needs to be consideration to whether this model should be classified as a 2D or 3D model. With regards to biomaterial infiltration, it is also not possible to rule out that cells infiltrate underneath the biomaterial and then grow upwards into the biomaterial. DuraGen Plus™ is a 3D collagen matrix with a porous structure and thus supports bilateral cellular movement within the hydrogel. In addition, there is evidence both for and against classifying Model 1 as 3D. Firstly, the

astrocytes initially adhere to the coverslips and eventually become confluent with additional glial cell types including the microglia and OPCs eventually appearing on top of the astrocytic bed layer. Thus, based on this, the mixed-glial culture is multi-cellular and to some extent a 3D culture system. Indeed, this model is not as 3D as organotypic brain slice cultures nor in vivo brain tissue, thus given these discrepancies further research and investigation is required determine whether this model is truly 3D.

4.4.1 Model 1 replicates foreign body reactions to neural implants

In addition, Model 1 could provide researchers with a novel, in vitro model to study the foreign body reaction to neural implants. The reactive gliosis and OPC responses seen in Model 1 allows this model to be used to study not only implants in the context of pTBI, but also the foreign body reaction to microelectrodes. Implantable microelectrodes have been used in the management of traumatic and neurodegenerative pathologies. However,

although this intervention shows promise, specifically the glial cell responses at the injury site to BBB dysfunction and neuronal death results in failure of the implant over time (***figure 35***).

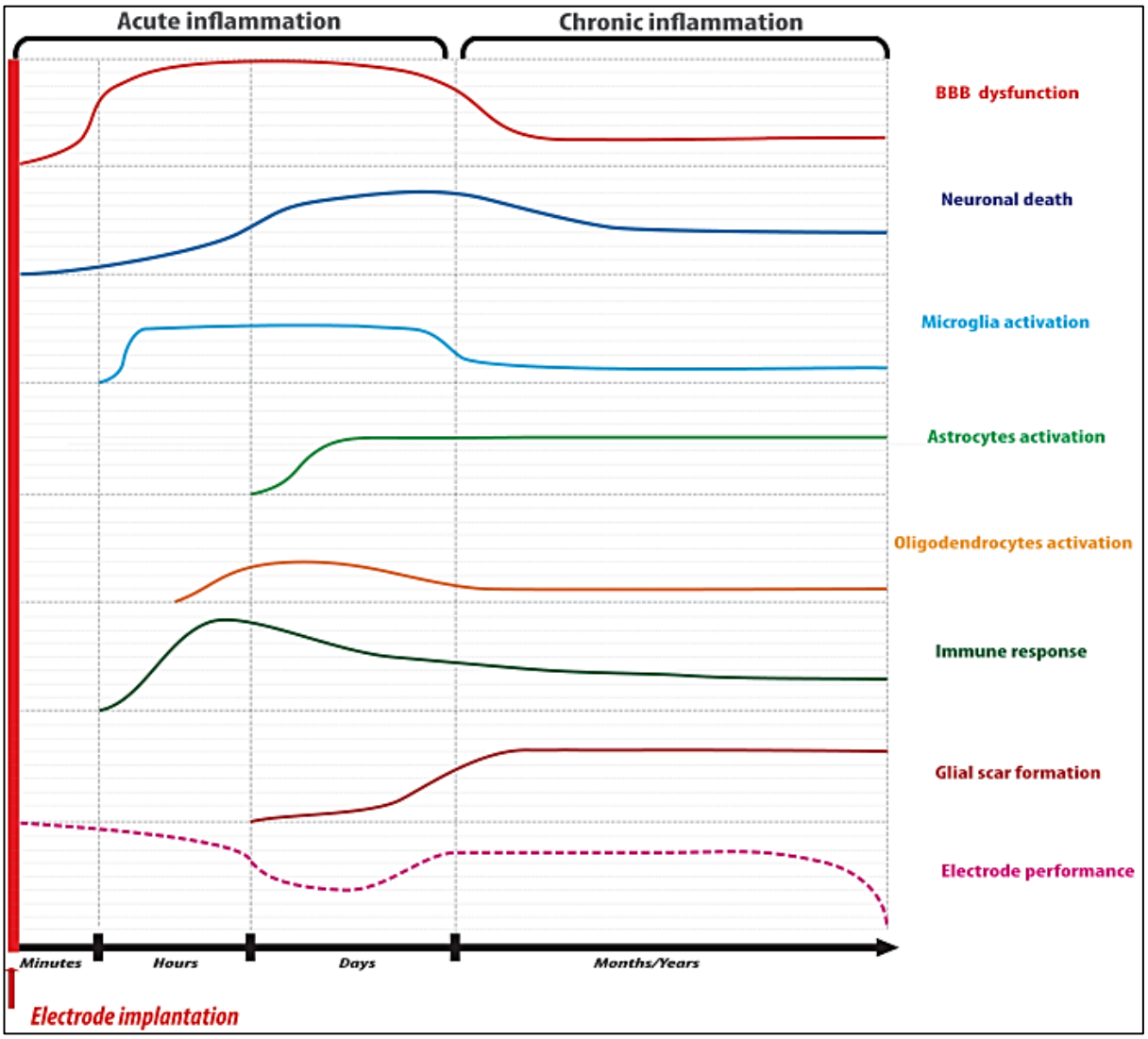

Figure 35: A schematic displaying how neural cell responses to microelectrodes correlates with subsequent electrode performance (170)**.**

Gulino et al mentions that in response to a foreign body, astrocytes extend long processes and upregulate GFAP, while microglia are acutely activated and are responsible for the secretion of pro-inflammatory cytokines, phagocytosis of cellular debris and astrocyte/oligodendrocyte cross talk (102,170). Oligodendrocyte cell death occurs at the implantation site, OPCs migrate towards the implant where they can differentiate into astrocytes. After 2 weeks, the glial scar matures, here astrocyte process extension contacts

the implant forming a non-permeable barrier (to cells) between the implant and tissue. Fibroblasts then secrete ECM proteins such as fibronectin, type IV collagen, laminin and CSPGs, further encapsulating the microelectrodes. This forms an “insulation” barrier which hampers electrophysiological performance due to the absence of contact between the electrode and neurons, thus leading to implant failure. Although Model 1 cannot replicate BBB dysfunction and neuronal death, the glial responses could be replicated. Early evidence indicates that Model 2 contains a neuronal component and thus could provide a more neuromimetic model, of greater value for testing electroactive biomaterials, especially those intended to stimulate neuronal cells. Furthermore, macrophages, fibroblasts and additional cell types can be added to Model 1 which in conjunction with the astrocytes could attenuate the formation of an insulation barrier to microelectrodes.

Chapter 5

Future direction and concluding comments

5.1 Summary of key thesis findings

I have shown that Model 1 is a capable of supporting biomaterial implantation into lesion sites to assess regenerative strategies. Specifically, I have shown:

- In response to injury peri-lesional astrocytes upregulate greater amounts of GFAP versus distal lesional astrocytes and that DuraGen Plus^{TM} implantation did not significantly alter these responses.
- Microglia infiltrate both the lesion and DuraGen Plus^{TM} and appear to adopt amoeboid morphologies.
- OPCs infiltrate the lesion core and early evidence of DuraGen Plus^{TM} infiltration.
- The development of a novel, double histological staining protocol, which enables researchers to visualize cell-biomaterial interactions through simple light microscopy.
- The first steps have been taken to develop a neuronal model, which contains all of the neural cell types available in a micro-well format.

5.1.2 The future direction for this research

I have developed a protocol which enables researchers to implant biomaterials into a lesion within a micro-well format. Although, this study implanted DuraGen Plus^{TM}, additional biomaterials could also be implanted and screened within the model. Furthermore, I found a novel and interesting finding: an FDA approved, neurosurgical grade biomaterial DuraGen Plus ^{TM} is preferentially infiltrated by the major immune cell type of the CNS; the microglia. This raises considerable questions specifically with regards to whether such biomaterials can be classified as immunogenic, minimally immunogenic or cytotoxic. Whether microglial infiltration was transient in nature or due to the immunogenic profile of DuraGen Plus^{TM}, remains in question. In the future, detailed gene profiling and expression studies to determine whether the microglia inside the biomaterial upregulate or downregulate key immunological markers such as pro-inflammatory cytokines and select matrix metalloproteinases (45,60,103,171). Furthermore, this study could provide a model for detailed live in vitro biomaterial degradation and biodegradability studies, as it is likely that

biomaterial biodegradability profiling is subject to microglial infiltration and enzymatic breakdown of the biomaterials.

Researchers have successfully transplanted neural cells in biomaterial constructs in animals to promote regeneration and repair in lesioned CNS (79,90,105). However, the majority of these studies, have tested laboratory grade and unapproved biomaterial constructs. Finch et al has shown that transplant populations such as NSC and astrocytes have high viability and retain their differentiation potential in DuraGen Plus™. However, the viability of these cells was assessed in a non-injury environment. Thus, neural cell laden DuraGen Plus™ constructs could be implanted into Model 1 to determine whether the injury environment, and microglial infiltration into the biomaterial, affects transplant cell morphology and differentiation potentials, and thus whether such a concept could be considered for clinical translation. In addition, previously clinical -grade magnetic nanoparticles have been successfully incorporated within the neural transplant populations with biomaterial constructs (172). Non-invasive magnetic resonance imaging can then be used to track transplant populations. Model 1 could easily be adapted to test the uptake, toxicity and efficacy of nanoparticles. Furthermore, nanoparticle laden transplant populations could be incorporated within biomaterial matrices and implanted into the lesion in Model 1 to determine their functional efficacy.

The pilot study in this thesis shows that a neuronal-glia model can be developed and requires further experiments to reproduce this finding. Furthermore, given the same experimental formats as Model 1, Model 2 could also be adapted to support a lesion and biomaterial implantation into lesion sites to assess regenerative strategies.

5.2 Concluding comment

I have developed a novel, in vitro TBI model in which the regenerative potential of biomaterials can be assessed. This model could provide a higher throughput and more ethically viable platform to screen neuroregenerative therapies prior to in vivo animal experimentation enabling the identification of key regenerative biomaterials/strategies, with the ultimate aim of clinical translation.

Bibliography

1. Hyder AA, Wunderlich CA, Puvanachandra P, Gururaj G, Kobusingye OC. The impact of traumatic brain injuries: A global perspective. NeuroRehabilitation. 2007;22(5):341–53.

2. American Association of Neurological Surgeons: Traumatic brain injury [Internet]. 2020. Available from: https://www.aans.org/en/Patients/Neurosurgical-Conditions-and-Treatments/Traumatic-Brain-Injury

3. Vella MA, Crandall M, Patel MB, Surgery AC, Sciences S, Care SC, et al. Acute management of TBI. Surg Clin North Am. 2017;97(5):1015–30.

4. Ren Z, Iliff JJ, Yang L, Yang J, Chen X, Chen MJ, et al. 'Hit & Run' model of closed-skull traumatic brain injury (TBI) reveals complex patterns of post-traumatic AQP4 dysregulation. J Cereb Blood Flow Metab. 2013;33(6):834–45.

5. Chapman JC, Diaz-Arrastia R. Military traumatic brain injury: A review. Alzheimer's Dement [Internet]. 2014;10(3):S97–104. Available from: http://linkinghub.elsevier.com/retrieve/pii/S155252601400140X

6. Infographic B. https://www.brainline.org/slideshow/infographic-leading-causes-traumatic-brain-injury.

7. Van Wyck DW, Grant GA. Penetrating Traumatic Brain Injury: A Review of Current Evaluation and Management Concepts. J Neurol Neurophysiol. 2015;06(06).

8. Okidi R, Ogwang DM, Okello TR, Ezati D, Kyegombe W, Nyeko D, et al. Factors affecting mortality after traumatic brain injury in a resource-poor setting. BJS Open. 2019;320–5.

9. Al. D et. Pathophysiology of battlefield associated traumatic brain injury. Pathophysiology. 20:23–30.

10. Gutiérrez-González R, Boto GR, Rivero-Garvía M, Pérez-Zamarrón Á, Gómez G. Penetrating brain injury by drill bit. Clin Neurol Neurosurg. 2008;110(2):207–10.

11. Oehmichen M, Meissner C, König HG. Brain injury after survived gunshot to the head: Reactive alterations at sites remote from the missile track. Forensic Sci Int. 2001;115(3):189–97.

12. Mckee A. military TBI. Alzheimers Dement [Internet]. 2014;10(3 0):S242-53. Available from: http://www.ncbi.nlm.nih.gov/pubmed/24924675%0Ahttp://www.pubmedcentral.nih.gov/articlerender.fcgi?artid=PMC4255273

13. Waterhouse C. The Glasgow Coma Scale and other neurological observations. Nurs Stand (Royal Coll Nurs (Great Britain) [Internet]. 2005; Available from: https://www.semanticscholar.org/paper/The-Glasgow-Coma-Scale-and-other-neurological-Waterhouse/ec2dd592fb06d22e55071311c96f850611e281d3

14. Article O. A Comparative Study of Injury Severity Scales as Predictors of Mortality in Trauma Patients: Which Scale Is the Best? 2020;8(1):27–33.

15. Simon DW, McGeachy M, Bayir H, Clark RSB, Loane DJ, Kochanek PM. Neuroinflammation in the Evolution of Secondary Injury, Repair, and Chronic Neurodegeneration after Traumatic Brain Injury. Nat Rev Neurol. 2017;13(3):171–91.

16. Mena JH, Sanchez AI, Rubiano AM, Peitzman AB, Sperry JL, Gutierrez MI, et al. Effect of the modified glasgow coma scale score criteria for mild traumatic brain injury on mortality prediction: Comparing classic and modified glasgow coma scale score model scores of 13. J Trauma - Inj Infect Crit Care. 2011;71(5):1185–93.

17. Majdan M, Steyerberg EW, Nieboer D, Mauritz W, Rusnak M, Lingsma HF. Glasgow coma scale motor score and pupillary reaction to predict six-month mortality in patients with traumatic brain injury: Comparison of field and admission assessment. J Neurotrauma. 2015;32(2):101–8.

18. Xiong Y, Mahmood A, Chopp M. Current understanding of neuroinflammation after traumatic brain injury and cell-based therapeutic opportunities. Chinese J Traumatol - English Ed [Internet]. 2018;21(3):137–51. Available from: https://doi.org/10.1016/j.cjtee.2018.02.003

19. ATLS-RCS [Internet]. Available from: https://www.rcseng.ac.uk/education-and-exams/courses/search/advanced-trauma-life-support-atls-provider-programme/

20. Bakir A, Temiz C, Umur S, Aydin V, Torun F. High-velocity gunshot wounds to the head: Analysis of 135 patients. Neurol Med Chir (Tokyo). 2005;45(6):281–7.

21. Radiopaedia [Internet]. Available from: https://radiopaedia.org/articles/marshall-classification-of-traumatic-brain-injury

22. Shah A, Almenawer S, Hawryluk G. Timing of decompressive craniectomy for ischemic stroke and traumatic brain injury: A review. Front Neurol. 2019;10(JAN).

23. Meng E, Duan Y, Wang X. Therapeutic mechanism of intracranial infection in patients with hydrocephalus after craniocerebral injury based on decompressive craniectomy. Saudi J Biol Sci [Internet]. 2020;27(3):873–80. Available from: https://doi.org/10.1016/j.sjbs.2019.12.039

24. Karve IP, Taylor JM, Crack PJ. The contribution of astrocytes and microglia to traumatic brain injury. Br J Pharmacol. 2016;173(4):692–702.

25. Müller C, Plewnia A, Becker S, Rundel M, Zimmermann L, Körner M. Expectations and requests regarding team training interventions to promote interdisciplinary collaboration in medical rehabilitation - A qualitative study. BMC Med Educ [Internet]. 2015;15(1):1–14. Available from: http://dx.doi.org/10.1186/s12909-015-0413-3

26. Letourneau PC. Actin in Axons. Results Probl Cell Differ Author Manuscr. 2009;48:339–51.

27. Filbin MT. Myelin-associated inhibitors of axonal regeneration in the adult mammalian CNS. Nat Rev Neurosci. 2003;4(9):703–13.

28. Siddiqui TA, Lively S, Schlichter LC. Complex molecular and functional outcomes of single versus sequential cytokine stimulation of rat microglia. J Neuroinflammation [Internet]. 2016;13(1):1–22. Available from: http://dx.doi.org/10.1186/s12974-016-0531-9

29. Bonci A, Lupica CR, Morales M. NgR1 and NgR3 are receptors. 2015;18(3):386–92.

30. Lee J, Zheng B. Role of myelin-associated inhibitors in axonal repair after spinal cord injury. Exp Neurol. 2012;1(235):33–42.

31. Asher JWF and RA. The glial scar and central nervous system repair. Brain Res Bull. 1999;

32. Silver J, Miller JH. Regeneration beyond the glial scar. Nat Rev Neurosci. 2004;5(2):146–56.

33. Lau LW, Cua R, Keough MB, Haylock-Jacobs S, Yong VW. Pathophysiology of the brain extracellular matrix: A new target for remyelination. Nat Rev Neurosci [Internet]. 2013;14(10):722–9. Available from: http://dx.doi.org/10.1038/nrn3550

34. Kale A, Novozhilova E, Englund-Johansson U, Stupp SI, Palmgren B, Olivius P. Exogenous BDNF and Chondroitinase ABC Consisted Biomimetic Microenvironment Regulates Survival, Migration and Differentiation of Human Neural Progenitor Cells Transplanted into a Rat Auditory Nerve. Neurosci Med. 2014;05(02):86–100.

35. S.J. Davies, D.R. Goucher, C. Doller JS. Robust regeneration of adult sensory axons in degenerating white matter of the adult rat spinal cord. J Neurosci. 1999.

36. Ouyang L, Martin DC. Glial Scar Brain Machine Interfaces : Implications for Science , Clinical Practice and Soci- ety Up-Regulation of Glial Fibrillary Acidic Protein in Response to Retinal Injury : Its Potential Role in Glial Remodeling and a Comparison

to Vimentin Expres- s. 2011;

37. T.LangAmandaTranJerrySilver JMCADRF. Functional regeneration beyond the glial scar. Exp Neurol. 2014;253:197–207.

38. Dong Y, Benveniste EN. Immune function of astrocytes. Glia. 2001;36(2):180–90.

39. Cernak I, Wing ID, Davidsson J, Plantman S. A Novel Mouse Model of Penetrating Brain Injury. Front Neurol. 2014;5(October):1–10.

40. Aloisi F. Immune function of microglia. Glia. 2001;36(2):165–79.

41. Compston A, Zajicek J, Sussman J, Webb A, Hall G, Muir D, et al. Glial lineages and myelination in the central nervous system. J Anat. 1997;190(2):161–200.

42. Caldeira C, Oliveira AF, Cunha C, Vaz AR, Falcão AS, Fernandes A, et al. Microglia change from a reactive to an age-like phenotype with the time in culture. Front Cell Neurosci. 2014;8(JUN):1–16.

43. Giulian D, Baker TJ. Characterization of ameboid microglia isolated from developing mammalian brain. J Neurosci. 1986;6(8):2163–78.

44. Felsky D, Roostaei T, Nho K, Risacher SL, Bradshaw EM, Petyuk V, et al. Neuropathological correlates and genetic architecture of microglial activation in elderly human brain. Nat Commun [Internet]. 2019;10(1):1–12. Available from: http://dx.doi.org/10.1038/s41467-018-08279-3

45. Lam D, Lively S, Schlichter LC. Responses of rat and mouse primary microglia to pro- and anti-inflammatory stimuli: Molecular profiles, K+ channels and migration. J Neuroinflammation. 2017;14(1):1–30.

46. Zanier ER, Fumagalli S, Perego C, Pischiutta F, De Simoni M-G. Shape descriptors of the “never resting” microglia in three different acute brain injury models in mice. Intensive Care Med Exp. 2015;3(1):1–18.

47. Fernández-Arjona M del M, Grondona JM, Granados-Durán P, Fernández-Llebrez P, López-Ávalos MD. Microglia morphological categorization in a rat model of neuroinflammation by hierarchical cluster and principal components analysis. Front Cell Neurosci. 2017;11(August):1–22.

48. Colonna M, Butovsky O. Microglia Function in the Central Nervous System During Health and Neurodegeneration. Annu Rev Immunol. 2017;35(1):441–68.

49. Lively S, Lam D, Wong R, Schlichter LC. Comparing effects of transforming growth factor β1 on microglia from rat and mouse: Transcriptional profiles and potassium

channels. Front Cell Neurosci. 2018;12(May):1–24.

50. Ferreira R, Lively S, Schlichter LC. IL-4 type 1 receptor signaling up-regulates KCNN4 expression, and increases the KCa3.1 current and its contribution to migration of alternative-activated microglia. Front Cell Neurosci. 2014;8(JULY):1–15.

51. Lively S, Wong R, Lam D, Schlichter LC. Sex- and development-dependent responses of rat microglia to pro- and anti-inflammatory stimulation. Front Cell Neurosci. 2018;12(November):1–20.

52. Lively S, Schlichter LC. The microglial activation state regulates migration and roles of matrix-dissolving enzymes for invasion. J Neuroinflammation. 2013;10:1–14.

53. Pires LR, Rocha DN, Ambrosio L, Pêgo AP. The role of the surface on microglia function: implications for central nervous system tissue engineering. J R Soc Interface [Internet]. 2015;12(103):20141224-. Available from: http://rsif.royalsocietypublishing.org/content/12/103/20141224.long

54. von Ehr A, Attaai A, Neidert N, Potru PS, Ruß T, Zöller T, et al. Inhibition of Microglial TGFβ Signaling Increases Expression of Mrc1. Front Cell Neurosci. 2020;14(March):1–10.

55. Cargill R, Kohama SG, Struve J, Su W, Banine F, Witkowski E, et al. Astrocytes in aged nonhuman primate brain gray matter synthesize excess hyaluronan. Neurobiol Aging. 2012;33(4):830.e13-830.e24.

56. Miron VE, Boyd A, Zhao JW, Yuen TJ, Ruckh JM, Shadrach JL, et al. M2 microglia and macrophages drive oligodendrocyte differentiation during CNS remyelination. Nat Neurosci. 2013;16(9):1211–8.

57. Shigemoto-Mogami Y, Hoshikawa K, Goldman JE, Sekino Y, Sato K. Microglia enhance neurogenesis and oligodendrogenesis in the early postnatal subventricular zone. J Neurosci. 2014;34(6):2231–43.

58. Dubbelaar M l, Krach L, Boddeke E. The Kaleidoscope of Microglial Phenotypes. Front Immunol. 2018;(9):1753.

59. Sekton B. Matrix metalloproteinases – an overview. Res Rep Biol. 2010;1.

60. Lively S, Hutchings S, Schlichter LC. Molecular and cellular responses to interleukin-4 treatment in a rat model of transient ischemia. J Neuropathol Exp Neurol. 2016;75(11):1058–71.

61. Blackburn D, Sargsyan S, Monk PN, Shaw PJ. Astrocyte function and role in motor neuron disease: A future therapeutic target? Glia. 2009;57(12):1251–64.

62. Priego N, Valiente M. The potential of astrocytes as immune modulators in brain tumors. Front Immunol. 2019;10(JUN):1–9.

63. Colombo E, Farina C. Astrocytes: Key Regulators of Neuroinflammation. Trends Immunol. 2016;37(9):608–20.

64. Liddelow SA, Guttenplan KA, Clarke LE, Bennett FC, Bohlen CJ, Schirmer L, et al. Neurotoxic reactive astrocytes are induced by activated microglia. Nature [Internet]. 2017;541(7638):481–7. Available from: http://dx.doi.org/10.1038/nature21029

65. Wang H, Song G, Chuang H, Chiu C, Abdelmaksoud A, Ye Y, et al. Portrait of glial scar in neurological diseases. Int J Immunopathol Pharmacol. 2018;31:1–6.

66. Zhao J, Wang B, Huang T, Guo X, Yang Z, Song J, et al. Glial response in early stages of traumatic brain injury. Neurosci Lett [Internet]. 2019;708(157):134335. Available from: https://doi.org/10.1016/j.neulet.2019.134335

67. Cernak I, Vink R, Zapple DN, Cruz MI, Ahmed F, Chang T, et al. The pathobiology of moderate diffuse traumatic brain injury as identified using a new experimental model of injury in rats. Neurobiol Dis. 2004;17(1):29–43.

68. Williams AJ, Wei HH, Dave JR, Tortella FC. Acute and delayed neuroinflammatory response following experimental penetrating ballistic brain injury in the rat. J Neuroinflammation. 2007;4:1–12.

69. Faulkner JR, Herrmann JE, Woo MJ, Tansey KE, Doan NB, Sofroniew M V. Reactive Astrocytes Protect Tissue and Preserve Function after Spinal Cord Injury. J Neurosci. 2004;24(9):2143–55.

70. Bardehle S, Krüger M, Buggenthin F, Schwausch J, Ninkovic J, Clevers H, et al. Live imaging of astrocyte responses to acute injury reveals selective juxtavascular proliferation. Nat Neurosci. 2013;16(5):580–6.

71. Robel S, Bardehle S, Lepier A, Brakebusch C, Götz M. Genetic deletion of Cdc42 reveals a crucial role for astrocyte recruitment to the injury site in vitro and in vivo. J Neurosci. 2011;31(35):12471–82.

72. Sidiropoulou K, Pissadaki EK, Poirazi P. Inside the brain of a neuron. EMBO Rep. 2006;7(9):886–92.

73. Neuronal anatomy [Internet]. Available from: https://www.dreamstime.com/diagram-neuron-anatomy-illustration-image121138040

74. Sardi S, Vardi R, Sheinin A, Goldental A, Kanter I. New Types of Experiments Reveal that a Neuron Functions as Multiple Independent Threshold Units. Sci Rep [Internet].

2017;7(1):1–17. Available from: http://dx.doi.org/10.1038/s41598-017-18363-1

75. Nimchinsky EA, Sabatini BL, Svoboda K. Structure and Function of Dendritic Spines. Annu Rev Physiol. 2002;64(1):313–53.

76. Richardson PM, McGuinness UM AA. Axons from CNS neurons regenerate into PNS grafts. Nature. 1980;

77. Nihal C. de Lanerolle, Jung H. Kim FAB. Neuropathology of Traumatic Brain Injury: Comparison of Penetrating, Nonpenetrating Direct Impact and Explosive Blast Etiologies. Semin Neurol. 2015;

78. MANFRED OEHMICHEN, CHRISTOPH MEISSNER and HGK. Brain Injury After Gunshot Wounding: Morphometric Analysis of Cell Destruction Caused by Temporary Cavitation. J Neurotrauma. 2009;17(2).

79. Li N, Leung GKK. Oligodendrocyte Precursor Cells in Spinal Cord Injury: A Review and Update. Biomed Res Int. 2015;2015.

80. RabchevskyAG, SullivanPG, ScheffSW. Temporal-spatial dynamics in oligodendrocyte and glial progenitor cell numbers throughout ventrolateral white matter following contusion spinal cord injury. Glia. 2007;55:831–43.

81. Almad A, Sahinkaya FR, McTigue DM. Oligodendrocyte Fate after Spinal Cord Injury. Neurotherapeutics. 2011;8(2):262–73.

82. Hampton DW, Rhodes KE, Zhao C, Franklin RJM, Fawcett JW. The responses of oligodendrocyte precursor cells, astrocytes and microglia to a cortical stab injury, in the brain. Neuroscience. 2004;127(4):813–20.

83. Buffo A, Vosko MR, Ertürk D, Hamann GF, Jucker M, Rowitch D, et al. Expression pattern of the transcription factor Olig2 in response to brain injuries: Implications for neuronal repair. Proc Natl Acad Sci U S A. 2005;102(50):18183–8.

84. Hughes EG, Kang SH, Fukaya M, Bergles DE. Oligodendrocyte progenitors balance growth with self-repulsion to achieve homeostasis in the adult brain. Nat Neurosci. 2013;16(6):668–76.

85. Takase H, Washida K, Hayakawa K, Arai K, Wang X, Lo EH, et al. Oligodendrogenesis after traumatic brain injury. Behav Brain Res [Internet]. 2018;340:205–11. Available from: https://doi.org/10.1016/j.bbr.2016.10.042

86. Van Den Bosch L. Amyotrophic lateral sclerosis: Mechanisms and therapeutic strategies. Dis Targets Neurodegener Disord Paving W Dis Ther. 2017;277–96.

87. Moshayedi P, Nih LR, Llorente IL, Berg AR, Cinkornpumin J, Lowry WE, et al. Systematic optimization of an engineered hydrogel allows for selective control of human neural stem cell survival and differentiation after transplantation in the stroke brain. Biomaterials [Internet]. 2016;105:145–55. Available from: http://dx.doi.org/10.1016/j.biomaterials.2016.07.028

88. Wang Y, Cooke MJ, Sachewsky N, Morshead CM, Shoichet MS. Bioengineered sequential growth factor delivery stimulates brain tissue regeneration after stroke. J Control Release [Internet]. 2013;172(1):1–11. Available from: http://dx.doi.org/10.1016/j.jconrel.2013.07.032

89. Haw RTY, Tong CK, Yew A, Lee HC, Phillips JB, Vidyadaran S. A three-dimensional collagen construct to model lipopolysaccharide-induced activation of BV2 microglia. J Neuroinflammation [Internet]. 2014 Jan [cited 2014 Oct 24];11(1):134. Available from: http://www.pubmedcentral.nih.gov/articlerender.fcgi?artid=4128540&tool=pmcentrez&rendertype=abstract

90. Zhong J, Chan A, Morad L, Kornblum HI, Guoping Fan, Carmichael ST. Hydrogel matrix to support stem cell survival after brain transplantation in stroke. Neurorehabil Neural Repair. 2010;24(7):636–44.

91. Adil MM, Vazin T, Ananthanarayanan B, Rodrigues GMC, Rao AT, Kulkarni RU, et al. Engineered hydrogels increase the post-transplantation survival of encapsulated hESC-derived midbrain dopaminergic neurons. Biomaterials [Internet]. 2017;136:1–11. Available from: http://dx.doi.org/10.1016/j.biomaterials.2017.05.008

92. Kornev VA, Grebenik EA, Solovieva AB, Dmitriev RI, Timashev PS. Hydrogel-assisted neuroregeneration approaches towards brain injury therapy: A state-of-the-art review. Comput Struct Biotechnol J [Internet]. 2018;16:488–502. Available from: https://doi.org/10.1016/j.csbj.2018.10.011

93. Li L, Yan B, Yang J, Chen L, Zeng H. Novel mussel-inspired injectable self-healing hydrogel with anti-biofouling property. Adv Mater. 2015;27(7):1294–9.

94. Banerjee A, Arha M, Choudhary S, Ashton RS, Bhatia SR, Schaffer D V., et al. The influence of hydrogel modulus on the proliferation and differentiation of encapsulated neural stem cells. Biomaterials [Internet]. 2009;30(27):4695–9. Available from: http://dx.doi.org/10.1016/j.biomaterials.2009.05.050

95. Aurand E, Wagner J, Lanning C, Bjugstad K. Building Biocompatible Hydrogels for Tissue Engineering of the Brain and Spinal Cord. J Funct Biomater. 2012;3(4):839–63.

96. Thiele J, Ma Y, Bruekers SMC, Ma S, Huck WTS. 25th anniversary article: Designer

hydrogels for cell cultures: A materials selection guide. Adv Mater. 2014;26(1):125–48.

97. Zhou S, Bismarck A, Steinke JHG. Ion-responsive alginate based macroporous injectable hydrogel scaffolds prepared by emulsion templating. J Mater Chem B. 2013;1(37):4736–45.

98. Zhu W, Chu C, Kuddannaya S, Yuan Y, Walczak P, Singh A, et al. In Vivo Imaging of Composite Hydrogel Scaffold Degradation Using CEST MRI and Two-Color NIR Imaging. Adv Funct Mater. 2019;1903753:1–10.

99. Yan C, Altunbas A, Yucel T, Nagarkar RP, Schneider JP, Pochan DJ. Injectable solid hydrogel: Mechanism of shear-thinning and immediate recovery of injectable β-hairpin peptide hydrogels. Soft Matter. 2010;6(20):5143–56.

100. Guvendiren M, Lu HD, Burdick JA. Shear-thinning hydrogels for biomedical applications. Soft Matter. 2012;8(2):260–72.

101. Haines-Butterick L, Rajagopal K, Branco M, Salick D, Rughani R, Pilarz M, et al. Controlling hydrogelation kinetics by peptide design for three-dimensional encapsulation and injectable delivery of cells. Proc Natl Acad Sci U S A. 2007;104(19):7791–6.

102. Bollmann L, Koser DE, Shahapure R, Gautier HOB, Holzapfel GA, Scarcelli G, et al. Microglia mechanics: Immune activation alters traction forces and durotaxis. Front Cell Neurosci. 2015;9(September):1–16.

103. Lam D, Lively S, Schlichter LC, Siddiqui TA, Lively S, Schlichter LC, et al. In Vivo Imaging of Composite Hydrogel Scaffold Degradation Using CEST MRI and Two-Color NIR Imaging. Front Cell Neurosci [Internet]. 2018;12(1):1–16. Available from: https://doi.org/10.1016/j.csbj.2018.10.011

104. Oliveira JM, Carvalho L, Silva-Correia J, Vieira S, Majchrzak M, Lukomska B, et al. Hydrogel-based scaffolds to support intrathecal stem cell transplantation as a gateway to the spinal cord: clinical needs, biomaterials, and imaging technologies. npj Regen Med. 2018;

105. Führmann T, Tam RY, Ballarin B, Coles B, Elliott Donaghue I, van der Kooy D, et al. Injectable hydrogel promotes early survival of induced pluripotent stem cell-derived oligodendrocytes and attenuates longterm teratoma formation in a spinal cord injury model. Biomaterials [Internet]. 2016;83:23–36. Available from: http://dx.doi.org/10.1016/j.biomaterials.2015.12.032

106. Preul MC, Campbell PK, Garlick DS, Spetzler RF. Application of a new hydrogel dural

sealant that reduces epidural adhesion formation: Evaluation in a large animal laminectomy model. J Neurosurg Spine. 2010;

107. Tian Z, Liu W, Li G. The microstructure and stability of collagen hydrogel cross-linked by glutaraldehyde. Polym Degrad Stab [Internet]. 2016;130:264–70. Available from: http://dx.doi.org/10.1016/j.polymdegradstab.2016.06.015

108. Leipzig ND, Shoichet MS. The effect of substrate stiffness on adult neural stem cell behavior. Biomaterials [Internet]. 2009;30(36):6867–78. Available from: http://dx.doi.org/10.1016/j.biomaterials.2009.09.002

109. Zimmermann JA, Schaffer D V. Engineering biomaterials to control the neural differentiation of stem cells. Brain Res Bull. 2019;150(April):50–60.

110. George J, Hsu CC, Nguyen LTB, Ye H, Cui Z. Neural tissue engineering with structured hydrogels in CNS models and therapies. Biotechnol Adv [Internet]. 2019;(March):1–17. Available from: https://doi.org/10.1016/j.biotechadv.2019.03.009

111. NHS. https://www.nhs.uk/conditions/lumbar-puncture/ [Internet]. Available from: https://www.nhs.uk/conditions/lumbar-puncture/

112. Hu W, Wang Z, Xiao Y, Zhang S, Wang J. Advances in crosslinking strategies of biomedical hydrogels. Biomater Sci. 2019;7(3):843–55.

113. Trimaille T, Pertici V, Gigmes D. Hydrogels à base de polymères synthétiques pour la réparation médullaire. Comptes Rendus Chim [Internet]. 2016;19(1–2):157–66. Available from: http://dx.doi.org/10.1016/j.crci.2015.03.016

114. Ooi HW, Hafeez S, Van Blitterswijk CA, Moroni L, Baker MB. Hydrogels that listen to cells: A review of cell-responsive strategies in biomaterial design for tissue regeneration. Mater Horizons [Internet]. 2017;4(6):1020–40. Available from: http://dx.doi.org/10.1039/C7MH00373K

115. Rosenberg GA. Matrix metalloproteinases and their multiple roles in neurodegenerative diseases. Lancet Neurol [Internet]. 2009;8(2):205–16. Available from: http://dx.doi.org/10.1016/S1474-4422(09)70016-X

116. Hou S, Xu Q, Tian W, Cui F, Cai Q, Ma J, et al. The repair of brain lesion by implantation of hyaluronic acid hydrogels modified with laminin. J Neurosci Methods. 2005;148(1):60–70.

117. Ajioka I, Ichinose S, Nakajima K, Mizusawa H. Basement membrane-like matrix sponge for the three-dimensional proliferation culture of differentiated retinal horizontal interneurons. Biomaterials [Internet]. 2011;32(25):5765–72. Available from:

http://dx.doi.org/10.1016/j.biomaterials.2011.04.062

118. Deguchi K, Tsuru K, Hayashi T, Takaishi M, Nagahara M, Nagotani S, et al. Implantation of a new porous gelatin-siloxane hybrid into a brain lesion as a potential scaffold for tissue regeneration. J Cereb Blood Flow Metab. 2006;26(10):1263–73.

119. Zuidema JM, Gilbert RJ, Gottipati MK, Diego S, Jolla L, Studies I, et al. HHS Public Access. 2019;205(205):372–95.

120. Cho IS, Ooya T. An injectable and self-healing hydrogel for spatiotemporal protein release via fragmentation after passing through needles. J Biomater Sci Polym Ed [Internet]. 2018;29(2):145–59. Available from: https://doi.org/10.1080/09205063.2017.1405573

121. Shruti V. Kabadi1, 2, Genell D. Hilton2, 3, Bogdan A. Stoica1, 2, David N. Zapple4, and Alan I. Faden1 2. Fluid-percussion–induced traumatic brain injury model in rats. Nat Protoc. 2011;23(1):1–7.

122. Park GK, Kim S-H, Kim K, Das P, Kim B-G, Kashiwagi S, et al. Dual-Channel Fluorescence Imaging of Hydrogel Degradation and Tissue Regeneration in the Brain. Theranostics. 2019;9(15):4255–64.

123. Rosenberg GA. Matrix Metalloproteinases and Extracellular Matrix in the Central Nervous System. Prim Cerebrovasc Dis Second Ed. 2017;291–5.

124. Chen JH, Hsu WC, Huang KF, Hung CH. Neuroprotective effects of collagen-glycosaminoglycan matrix implantation following surgical brain injury. Mediators Inflamm. 2019;2019.

125. Beyens A, Albuisson J, Boel A, Al-Essa M, Al-Manea W, Bonnet D, et al. Arterial tortuosity syndrome: 40 new families and literature review. Genet Med. 2018;20(10):1236–45.

126. Huang KF, Hsu WC, Hsiao JK, Chen GS, Wang JY. Collagen-Glycosaminoglycan Matrix Implantation Promotes Angiogenesis following Surgical Brain Trauma. Biomed Res Int. 2014;2014.

127. Zyck S, Toshkezi G, Krishnamurthy S, Carter DA, Siddiqui A, Hazama A, et al. Treatment of Penetrating Nonmissile Traumatic Brain Injury. Case Series and Review of the Literature. World Neurosurg [Internet]. 2016;91:297–307. Available from: http://dx.doi.org/10.1016/j.wneu.2016.04.012

128. Finch L, Adams C, Sen J, Tickle J, Tzerakis N, Chari DM. Neurosurgical grade biomaterial, DuraGen TM , offers a promising matrix for protected delivery of neural

stem cells in clinical cell therapies . Futur Healthc J. 2019;6(Suppl 1):76–76.

129. Finch L, Harris S, Solomou G, Sen J, Tzerakis N, Emes RD, et al. Safe nanoengineering and incorporation of transplant populations in a neurosurgical grade biomaterial, DuraGen PlusTM, for protected cell therapy applications. J Control Release [Internet]. 2020;321(February):553–63. Available from: https://doi.org/10.1016/j.jconrel.2020.02.028

130. Shin, Samuel S.; ; | Grandhi, Ramesh | Henchir, Jeremy; | Yan, Hong Q.; ; | Badylak, Stephen F. | Dixon CE; ; Neuroprotective effects of collagen matrix in rats after traumatic brain injury. Restor Neurol Neurosci vol 33, no 2, pp 95-104, 2015. 2015;33(2):95–104.

131. Shruti V. Kabadi1, 2, Genell D. Hilton2, 3, Bogdan A. Stoica1, 2, David N. Zapple4 and AI, Faden1 2. Fluid-percussion–induced traumatic brain injury model in rats. Nat Protoc.

132. Mychasiuk R, Farran A, Angoa-Perez M, Briggs D, Kuhn D, Esser MJ. A novel model of mild traumatic brain injury for juvenile rats. J Vis Exp. 2014;(94):1–7.

133. Skotak M, Alay E, Chandra N. On the accurate determination of shock wave time-pressure profile in the experimental models of blast-induced neurotrauma. Front Neurol. 2018;9(FEB):1–11.

134. Carey ME, Sarna GS, Farrell JB HL. Experimental missile wound to the brain. J Neurosur. 1989;71:754–64.

135. Zhou S, Li Z. A Gross and Microscopic Injuries Accompanying Projectile Study of Cerebral Maxillofacial Wounding in Dogs. 1998;345–8.

136. Crockard HA, Brown FD, Johns LM MS. An experimental cerebral missile injury model in primates. J Neurosurg. 1977;6:776–83.

137. J.W.Finnie. Pathology of experimental traumatic craniocerebral missile injury. J Comp Pathol Vol , Issue 1, January 1993, Pages. 1993;108(1):93–101.

138. Schiweck J, Eickholt BJ, Murk K. Important shapeshifter: Mechanisms allowing astrocytes to respond to the changing nervous system during development, injury and disease. Front Cell Neurosci. 2018;12(August):1–17.

139. Morrison B, Elkin BS, Dollé J-P, Yarmush ML. In Vitro Models of Traumatic Brain Injury. Vol. 13, Annual Review of Biomedical Engineering. 2011. 91–126 p.

140. Kumaria A. In vitro models as a platform to investigate traumatic brain injury. Altern Lab Anim [Internet]. 2017 Sep;45(4):201–11. Available from:

http://www.ncbi.nlm.nih.gov/pubmed/28994300

141. Morin-Brureau M, De Bock F, Lerner-Natoli M. Organotypic brain slices: A model to study the neurovascular unit micro-environment in epilepsies. Fluids Barriers CNS. 2013;10(1):1–12.

142. Krings M, Höllig A, Liu J, Grüsser L, Rossaint R, Coburn M. Desflurane impairs outcome of organotypic hippocampal slices in an in vitro model of traumatic brain injury. Med Gas Res. 2016;6(1):3–9.

143. Weightman AP, Pickard MR, Yang Y, Chari DM. An in vitro spinal cord injury model to screen neuroregenerative materials. Biomaterials [Internet]. 2014;35(12):3756–65. Available from: http://dx.doi.org/10.1016/j.biomaterials.2014.01.022

144. Cho S, Wood A, Bowlby M. Brain Slices as Models for Neurodegenerative Disease and Screening Platforms to Identify Novel Therapeutics. Curr Neuropharmacol. 2007;5(1):19–33.

145. Kumaria A. In vitro models as a platform to investigate traumatic brain injury. ATLA Altern to Lab Anim. 2017;45(4):201–11.

146. Skvortsova E V., Sinenko SA, Tomilin AN. Immortalized murine fibroblast cell lines are refractory to reprogramming to pluripotent state. Oncotarget. 2018;9(81):35241–50.

147. Etienne-Manneville S, Manneville JB, Nicholls S, Ferenczi MA, Hall A. Cdc42 and Par6-PKCη regulate the spatially localized association of Dlg1 and APC to control cell polarization. J Cell Biol. 2005;170(6):895–901.

148. Nishio T, Kawaguchi S, Yamamoto M, Iseda T, Kawasaki T, Hase T. Tenascin-C regulates proliferation and migration of cultured astrocytes in a scratch wound assay. Neuroscience. 2005;132(1):87–102.

149. Park LCH, Zhang H, Gibson GE. Co-culture with astrocytes or microglia protects metabolically impaired neurons. Mech Ageing Dev. 2001;123(1):21–7.

150. The national centre for the Reduction, Replacement and Refinement of animal models [Internet]. Available from: https://www.nc3rs.org.uk/the-3rs#:~:text=Definitions of the 3Rs ,Advancing research into animal welfare b ...

151. Maclean FL, Horne MK, Williams RJ, Nisbet DR. Review: Biomaterial systems to resolve brain inflammation after traumatic injury. APL Bioeng [Internet]. 2018;2(2):021502. Available from: http://dx.doi.org/10.1063/1.5023709

152. Qu C, Mahmood A, Liu XS, Xiong Y, Wang L, Wu H, et al. The treatment of TBI with human marrow stromal cells impregnated into collagen scaffold: Functional outcome

and gene expression profile. Brain Res. 2011;1371:129–39.

153. Mccarthy KD, De Vellis J. PREPARATION OF SEPARATE ASTROGLIAL AND OLIGODENDROGLIAL CELL CULTURES FROM RAT CEREBRAL TISSUE A novel method has been developed for the preparation of nearly pure separate cultures of astrocytes and oligodendrocytes . The method is based on (a) the abs. J Cell Biol. 1980;85(June):890–902.

154. Reduction, Replacement and Refinement of animal models [Internet]. Available from: https://www.rvc.ac.uk/research/about/animals-in-research/replacement-refinement-reduction

155. Gao HM, Hong JS, Zhang W, Liu B. Distinct role for microglia in rotenone-induced degeneration of dopaminergic neurons. J Neurosci. 2002;22(3):782–90.

156. Lööv C, Shevchenko G, Geeyarpuram Nadadhur A, Clausen F, Hillered L, Wetterhall M, et al. Identification of Injury Specific Proteins in a Cell Culture Model of Traumatic Brain Injury. PLoS One. 2013;8(2).

157. Schildge S, Bohrer C, Beck K, Schachtrup C. Isolation and culture of mouse cortical astrocytes. J Vis Exp. 2013;(71):1–7.

158. Király K, Hyttinen MM, Lapveteläinen T et al. Specimen preparation and quantification of collagen birefringence in unstained sections of articular cartilage using image analysis and polarizing light microscopy. Histochem J. 1997;29(4):317-327.

159. Patel B, Xu Z, Pinnock CB, Kabbani LS, Lam MT. Self-assembled Collagen-Fibrin Hydrogel Reinforces Tissue Engineered Adventitia Vessels Seeded with Human Fibroblasts. Sci Rep [Internet]. 2018;8(1):1–13. Available from: http://dx.doi.org/10.1038/s41598-018-21681-7

160. Ding S. Dynamic reactive astrocytes after focal ischemia. Neural Regen Res. 2014 Dec 1;9(23):2048-52. doi: 10.4103/1673-5374.147929. PMID: 25657720; PMCID: PMC4316467.

161. Chen Y, Balasubramaniyan V, Peng J, Hurlock EC, Tallquist M, Li J, et al. Isolation and culture of rat and mouse oligodendrocyte precursor cells. Nat Protoc. 2007;2(5):1044–51.

162. Var SR, Byrd-jacobs CA. Role of Macrophages and Microglia in Zebrafish Regeneration. 2020;1–17.

163. Bar-Or A, Nuttall RK, Duddy M, Alter A, Kim HJ, Ifergan I, et al. Analyses of all matrix metalloproteinase members in leukocytes emphasize monocytes as major

inflammatory mediators in multiple sclerosis. Brain. 2003;126(12):2738–49.

164. Jiang D, Liang J, Noble PW. Hyaluronan in Tissue Injury and Repair. Annu Rev Cell Dev Biol. 2007;23(1):435–61.

165. McKee CM, Lowenstein CJ, Horton MR, Wu J, Bao C, Chin BY, et al. Hyaluronan fragments induce nitric-oxide synthase in murine macrophages through a nuclear factor κB-dependent mechanism. J Biol Chem. 1997;272(12):8013–8.

166. Rustenhoven J, Park TIH, Schweder P, Scotter J, Correia J, Smith AM, et al. Isolation of highly enriched primary human microglia for functional studies. Sci Rep. 2016;6:1–11.

167. Ray B, Chopra N, Long JM, Lahiri DK. Human primary mixed brain cultures: Preparation, differentiation, characterization and application to neuroscience research. Mol Brain. 2014;7(1):1–15.

168. Russell LN, Lampe KJ. Oligodendrocyte Precursor Cell Viability, Proliferation, and Morphology is Dependent on Mesh Size and Storage Modulus in 3D Poly(ethylene glycol)-Based Hydrogels. ACS Biomater Sci Eng. 2017;3(12):3459–68.

169. Li X et al. “Engineering an in situ crosslinkable hydrogel for enhanced remyelination.” FASEB J Off Publ Fed Am Soc Exp Biol vol. 27,3:1127–36.

170. Gulino M, Kim D, Pané S, Santos SD, Pêgo AP. Tissue response to neural implants: The use of model systems toward new design solutions of implantable microelectrodes. Front Neurosci. 2019;13(JUL):1–24.

171. Lively S, Schlichter LC. Microglia responses to pro-inflammatory stimuli (LPS, IFNγ+TNFα) and reprogramming by resolving cytokines (IL-4, IL-10). Front Cell Neurosci. 2018;12(July):1–19.

172. Tickle J. Engineering neural cells in implantable materials. Keele Univ. 2017;(September).